



Title: Design and Analysis of Safety Link for Emergency Disconnect of Completion and Work-over Marine Risers	Delivered: 08.06.2011
	Availability: CONFIDENTIAL
Student: Stud. Techn. Harald Nyhus	Number of pages: 103 + Appendices

Abstract:

This master thesis is done in collaboration with Aker Solutions Subsea AS and proposes how one could securely cope with uncontrolled drift-off where the marine riser experience excessive moments and/or tension that will damage the well integrity and structure while the well is undergoing workover or intervention. This weak link design is meant to release the riser from the well structure before damage occurs, either when excessive moments, tension or both have the potential to damage the structure. The release mechanism should work as a 3rd barrier, and by itself, with no input from the operator, make the riser disconnect safely. The mechanism should also secure the well so that the surface vessel can safely drift-off from position.

The preliminary study project, which was finished in December 2010, produced several interesting concepts. One was chosen for further study and analysis in the master thesis by the candidate, Aker Solutions representatives and the supervisor from NTNU. In this thesis, the concept has been further developed, analyzed and dimensioned to cope with relevant example and extreme loading conditions provided by Aker Solutions Subsea AS.

The concept developed in this thesis is based on an idea of a standard ANSI flanged connection. By using pressurized CO₂, the flange geometry produces a separation pressure which forces the flange bolts to break, thus separating the riser connection and disrupting the communication between the surface vessel and the subsea equipment. The system is initiated by a battery powered offset monitoring system which measures the riser offset at a position 55 meters above the EDP. When the separation has been initiated, the hydraulic pressure and control signal connection between the operator and the subsea well is terminated, thus closing the wellbore by utilization of the failsafe valves in the subsea tree and/or well control package.

Analyses of the final concept in Abaqus show that the dimensions and geometry copes well with the applied loading condition. The weak link bolts are designed to break if subjected to a limited tension force. This enables the present weak link to be applied as a replacement for existing links which are solely based on tension response.

Keyword:

Offshore, Workover, Intervention, Weak Link, Safety Joint, Concept generation, Abaqus, Autodesk Inventor

Advisor:

Professor Bernt J. Leira



Master Thesis, Spring, 2011

for

Stud. Techn. Harald Nyhus

**Design and Analysis of Safety Link for Emergency Disconnect of
Completion and Work-over Marine Risers**



SCOPE OF WORK

Master thesis, Spring 2011

for

Stud. Techn. Harald Nyhus

Design and Analysis of Safety Link for Emergency Disconnect of Completion and Work-over Marine Risers

*Utvikling og Analyse av Sikkerhetsledd for Nødfrakopling av Marine
Intervensjonsstigerør*

The possibility of using a weak link in marine risers which is capable of protecting the subsea equipment against unwanted moment and tension damage is to be investigated based on a request from Aker Solutions. If this positioning system of the vessel to which the riser is attached fails for some reason, emergency disconnect of the interface to the bottom equipment should occur. In the case that the emergency disconnect procedures do not work, the safety link should ensure a secure break-off from the bottom equipment when the moments acting on the components of the subsea equipment become large enough for damage to occur. The weak link should also function as a safety barrier against unwanted tension forces.

The main objective of the master thesis is to consider a more detailed design of a promising concept that was identified as part of the work with the project thesis

The following subjects are to be examined in this thesis:

1. When placing the SL in the well stack or riser string, loading that affects the wellhead and critical components could be changed. The implications of making these changes should be discussed and the best position for the SL should be decided. If the SL makes the well stack higher the effects should be assessed to ensure that limits are not breached, or that the wellhead suffers from decreased fatigue life due to the extended height.



2. The interface of the Safety Link (SL) to adjacent components in the riser should be set and modeled in Autodesk Inventor. Based on the project design of the SJ, further design work towards a final design should be done in Autodesk Inventor. Relevant design calculations regarding the SL functions should be done to ensure that the SL will work as intended. Also, design review and discussion regarding the final design should be done in collaboration with Aker Subsea AS and the supervisor at NTNU. It should further be assessed whether the new SL can be applied as replacement for existing links which are solely based on tension response.
3. A static analysis in Abaqus of the final design made in Autodesk Inventor should identify the final and optimal dimensions of the SL. This process could result in great changes in the initial design. An iterative process at this stage should be done to further develop the final design.
4. By using the Abaqus analysis software, the SL should be analyzed with respect to local response during the separation process to identify possible design problems with the SL. While separating, the SL could be subjected to extreme loads both in tension and bending. The geometry and functionality of the SL could then be altered as a result of the separating forces (the piston solution). Interesting effects to look at are the recoil of the riser when the bolts are torn.
5. An outline and more specific design work should be done regarding the set-off system and the system which closes the wellbore. No final design of these systems is necessary but a more detailed description of the system and how it works should be made.

The work-scope may prove to be larger than initially anticipated. Subject to approval from the supervisor, topics may be deleted from the list above or reduced in extent.

In the thesis the candidate shall present his personal contribution to the resolution of problems within the scope of the thesis work. Theories and conclusions should be based on mathematical derivations and/or logic reasoning identifying the various steps in the deduction. The candidate should utilise the existing possibilities for obtaining relevant literature.

The thesis should be organised in a rational manner to give a clear exposition of results, assessments, and conclusions. The text should be brief and to the point, with a clear language. Telegraphic language should be avoided.

The thesis shall contain the following elements: A text defining the scope, preface, list of contents, summary, main body of thesis, conclusions with recommendations for further work, list of symbols and acronyms, references and (optional) appendices. All figures, tables and equations shall be numerated.

The supervisor may require that the candidate, at an early stage of the work, presents a written plan for the completion of the work. The plan should include a budget for the use of computer and laboratory resources which will be charged to the department. Overruns shall be reported to the supervisor.



The original contribution of the candidate and material taken from other sources shall be clearly defined. Work from other sources shall be properly referenced using an acknowledged referencing system.

The thesis shall be submitted in 3 copies:

- Signed by the candidate
- The text defining the scope included
- In bound volume(s)
- Drawings and/or computer prints which cannot be bound should be organised in a separate folder.

Supervisor: Professor Bernt J. Leira

Contact person at Aker Solutions: Øystein Wærstad

Start: January 17th, 2011

Deadline: June 14th, 2011

Trondheim, 17 January 2011

Bernt J. Leira



PREFACE

This report is the result of my master thesis project carried out at Department of Marine Technology NTNU Trondheim. The master thesis is also the last part of my Master of Science in Subsea Technology degree at Norwegian university of science and technology-NTNU Trondheim.

The work done in this thesis is done by the candidate alone. If the work has halted because of critical questions, the supervisor at NTNU and the contact at Aker Solutions Subsea AS have helped by structuring thoughts and processes to an extent where the work has resumed.

Development of a totally new weak-link concept for a system as the Kristin W/CO riser, has been a highly iterative process, where the use of multiple analytical and modeling programs has proved to be challenging at times. The iterative process has of course influenced the report in some degree. To compensate for this, a large effort has been made to make the report as conclusive as possible.

Evaluating the intended scope of work for this thesis, most of my goals which were set are met. In a perfect world, I would have wanted to go deeper into some of the topics of this report. But, due to the number of topics which were assessed as necessary, this has naturally been limited due to the time schedule. Still, I am very pleased with how the master thesis turned out, especially the concept that was developed. And I am looking forward to possibly continuing the work in my new job at Aker Solutions Subsea AS in Oslo, Norway.

I would like to thank Professor Bernt J. Leira at The Department of Marine Technology for the guidance throughout this thesis and the help I have received when late nights and hard work does not seem to add up. The door to his office has always been open, thus making my work much easier and effective. I would also like to thank my contact at Aker Solutions Subsea AS, Øystein Wærstad. He has represented a perfect combination of useful answers and fast-reply e-mailing. Mr. Wærstad has also been a big help in understanding all the equipment to account for in developing tomorrows safety link in a workover marine riser.

It is assumed that the person reading this thesis possesses some knowledge of the subsea oil and gas systems and also the terminology of the oil and gas industry.

The reference system used in the report is according to ISO 690 in Microsoft Office Word 2007.

Trondheim, June 10. 2011

Harald Nyhus



LIST OF CONTENTS

Scope of work.....	III
Preface.....	VI
List of contents.....	VII
List of figures.....	X
List of tables.....	XII
List of abbreviations.....	XIII
1.0 Introduction.....	1
1.1 Preliminary Continuations of Project Thesis Work.....	2
2.0 The SL's Location in the Riser Stack.....	3
2.1 The well stack Location.....	3
2.2 The riser string location.....	5
2.3 Conclusion on SL Location.....	7
3.0 Trigger system design.....	8
3.1 Acoustic inclination monitoring.....	8
3.2 The trigger system.....	9
3.3 The separation gas.....	11
3.4 Controllers.....	11
3.5 Operator control.....	12
3.6 Valves controlling the pressure batteries.....	12
4.0 The Safety Link Design.....	14
4.1 The interface to adjacent riser components.....	15
4.2 Design criteria, loading and limitations.....	17
4.3 SL Concept- Integrated Pressure Batteries.....	18
4.3.1 Finite Element Analysis.....	19
4.3.2 Concept conclusion.....	21
4.4 SL Final Concept- External Pressure Batteries.....	22
4.4.1 Top connector- Piston.....	23
4.4.2 Bottom connector- Cylinder.....	26
4.4.3 Trigger system.....	27
4.4.3.1 Pressure battery.....	27



4.4.3.2	Bottle rack, pressure battery and control valve	31
4.4.3.3	Control rack	33
4.4.4	Bolts	34
4.4.4.1	Bolt material	34
4.4.4.2	Standard Summary: ISO 13628-7:2005	37
4.4.4.3	Bolt dimensions	38
4.4.4.4	Bolt design	45
4.4.5	The assembly of the SL	46
5.0	Finite Element Analysis	49
5.1	Loading scenario	49
5.2	The Top Connector	52
5.2.1	Element type	53
5.2.2	Results- Triggered Separation	53
5.2.2.1	Checking the model	54
5.2.3	Results- Accidental Pull	56
5.2.3.1	Checking the model	57
5.2.4	Comparing the model	59
5.2.5	Conclusion- Top Connector	60
5.3	Bottom Connector	61
5.3.1	Results- Triggered Separation	62
5.3.2.1	Checking the Model	63
5.3.2	Conclusion- Bottom connector	64
5.4	Bolt	64
5.4.1	Results- Bolt	65
5.4.2	Conclusion- Bolt	66
5.5	Parameter study- SL separation	67
5.5.1	Results	68
5.5	FEA conclusion	72
6.0	Closing of the Wellbore	73
6.1	Utilizing the existing systems	73
6.2	Cutting the Umbilical	74
6.3	The design of the cutting system	76



7.0	Reliability Study.....	79
7.1	Normal Operation.....	80
7.2	Excessive Top Tension.....	81
7.3	Excessive Moment Loading	82
7.4	Combined loading	83
7.5	Reliability Study Conclusion.....	83
8.0	Conclusion.....	85
9.0	Further Work	87
9.1	Trigger system.....	87
9.2	Umbilical cutting mechanism.....	87
9.3	The Geometry of the Safety Link.....	88
10.0	References	89
10.1	Figure reference.....	90

Appendix A: Drawings of developed SL components and systems.

Appendix B: Datasheet; GT-rings 13000-14000 series.

Appendix C: MatLab codes applied for pressure change calculation when SL separates.

Appendix D: Material datasheet; AISI 8630, AISI 4340 and Ti-20%TiC.

Appendix E: SL design standard; ISO 13628-7:2005

Appendix F:

1. Maximum Bending Loads on Riser System for Connected Mode Operation
2. Schematic Representation of Riser System for Kristin Workover Riser
3. Riser Joint Interface Drawing from AKSO



LIST OF FIGURES

Figure 1: Schematic representation	4
Figure 2: Schematic representation	6
Figure 3: The trigger system sketch, showing the primary and secondary system working independently.	10
Figure 4: The preliminary project thesis final design. Pressure batteries are placed outside in a protective housing. The interface to other riser joints has not been decided upon.....	15
Figure 5: Section view of the piston concept. The piston shaped top connector flange fits inside the bottom connector geometry, enabling the bolts to be loaded to the breaking point by introducing a separation pressure.	15
Figure 6: Female interface of the riser joint. Red circle shows two lifting and handling edges built into the geometry.....	16
Figure 7: Male interface of the riser joint.....	16
Figure 8: The SL design, presenting the integrated pressure batteries.....	19
Figure 9: The section view of the SL design, presenting the integrated pressure batteries.....	19
Figure 10: The integrated pressure battery model from Abaqus. The model is showing von Mises stress. Highest stress was shown to be approximately 500 MPa.....	20
Figure 11: The SL final design. Bottom connector has been given a longer pipe section to make room for the trigger system shown in the inset picture.....	22
Figure 12: The top connector.	23
Figure 13: The piston geometry of the top connector. Seals are placed on the inside and outside of the lower part of the piston geometry.....	23
Figure 14: Half section view of the piston geometry.	23
Figure 15: When forces are acting on the seal from pressure, the seal becomes tighter.	25
Figure 16:G-T RING, 13000 Non-radiused and 14000 radiused seal series.....	25
Figure 17: As the piston is moving out from the annular cylinder, the friction causes torque to the seal cross section. This causes the sealing to seal even more.....	25
Figure 18: The bottom connector.	26
Figure 19: The cylinder geometry of the bottom connector.....	26
Figure 20: Half section view of the bottom connector.	26
Figure 21: The pressurized gas container.....	27
Figure 22: Half section view of the pressurized gas container.....	27
Figure 23: System pressure is decreasing as the SL separates.	30



Figure 24: The separation pressure is acting on nearly the same surface area as the hydrostatic pressure when separation is initiated.	30
Figure 25: The bottle rack, holding the pressure battery. The rack is designed to allow easy handling of the bottles	31
Figure 26: The multi directional electronically actuated valve, also called the control valve, mounted on the bottle rack along with hoses, bottles and connectors.....	31
Figure 27: Schematic presentation of the multi directional electronically actuated control valve.....	32
Figure 28: The control rack housing with cover. The opening on the right allows the transducer to signal the transponder on the well stack for position monitoring.....	33
Figure 29: Control rack housing, exploded view. From the right; Primary Controller and Operator Monitoring systems, primary battery and positioning system.....	33
Figure 30: The bolt-joint diagram. The diagram shows how the joint acts as a unit where the forces are transferred mostly into the joint and a fraction is transferred to the bolts.(18)	40
Figure 31: The shape similarities of the triangles made in the bolt-joint diagram.	40
Figure 32: The Bolt design for the SL.....	45
Figure 33: The final design of the SL.....	47
Figure 34: Final design of the SL installed in the C/WO riser string.....	48
Figure 35: The bottom connector is encastred to resemble the riser fastening point.	51
Figure 36: A vertical symmetry plane split the model in half.	51
Figure 37: The top tension is modeled as a vertical pulling force.....	51
Figure 38: The well pressure is set to an inside pressure force.	51
Figure 39: A kinematic coupling locks a centered reference point in all degrees of freedom to the top surface. The moment load is then put to work in this point.	51
Figure 40: The top connector Abaqus model, loaded by triggered separation forces. Red line shows the nodal path of highest stresses.	54
Figure 41: Von Mises Stress along the path of interest. Highest value of interest is below 200 MPa..	54
Figure 42: Hoop stress inside the SL, varying along the path shown in figure 40.....	55
Figure 43: The top connector Abaqus model, loaded by maximum pull forces. Red line shows the path of highest stresses.....	57
Figure 44: Von Mises Stress along the path of interest. Highest value of interest is directly above 200 MPa.	57
Figure 45: Vertical stress component along the path of interest.	58
Figure 46: The encastred, resembling the bolts effect.....	61
Figure 47: The separation pressure acting as a downward force to the SL, balanced by the bolts.	61



Figure 48: The pulling force of 300 Mg is modeled as a negative pressure force on the bolted surface.	61
Figure 49: The moment is acting in the reference point which is kinematically coupled to the bolted surface.	61
Figure 50: The bottom connector Abaqus model, loaded by all forces. Red line shows the path of highest stresses.	63
Figure 51: Von Mises Stress along the path of interest. The mean stress along the pipe section is approximately just beneath 240 MPa.	63
Figure 52: The test geometry made from the pipe section in the bottom connector. Red line indicates the path of interest.	64
Figure 53: Von Mises Stress along the path of interest. The mean stress along the pipe section is 244 MPa. NB: Please notice the vertical axis variation from 243.575 MPa to 243.755 MPa.....	64
Figure 54: The bolt from Abaqus analysis model. The von Mises stress level is reaching the tensile limit of 1000 MPa. Yellow line indicates nodes of interest.	66
Figure 55: Von Mises stress at nodes following the yellow line in the figure from bottom to top. Stress levels are reaching the tensile stress limit of 1000±50 MPa.	66
Figure 56: The Shear-ram cutting mechanism used for cutting standard drill pipe.(21).....	75
Figure 57: The mounting ring with the cutting system attached.	76
Figure 58: The actuator pushes the cutting block towards the adjacent cutting geometry, creating large shear forces which cut the umbilical.	76
Figure 59: The cutting system mounted on the bottom connector. The umbilical line passes through the cutter.....	77
Figure 60: Valve schematic showing the line which is planned to power the umbilical cutting actuator.	78

LIST OF TABLES

Table 1: Design criteria, loading and limitations.....	17
Table 2: Selected search parameter used in material selection.	36
Table 3: The imaginary bolt material data.	37
Table 4: Load data provided from AKSO.....	38
Table 5: Test result of the comparison model.	60
Table 6: Change in stress level as the SL separates.	69



LIST OF ABBREVIATIONS

AKSO	Aker Solutions	RKB	Rotary Kelly Bushing
BOP	Blow Out Preventer	SFT	Lower Riser Package
C/WO	Completion/Workover	SJ	Stress Joint
DNV	Det Norske Veritas	SL	Safety Link
DP	Dynamic Positioning	TSJ	Tapered Stress Joint
ED	Emergency Disconnect	VXT	Vertical X-mas Tree
EDP	Emergency Disconnect Package	WCP	Well Control Package
ESD	Emergency Shut Down	WH	WellHead
EQD	Emergency Quick Disconnect	WL	Weak Link
ISO	Int. Org. for Standardization	WL	Wire Line
LMRP	Lower Marine Riser Package	WLA	Wire Line Adapter
LRP	Lower Riser Package		



1.0 INTRODUCTION

The offshore exploration of oil and gas dates back to the nineteenth century. The first offshore oil wells were drilled from extended piers into the water of the Pacific Ocean, offshore Summerlands, California in the 1890's. However, the birth of the offshore industry is commonly considered as in 1947, when Kerr-McGee completed the first successful offshore well in the Gulf of Mexico in 4.6 m of water off Louisiana. Since then, the offshore industry has developed techniques enabling extreme deepwater wells to be created.(1) Eni's Devil's Tower located in 5,610 ft (1,710 m) of water, in the Gulf of Mexico, was the world's deepest spar until 2010. The world's deepest platform is currently the Perdido spar in the Gulf of Mexico, floating in 2,438 meters of water. It is operated by Royal Dutch Shell and was built at a cost of \$3 billion.(2)

On the 20th of April 2010 an explosion occurred on a semi submersible rig called Deepwater Horizon. Eleven workers died in the incident and seventeen were injured. Fire vessels fought the flames for 36 hours until the rig capsized and sank. In the weeks that followed, BP the operator of the rig, tried to stop the enormous spill of oil emerging from the deep waters of Mississippi Canyon Block 252 with all means necessary, and succeeded with sealing off the well after 85 days, 16 hours and 25 minutes. (3)(4)

In the aftermath of the Deepwater Horizon incident, one can observe increased initiative to study and try to prevent, even harder, a similar kind of disaster in the future. By doing this, more resources are routed towards research and development projects regarding safety barriers and other fail-safe mechanisms. (5)

In offshore oil production, the philosophy regarding safety barriers and redundancy has been under constant development. Basically this means that if a system should fail, another system will ensure the safety of people, environment and assets. Some of these systems are redundant many times over because their operational safety tasks are of extreme importance.

One system which is of extreme operational and safety importance is the marine riser. The riser is a high strength durable pipe, connecting the platform or intervention vessel physically to the subsea well and allows tools, drill-strings or fluids to run from and to the well. It is of extreme importance that the riser has a maintained tension control and is not exposed to excessive bending moments. The tension in the Riser is controlled by tension systems on the deck of the surface vessel which allows the surface vessel to move freely from the forces excited from the open sea. In addition, the



vessel has a controlled position directly above the well to ensure that the riser do not exceed the bending moment limits that could damage the well structure and components.

Should the system that control the positioning fail and the surface vessel experience an uncontrolled drift-off , the Emergency Disconnect Package (EDP) should be able to release the riser from the well structure. The EDP is then the only system that can save the well structure and ensure no damage to the well integrity. But, if the EDP- system does not work the surface vessel will drift off and damage the well integrity which could lead to a fatal disaster where an uncontrolled leak to the sea from the well could occur. (6)

Aker Solutions Subsea AS, has taken the initiative to this project and master thesis. The thesis studies an innovative solution to the drift-off problem where the main goal is to protect the well integrity and ensure safe operations even though the two safety mechanisms regarding drift-off should fail and the operator has lost control. By introducing a safety joint that monitor the moment and tension load, specially designed to disconnect the surface vessel from the well if limits are breached, one can prevent disasters in the future.

1.1 PRELIMINARY CONTINUATIONS OF PROJECT THESIS WORK

As an introduction to this thesis it has been assessed natural to summarize some of the conclusions made from the preliminary project thesis.

The final concept developed in the preliminary study, was developed to protect the well head and well integrity against excessive moment loading only. The idea is based on a standard ANSI flanged connection. By using pressurized gas, the flange geometry produces a separation pressure which forces the flange bolts to fail and by this separating the connection and thus breaking the connection between the surface vessel and the subsea equipment. The system is initiated by a battery powered measuring device which measures the riser offset angle thus protecting crucial well equipment against excessive moments. When the separation has been fulfilled, the communication between the operator and the subsea well is terminated, thus closing the wellbore by utilization of the failsafe valves and mechanisms in the subsea tree and/or well control package.

In this thesis, the idea has been modified several times in an attempt to fulfill as many demands as possible. The final concept design has been analyzed and evaluated in order to make the result as effective, reliable and safe as possible.



2.0 THE SL'S LOCATION IN THE RISER STACK

Early in the development process of the new Safety Link (SL), the best location for the SL was discussed. Basically the discussion has evolved to focus on four main criterions;

- 1 The SL should be placed where it does the least damage during normal operation.
- 2 The SL should be placed where it is most suitable with respect to its functions.
- 3 The SL should be placed where the cost can be minimized with respect to production and handling.
- 4 If possible, the location should enable the design to replace other SL functions in the riser string, i.e. the tension weak link (WL).

In the design process, two locations have been discussed. Either the SL is to be placed in the well stack between the Emergency Disconnect Package (EDP) and the Stress Joint (SJ) (the well stack location), or the SL should be placed in the riser string in vicinity of the well stack (the riser string location). Due to the design work already done in the preliminary project thesis, the location of the SL should be in vicinity of the well stack to be able to monitor the moment and also to close the well bore within reasonable time. In this chapter the two locations are discussed and compared to be able to choose the most effective solution. Schematic drawings of the Kristin CO/W riser system and components are presented in appendix F.

2.1 THE WELL STACK LOCATION

1. When placing the SL between the EDP and the SJ, as the red circle indicates in figure 1, there are many considerations which need to be addressed. The main problem with this location is the increased height of the well stack. When the riser responds to the environmental forces, the Well Head (WH) and the well stack are designed to withstand the horizontal and vertical forces transferred. Since the well stack is much stiffer than the riser string, the stack will transfer the moment and horizontal load to the WH functioning much like a moment arm. By increasing the height of the well stack, all the moment loads transferred to the WH will increase and thus most importantly decrease fatigue life of the WH.

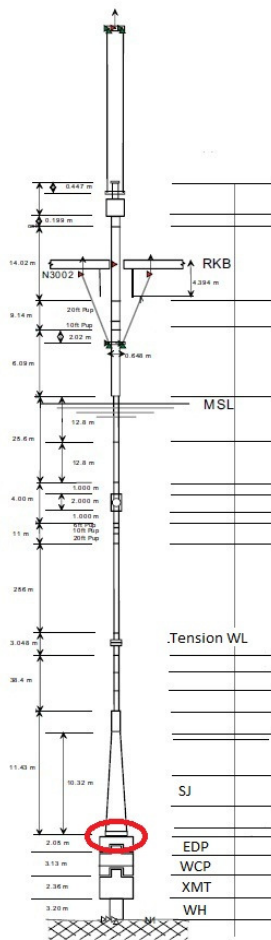


Figure 1: Schematic representation of the riser system. Red circle indicates lower SL location.

Thousands of man hours worldwide are dedicated every year to the investigation of how to increase the fatigue life of the WH. This is because a well's life is commonly determined from the assumed load history of the WH. A rupture or a sudden fatal breakdown of a WH could lead to serious accidents where people, environment and equipment could be seriously harmed. Therefore, a concept which decreases fatigue life of a WH is surely not preferable, and will probably be a concept that will not see the light of day. Of course, in the future the WH can be designed in a way that makes the WH less critical. Then this argument can be reevaluated.

With respect to tooling and running the installation procedures, there is not considered to be any special problems with this location except increased weight. By designing the SL to cope with the forces and moments at this location, the wall thickness and components will increase drastically in size thus increasing the handling weight. This makes the SL expensive to transport, move and in some degree operate.

2. The triggering system is not affected particularly by this location in the well stack since the moment is planned to be measured by acoustic signals powered by an independent power source. The closing of the wellbore is highly simplified by using this location. It is considered convenient to utilize the safety functions of the Well Control Package (WCP) and X-mas Tree (XMT) to close the wellbore by cutting the hydraulic and power supply thus safely cutting any tools or pipe in the bore and seal off the well. Also, the location may enable the closing of the wellbore to be done faster in some degree, because of short hydraulic signal travel distance.



Due to the high moments acting in this location, it is likely to assume that the SL will be totally damaged if initiated. Also, wedging problems and other effects could play a key role whether the SL will function properly.

3. The SL will be expensive to produce. To cope with high forces, the SL must be dimensioned more robust. This will result in high material and machining cost.
4. If the new SL should replace the tension SL, it has to be able to be dimensioned so that the SL will separate if the pull exceeds 300 Mg. Early calculations suggests that to dimension the SL sufficiently, so that the geometry can cope with moments up to 2500 kNm and at the same time limit the strength of bolts to fail at the pull limit of 300 Mg, seems to be difficult to balance with safety margin. Also, when placed in the well stack, the fatigue loads are considered excessive and could cause problems when dimensioning the bolts in the proposed concept.

2.2 THE RISER STRING LOCATION

1. At riser stack location, shown in figure 2, the moments are much smaller than in the well stack location. Here the maximum operation moment is set to 59 kNm, which is a significantly smaller moment force. Now, during normal operation, the SL will have little or no impact on the WH fatigue life. It does represent a slight change in geometry to the riser and of course some increase in weight, but the change is not expected to make the riser behave much different from the original. Locally the inertia forces and drag forces will change slightly but it is assumed to be not enough to be of significance to the riser behavior.

When installing the SL in this location it has not been identified any special problems. The SL will be installed in the riser stack as a normal riser joint. Of course, some extra time is assumed to be consumed as the section gets installed but this is not considered to be a major problem.

2. The triggering system is not affected particularly by this location since the moment is planned to be measured by acoustic signals powered by an independent power source. The distance from the riser stack location to the planned transponder in the well stack, should

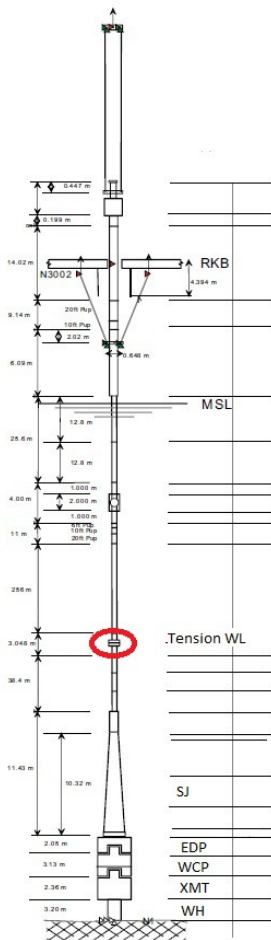


Figure 2: Schematic representation of the riser system. Red circle indicates upper SL location.

be about the same as between the well stack location and the planned transponder location in the riser stack.

As for the closing of the well bore, the riser stack location is more difficult. In conversation with Aker Solutions (AKSO), this should be solved by cutting the umbilical line which transports the hydraulic and electrical control signal to the well systems. The umbilical line runs beside the riser and past the SL. A cutting mechanism, triggered by the SL's separating forces, should release the Riser in full extent and also cut the hydraulic and/or electric signal to the well. By doing this the well control and safety systems (XMT,WCP), closes the wellbore and secures the well. If the well is a direct hydraulic system, the shutdown will be delayed in some extent, but if the system is a multiplex, electro/hydraulic or piloted hydraulic system, the shutdown could be relatively fast.(7)

If the SL is initiated when placed in this location the forces and moments should be much smaller compared to the well stack location. This will probably lead to a smoother separation without a total destruction of the SL.

3. Compared to the well stack location, this concept will be less expensive to produce. This is because of the material saves, but also because of less machining due to smaller dimensions.

Because of smaller dimensions and weight, the handling, transport and storage will be less expensive and generally easier compared to the well stack location.

4. This location enables the design of a SL which could possess two functions. The regular tension SL function where the specially designed flange bolts fail when tensioned past a tension limit, and also the moment SL function, known from the preliminary study as the piston concept.



2.3 CONCLUSION ON SL LOCATION

After assessing the analysis of the two locations in question, the favorable location is somewhat obvious. The design, cost and effectiveness gets better when placing the SL in the riser string. The SL basic functions are independent of where the SL is placed, so this will not affect the moment's measurement by acoustic signals. The main differences between the two locations are the forces, resulting in two very different designs. The SL separation by the piston concept has also been assessed to be working more efficient when the SL is placed in the riser string.



3.0 TRIGGER SYSTEM DESIGN

The trigger system is designed as a stored force which can force the SL to separate on command. Basically, the trigger system monitors the riser behavior and should secure safe operations even though multiple safety barriers are malfunctioning.

3.1 ACOUSTIC INCLINATION MONITORING

When the well stack is subjected to large moments the stack will experience some inclination, thus making the measuring of a critical moment at the SJ difficult if the measuring is based on riser inclination alone. The angle of inclination at a point on the riser above the SJ will be influenced by surface vessel motion and position, the environmental forces acting on the riser, soil properties (in contact with and in vicinity of the conductor housing) and somewhat deformation of the well stack.(8) First, the idea was to use some kind of a strain gauge system where continuously and accurate moment measurements on point of interest could be done and the tension forces in the riser are accounted for. The problem with strain gauges is that they need to be calibrated frequently to determine a reference point to measure the strain exactly. Also temperature variations could inflict the measuring results significantly making the system non-reliable. Further investigation on Kongsberg DP-systems showed that they use acoustic systems to accurately determine the position of the surface vessel relative to the well. The calculation of position is based on range, and vertical and horizontal angle measurements from a minimum of three hull mounted transducers. The system provides three-dimensional transponder positions relative to the vessel. The typical accuracy of the system is as narrow as 0.1 meter at 300 meters of water depth. The system is simple and seems accurate enough to be used as an off-set position monitoring system for the SL.

By using the Kongsberg DP-system positioning principle, one can monitor the position of a point on the well stack relative to the SL. The system uses an antenna (the transducer) which is to be fitted into the SL containing both a transmitter and a receiver. A pulse is transmitted from the SL aimed at a transponder placed somewhere in the well stack, preferably close to the SJ. The pulse activates the transponder, which will respond with a replay. The SL's transducer with corresponding electronics will calculate an accurate position of the transponder relative to the SL.(9)

By measuring the relative position between the SL location and a point on the well stack one can isolate the movement causing the moment, undisturbed by other effects. The relative position



measurement enables the SL off-set to be determined from the stiffer well stack which is caused by the moments. By measuring this in real-time, limitations could be set so that the SL will initiate when an accident is about to happen.

A concern which arises with sound waves travelling in water is the effect of deflection as the sound travel through different temperature layers and other obstacles which could disturb the signal. In a worst case scenario this could lead to an unwanted SL activation. In this design, the distance between the transducer and the transponder is meant to be no more than 55 meters. This allows very accurate measurements which could be set to behave somewhat conservative. Measurements can be done many times per second and the SL can be set not to initiate at the first limitation breach, but to await a certain confirmation period before activating. Also, since the sound beam does not come in contact with surface water the temperature is assumed relatively stable so deflection problems are assumed not to be significant.(10)

3.2 THE TRIGGER SYSTEM

In figure 3, a block diagram of the SL trigger system is presented. The diagram is made to get an overview of how the system could be designed to function with redundancy.

If the position monitoring is detecting a critical large offset, suggesting that high moment loads is affecting the well stack; a controller will send a logic signal to the main controller. This signal indicates that the SL should initiate the separation process. If the system is armed by the operator the main controller will open the valves and let the compressed gas flow into the SL. When the separation pressure is balanced, filling the SL with pressurized gas, the SL will be forced to disconnect.

If the SL separates because of excessive top tension, sensors monitoring the separation of the flanges will set-off the separation pressure, helping the separation process and most importantly cut the umbilical line by activating the umbilical cutting mechanism.

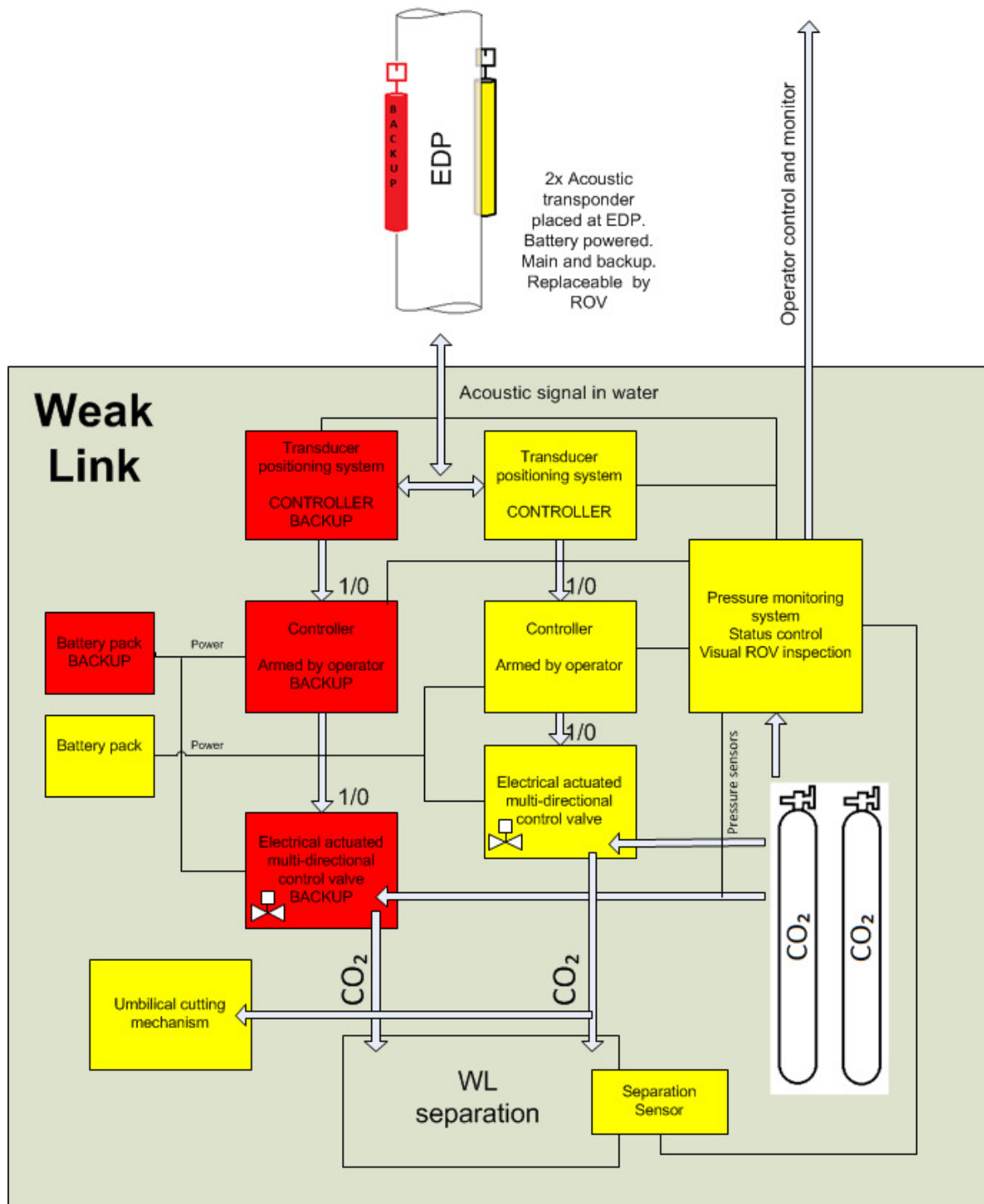


Figure 3: The trigger system sketch, showing the primary and secondary system working independently.



3.3 THE SEPARATION GAS

The gas used to separate the SL has been evaluated to hold certain properties. First of all, the gas used should be non reactive with its surroundings. In normal operation, the gas will be in contact with metal when stored. When used, the gas flows through connectors and hoses into the SL. While the SL separates the gas will come in contact with the flow from the well and salt water. The well stream could be a mix of water, drilling fluid containing chemicals, hydrocarbons, sand and gas. The pressurized gas containers will have a long-time exposure to the separation gas. The rest of the system will have short-time exposure. Also, the well stream will have a short time exposure and is likely to mix with the separation gas in some extent. While the system is not used, the gas has to be safe to store on deck and also to be safe to handle. It is of importance that the gas does not pollute the environment more than necessary when the SL is initiated.

At first, the gas which was evaluated was dry regular air, but after some research the gas which should be used is carbon dioxide (CO₂). To use CO₂ is convenient because of the existing extensive testing on how the gas behaves in contact with oil reservoirs. The gas is commonly known as an injection gas in oil reservoirs. The gas changes the viscosity of the reservoir, making the crude oil travel easier through dense rock and thus increases recovery. The gas is non-flammable and is inexpensive and safe to use. It is commonly known that CO₂ is used in many applications because of its non-flammable, non-reactive and inexpensive properties. Also, procedures and regulations on how the gas should be stored and treated on surface vessels, under transportation and storage areas are easy to come by because of the already common usage, making the gas a good candidate.(11)

3.4 CONTROLLERS

It is of most importance that the system being used is as fail safe as possible. Since the trigger system is electronically operated, the weakest link by far in the system is the trigger system. It seemed fairly easy to put a Programmable Logic Controller (PLC) to control the monitoring and setting off the SL. Further investigation showed that a PLC controller will not be reliable enough for the system because they tend to need maintenance frequently. AKSO meant that a microcontroller will be a lot less troublesome and should be the main operating controller along with simple switches which operates on logic signals. The controller system and operating switches are to be put in a tight pressure balanced oil filled canister to protect against interruptive forces and contamination. The main goal of designing this system is to make it as simple as possible, because of the importance of making this system reliable. A complete backup line is necessary if the system



should fail. The backup system could be designed so that when the main system fails the backup initiates. This will increase the complexity of the system, since controllers need to switch system when primary fails, but could prove to be more reliable. Another option is to operate both systems simultaneously, so that both systems will initiate if they are working properly. Of course, one of the two systems, primary and backup, should be designed to be able to separate the SL alone. This evaluation should be taken further in the actual design process of the final trigger system, but in this master thesis, the main system is assumed to function when operated, while the backup initiates when the main system fails.

3.5 OPERATOR CONTROL

As demanded from Statoil and AKSO, the operator should be able to enable and disable the SL. This is to ensure safe operations during critical well procedures. Also, a switch where the operator could manually override the system and set off the SL should be discussed further. In the system sketch, a signal line for operator monitoring of the SL system and possible control is drawn from a system control module. The operator monitor should show the system pressure at two system locations, valve positions, the riser offset relative to the SL or the calculated moment force and also the battery status. The operator should also be able to get warnings when a controller fails and the backup system is initiated. In subsea design, a visual inspection possibility is often used so that a Remotely Operated Vehicle (ROV) could manually inspect the system status if needed. The possibility of visually inspecting the system pressure and status could prove to be useful and is a commonly used tool for subsea applications. Not only if the operator monitor fails but also in case of comparison of measured values on surface vessel supposed to actual values. For instance, a green light could show that the system is operating normal. A red light could show that the system is operating in safety mode using the backup system. A mechanical pressure gauge could make possible a visual inspection of the system pressure and so on.

3.6 VALVES CONTROLLING THE PRESSURE BATTERIES

For the trigger system to be robust, the system needs both redundancy and reliable components. The valves which allow the system to contain the pressure and make use of it when needed are crucial pieces that need to operate fully during operation. Like all valves, some leakage is inevitable. Therefore pressure monitoring of the SL is needed to have control of the leakage situation. Also, it is desirable to use valves that can be operated fast and accurate, either the valve



should need little force to open so that high travel speed can open the valve fast, or the valve should need bigger force but short travel to open.

In the trigger system, more than one pressure bottle is connected to give as large volume as possible. It has been considered convenient to use a multi directional electronically actuated valve system, which not only direct the separation gas, but also function as a manifold, collecting the separation gas before delivered to the SL's pressure chamber. The valves should be able to operate precise, have a minimum of leakage and certified for the conditions at hand. The design of such a valve is complicated and should be discussed with a proper vendor, before deciding on which solutions are best.



4.0 THE SAFETY LINK DESIGN

In the preliminary project thesis done on the SL concept, the SL was intended to be placed between the EDP and SJ. The SL was designed as a massive pipe flange that would force to separate when initiated. The separation was powered by external pressure batteries which were thought to be located in a guide frame. The pressure batteries were designed as pressurized gas cylinders.

In this thesis the preliminary concept has been the inspiration and sketch basis to the design work and progress. All the main functions are adapted, but the dimensions and shape has been altered to match the new loading scenario. The pressure batteries where experimented with, as shown in chapter 4.3. This was an attempt to try to optimize the SL.

For simplification purposes, it has been decided convenient to name the main components of the SL. The SL geometry is built up of two components. As a normal flange, the connection is made from two adjacent components which are bolted together. In this SL design, it is appropriate to name the parts as the bottom connector and the top connector. The bottom connector is mounted to the riser pipes leading down to the WH and holds the pressure battery which separates the SL on initiation. The top connector is mounted to the riser pipes leading to the surface vessel. If the SL for some reason separates, the top connector will drift off with the surface vessel, while the bottom connector represent the reattachment point to the well.

The top connector flange design is based on a standard ANSI flange. The difference is that this flange has a special geometry which functions similarly to a piston in a combustion engine. The bottom connector contains the cylinder geometry adapted to the piston. Together these geometries allow pressurized gas to load the flange bolts so that the bolts fail and the SL separates.

In figures 4 and 5, the preliminary project thesis development is presented. As shown, the concept was studied and showed promising results leading to the development of a new and evolved concept in the master thesis.



Figure 4: The preliminary project thesis final design. Pressure batteries are placed outside in a protective housing. The interface to other riser joints has not been decided upon.

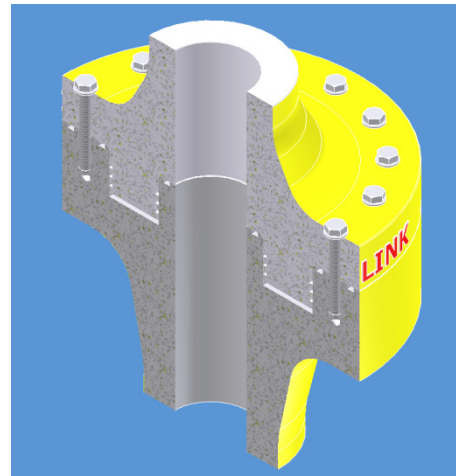
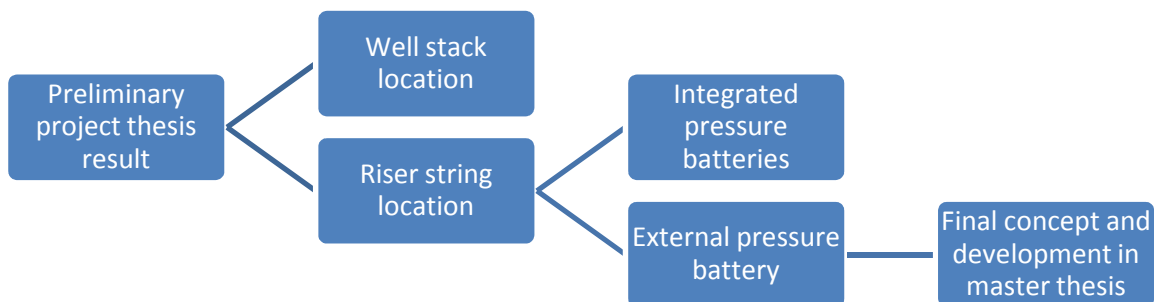


Figure 5: Section view of the piston concept. The piston shaped top connector flange fits inside the bottom connector geometry, enabling the bolts to be loaded to the breaking point by introducing a separation pressure.

In this master thesis, some fundamental design experimentation has been done to the SL. To sum up the results and what is presented in the following chapters, a block diagram has been made.



In the following chapters, a more detailed description of what these blocks represent will be given. The main purpose of this diagram is to give the reader some direction to the results in this thesis so that a higher understanding of the process is gained.

4.1 THE INTERFACE TO ADJACENT RISER COMPONENTS

Vital to the design was to evaluate how the system should be connected and built into the riser string. After some sketching and discussions with AKSO, it was decided that no special design work should be done to the interface. It was considered adequate to model the interfaces as a copy

of the regular riser joints. In figures 6 and 7, the male and female connectors are presented with their protection caps mounted. These are removed upon assembly.

When the interfaces are designed as regular riser connector joints, the SL will fit into the riser stack as a regular riser joint. This will ease the installation and not require any special tools or handling devices to install the SL.

In figure 6, the neck of the connector has two lifting and handling edges marked with a red circle. This geometry has to be implemented into the SL design because it is desirable to use the same tooling as for the riser joints. The handling and lifting edges are also discussed with AKSO and is decided to be implemented to the SL.

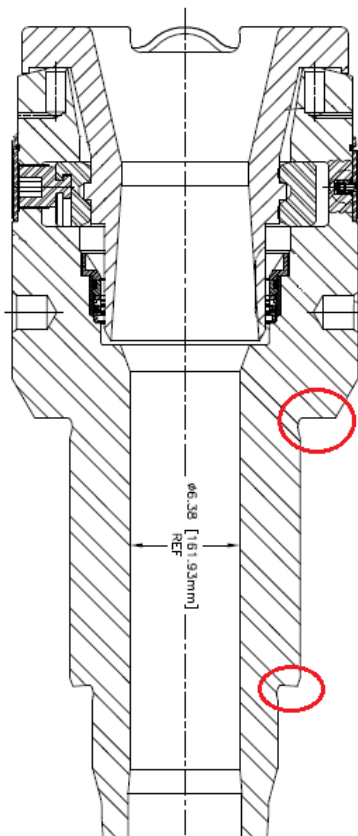


Figure 6: Female interface of the riser joint. Red circle shows two lifting and handling edges built into the geometry.

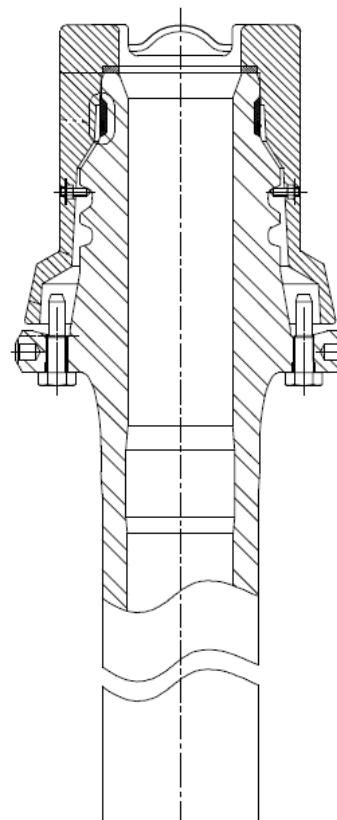


Figure 7: Male interface of the riser joint.



4.2 DESIGN CRITERIONS, LOADING AND LIMITATIONS

To be able to dimension and design the SL as effective as possible, a list of criterions where produced early in the design development. Both loading and design demands have been important to understand before any design work was done. To give a clear presentation of these criterions a list has been generated in table 1.

Table 1: Design criterions, loading and limitations.

<i>Description</i>	<i>Value</i>
Maximum geometry dimension due to RKB opening (diameter) and Catwalk length/Derrick height.	Max. Diameter (RKB opening): 47.5" or 1200 mm Max. Length/Height set to: 10 m
Maximum approximately weight of SL due to crane/Vessel, riser structure and handling limitations.	Max. weight is set to: 10 Mg
Inside diameter of SL, due to tooling size and general riser application. Same as riser joints (smallest passage of riser)	Min. ID: 6.462" or 165 mm Max. ID: 7.465" or 189 mm
Welding of cycle loaded components	No welding. Fatigue criterion.
Inside pressure, well pressure	Design pressure: 10 ksi or 690 bar
Maximum static riser pull. SL break load due to compensator lock-up.	Break load: Approximately 300 Mg
Maximum static riser moment at location.	Max. moment: 59 kNm
Minimum separation force when SL moment protection system is initiated.	Min. sep. force: 400Mg



Maximum production cost.	No limit at this stage.
Minimal use of hydraulic connection points is preferred for the moment protection system.	Max number of connections: Minimum
Operating time without service.	Approximate life without service is set to: 600 hours or 25 days
Maximum operation water depth in this design. (Kristin example case is 360 m.)	Max. water depth: 600 m
Ambient operational temperature range.	Submerged: -2 °C to +6 °C In air: -40 °C to +50 °C
Well stream temperature range.	Temperature range: -18 °C to +135 °C

4.3 SL CONCEPT- INTEGRATED PRESSURE BATTERIES

When the new concept was to be developed, it was tempting to see how it may be possible to design the SL with an integrated pressure battery. By doing this one could be able to make the design slimmer and maybe less complicated. In figures 8 and 9, the Autodesk Inventor model of the concept is presented. As shown, the piston-flange concept is kept. The interfaces (connectors) are modeled to their right dimensions according to data provided from AKSO. Here the piston-cylinder length is increased from earlier models. This is because it is desirable to model the connection as a “pipe in pipe” in an attempt to direct most of the moment away from the bolts and into the body itself. By doing this the possible stress cycles on the pretensioned bolts will hopefully be minimized.

The model is shaped like a pipe, making all vertical cross sections symmetrical. This gives the SL the same load response, regardless of which direction the moment or force, from both environmental loads and structural loads, are acting.



For fatigue purposes, all corners are rounded off. This prevents stress concentrations to form and allows the forces to transfer through the body in a smooth and even way.

The SL is planned to be manufactured by machining. A solid tube is to be machined to form the two components. By designing the components so that welding is not needed, the production cost get more effective and loss of fatigue life due to welding does not influence the fatigue life calculations.



Figure 8: The SL design, presenting the integrated pressure batteries.



Figure 9: The section view of the SL design, presenting the integrated pressure batteries.

4.3.1 FINITE ELEMENT ANALYSIS

To check the design, a model of the design was generated in Abaqus. When using Inventor to design the model one could easily transfer the geometries into Abaqus by exporting and importing the model as e.g. a *.SAT file. But when using this option, one cannot tweak the design dimensions in Abaqus because you only import the 3D-solid, not the sketches. Therefore the model had to be



drawn and produced in Abaqus Part environment because it is highly useful to be able to trim the dimensions while doing the analysis.

Because of the advanced geometry, which is simplified in this model, the automatic meshing features were not able to generate a suitable hex mesh. One could use the bottom-up meshing features, which was thoroughly tried, but this made the mesh too coarse with respect to the model geometry. To cope with this a quadratic TET mesh was selected with 10-noded tetrahedral elements. With the TET mesh Abaqus automatically seeded and meshed the model with no problems. To be able to track the forces and stresses in a TET-meshed model, partitions were made horizontal and vertical. This enables the program to plot stresses and deformation variations through the cross sections so that the user can compare the results. But this was not too interesting on this preliminary model. The interesting part was to look for stress concentrations. Especially in vicinity of the integrated pressure battery. As figure 10 implies, the curvature in the pressure battery is subjected to large forces which lies about 10% beneath yield limit. This is considered to be acceptable when the test pressure inside the battery which was used was calculated from ASME pressure vessel and boiler code. All other stresses and deformations are considered acceptable.

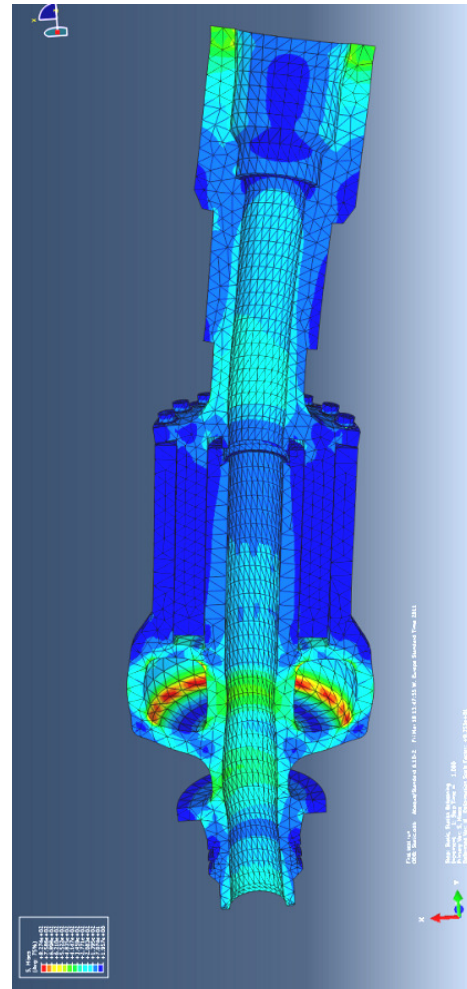


Figure 10: The integrated pressure battery model from Abaqus. The model is showing von Mises stress. Highest stress was shown to be approximately 500 MPa.



4.3.2 *CONCEPT CONCLUSION*

The problem with this design is obviously not the dimensioning. To make the SL withstand the forces which are acting is only a matter of wall thickness and material properties. The real problem lies with the production of this design. It has been a fundamental criterion not to include welds to the geometry. Therefore, the annular ring which represents the integrated pressure battery is preferably to be made by some kind of molding process. After discussions with several professors at institute of marine technology at NTNU, it was considered possible to make this geometry, but some kind of plugging will be necessary and therefore also implying welds to some degree. This addresses some points to be considered:

1. These kinds of welds are not considered to reduce fatigue life significantly in this design. This is because the geometry which is planned to be welded will not be subjected to load cycles of significance and is not the main load bearing geometry.
2. When designing the annular ring as a pressure vessel, high tolerance control on wall thickness is necessary. High tolerance is possible to achieve but will give an increase of production cost and time.
3. If the production of the annular ring should for some reason not be possible to make within the tolerances after further enquiries are done, the design has no future.

With these points in mind, the candidate has decided not to develop the design further in this thesis. Still, the design will be presented as a possible solution to AKSO, which could decide that the design could be of use on a later stage.

4.4 SL FINAL CONCEPT- EXTERNAL PRESSURE BATTERIES

As it was pointed out in chapter 4.3, the integrated-pressure-battery concept is not preferred in this project. By moving the pressure battery outside the SL, the specially designed flange geometry gets somewhat simpler. In this final design, shown in figure 11, the piston side of the flange is nearly unchanged. Due to the Abaqus analysis in previous designs, the length of the “pipe-in-pipe” geometry has been reduced. The geometry that enables the operator to handle and connect to the SL for lifting and running purposes is kept on the top connector side as before. The bottom connector side of the flange is modified to give room for the trigger and monitoring systems. The trigger system is planned placed underneath the bottom of the separation geometry, making use of the protection this geometry can give. Also, this design makes the SL slimmer and more effective with respect to the forces which will act on the SL while in operation. The basic dimensions of the SL are designed to resemble a regular riser pipe section where this is natural plus 5%. This will hopefully give positive results in the FEA calculations. All connecting geometries have been given smooth curvature transitions to cope with unwanted stress concentrations.

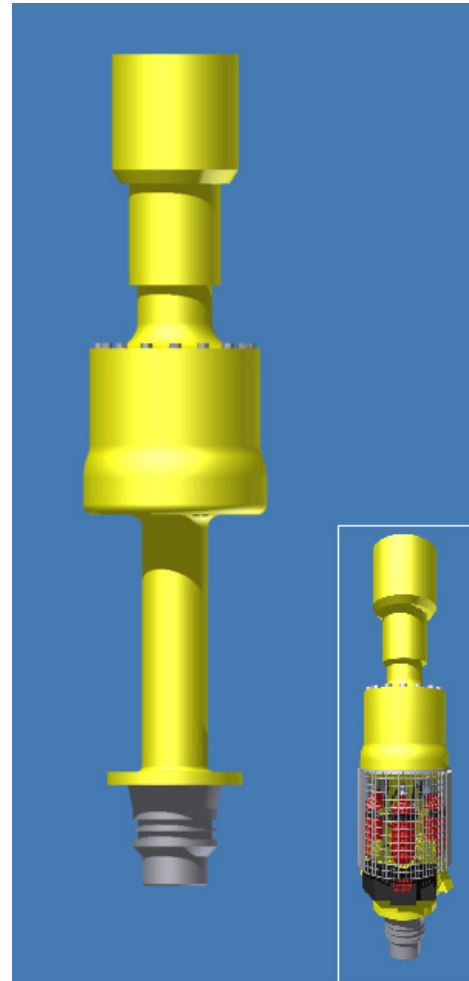


Figure 11: The SL final design. Bottom connector has been given a longer pipe section to make room for the trigger system shown in the inset picture.

4.4.1 TOP CONNECTOR- PISTON

Due to the interface to other riser components, all geometries above the flange are primarily fixed, except for the rounded transition from the SL flange plate to the riser pipe leading up to the riser interface. The large radius prohibits large stress concentrations to form. Early FEA testing of the geometry showed unacceptable deformation of the flange plate when subjected to the separation forces. This caused moment and shear loads to form in the SL bolts which were unacceptable. The flange thickness was then adjusted to 80 mm. This is to make the flange plate robust with respect to the large forces needed to break off the bolts when the SL is initiated. The top connector is shown in figures 12,13 and 14. In figure 13, the piston which transfer the separation pressure to the bolts is shown. The separation pressure will act on the horizontal bottom surface. The separation force is basically determined from the size of this area and the pressure delivered from the pressure batteries. The forces from the ambient hydrostatic pressure will also influence the separation. The pressure at 600 m water depth is:

$$P_{hyd,600} = 1030 * 9.81 * 600 = 6.063 MPa$$

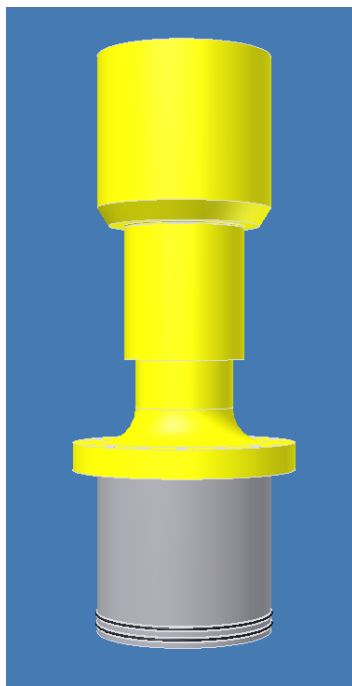


Figure 12: The top connector.

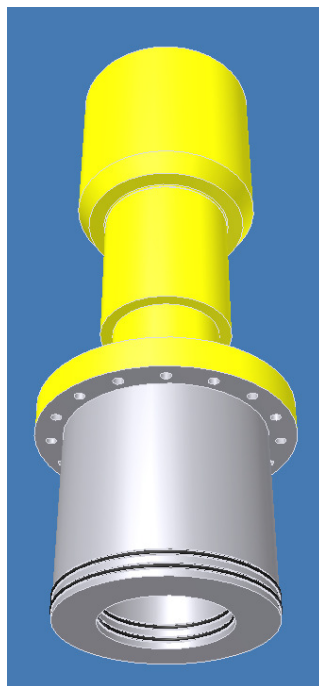


Figure 13: The piston geometry of the top connector. Seals are placed on the inside and outside of the lower part of the piston geometry.

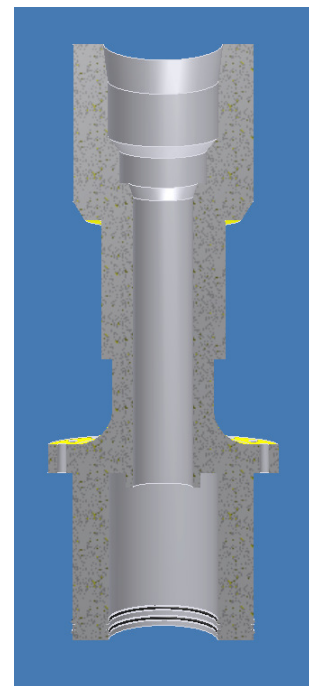


Figure 14: Half section view of the piston geometry.



The top tension from the surface vessel will only facilitate the wanted effects and is neglected.

To calculate the wanted separation force one has to assume a separation pressure delivered from the pressure batteries. At first the pressure was set to 400 bar. Because this kind of pressure is easily delivered from standard pressurized cylinders. More investigation showed that to give the right separation force it was necessary to use batteries which delivered 500 bar pressure. This is because the pressure loss from increasing volume in the trigger system on initiation did not make the system reliable enough. Still, the separation force that would act on the cross section was assumed to be 400 bar, losing around 100 bar in the system. The area of the piston cross section was calculated and dimensions was set to give a satisfying separation force:

$$\text{Preliminary dimensioned area: } A_{piston} = \left(\frac{\pi * 510^2}{4} - \frac{\pi * 310^2}{4} \right) = 128805 \text{ mm}^2$$

$$\text{Separation force: } F_{sep.} = A_{piston} * (40 \text{ MPa} - 6.06 \text{ MPa}) = 4371642 \text{ N}$$

This gives approximately 445 Mg separation force, which is satisfying when compared to the requirement set to 400 Mg.

Four seals, both on the inside and outside of the piston geometry, is shown in figure 13. Two seals are placed on each side to ensure a pressure tight seal. The piston would need a seal that will contain the separation pressure, allowing the force to be transferred to the bolts. The process of selecting the perfect seal is always preferred done in collaboration with sealing professionals, but as an example on what kind of seal that could be reviewed a G-T RINGS 13,000 and 14,000 series seal is presented in figures 15,16 and 17.



Figure 16: G-T RING, 13000 Non-radiused and 14000 radiused seal series.

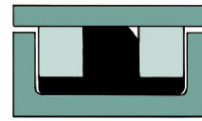


Figure 15: When forces are acting on the seal from pressure, the seal becomes tighter.

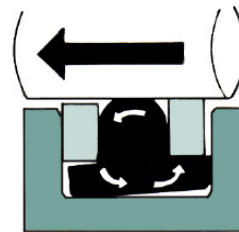


Figure 17: As the piston is moving out from the annular cylinder, the friction causes torque to the seal cross section. This causes the sealing to seal even more.

This seal is a robust seal designed for large hydraulic actuators. As shown, the seal is minimal loaded when not in use. As the separation pressure flow through the system and pressurises the SL the seals get tighter. As the SL separates the friction forces acting on the seals will tighten the seal even more. The seals are rated for 10 ksi or 690 bar and can be designed to cope with higher pressures. Further study of the data on this seal shows that other specifications seem to be appropriate for the SL such as environmental, robustness and temperature specifications. A complete datasheet for the G-T seal is presented in appendix B. In the datasheet, the appropriate size and dimensions for the SL application is not covered. Green Tweed, the manufacturer, states on their web page that sizes could be adjusted on request.(12) An invite to this discussion should be made to the manufacturer if the supplier is considered usable by AKSO.

A complete drawing of the top connector is presented in appendix A.



4.4.2 BOTTOM CONNECTOR- CYLINDER

Like the top connector, the design of the interface to adjacent riser components is fixed. Basically the design is a copy of a standard riser joint up until the flange-cylinder housing. The bottom connector is shown in figures 18,19 and 20.



Figure 18: The bottom connector.

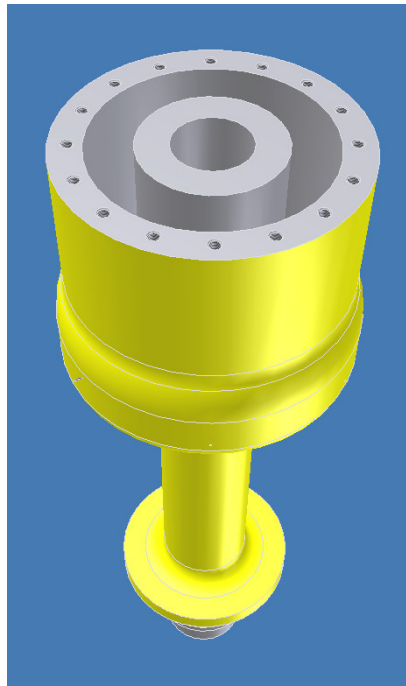


Figure 19: The cylinder geometry of the bottom connector.

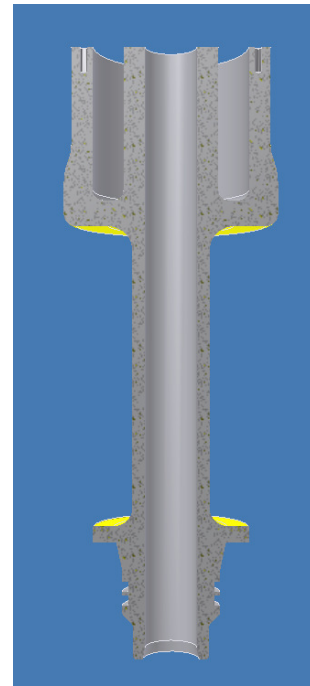


Figure 20: Half section view of the bottom connector.

The transition from standard riser pipe to the cylinder housing has been rounded off to prevent stress concentrations. Also, the transitions between horizontal and vertical sides of the pressurized compartment have been rounded off. When the SL is initiated the bottom of the cylinder annulus is loaded heavily. This is why the walls are reinforced. It is of importance that the deformation in this area does not inflict the sealing properties of the seals. This area is also the widest part of the complete assembly. As the drawing shows in appendix A, the largest diameter is 700 mm, which is well inside the limitation of 1200 mm. As the SL separates the loading from the separation pressure will decline, making less need for reinforcement of the walls. The wall thickness surrounding the cylinder annulus is generally thicker than the riser pipe, making the SL assembly in this region stiffer than the riser pipe. This is to prohibit wedging effects when initiated and allow bending



moments to be transferred through the geometry and into the riser beneath. This could show to be important in the parameter analysis because it is expected a fatal moment-to-surface relationship in the very last stages of the SL separation. A complete drawing of the bottom connector is presented in appendix A.

4.4.3 TRIGGER SYSTEM

In chapter 3.2, the block diagram and outline of the trigger system was presented. This has been the basic drawing of how the system should look like and function. To pick out all the components from manufacturers has been considered unnecessary time consuming. All the components in the inventor model are therefore made from basic calculations and assumptions to get a visual presentation of the complete model. For orientation, a system drawing is presented in appendix A.

4.4.3.1 Pressure battery

The first stage of this work was to calculate the volume of pressurized gas needed to make the SL perform as designed. A pressure bottle was generated in Autodesk Inventor with so called smart dimensioning sketch geometries. This was done to make the adjustment of the bottle volume easier. The design of the pressure bottle is shown in figures 21 and 22.



Figure 21: The pressurized gas container.

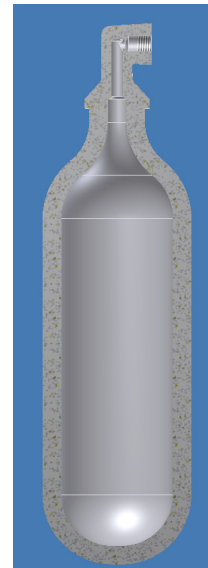


Figure 22: Half section view of the pressurized gas container.



These bottles should be selected in collaboration with a supplier. A brief search on the web showed multiple manufacturers which could deliver the bottles in many premanufactured and custom sizes.

As the outline of the trigger system shows, two separate systems are designed two gain redundancy. A number of six bottles were selected with three bottles coupled to each system as containers for the pressurized CO₂. The decision of using six bottles is rooted in an idea of making one of the two systems redundant in a way that enables the control system to leave one bottle out of the system in case of leakage. Exactly how the control system will control the bottles is not discussed in this thesis. This is considered to be discussed with a manufacturer of the multi directional, electronically actuated valve system and the control systems. The volume of three bottles is calculated to be:

Volume:

$$V_{bottles} = \left(\left(\frac{\pi * 0.12^2}{4} \right) * 0.3 + \frac{4}{3} \pi * 0.06^3 \right) * 3 = 0.01289 m^3$$

The temperature of the pressurized gas is considered to be as the ambient temperature. Since the bottles are completely surrounded by seawater, the temperature of the gas will be approximately 4 degrees Celsius and is considered to change to a slightly lower temperature when the SL is initiated.

In an attempt to predict the pressure which gives the separation force, the system volume that the gas has to fill has been calculated. From the Autodesk Inventor model, all length values of the hoses and connectors for one system are given to be 1.872 meters. The volume of the valve is set to one meter of flexible hose. The inner diameter of the hoses and connectors is ½ inch or 12.7mm.

System volume:

$$V_{system} = WL + \text{Hoses and connectors} + \text{Control Valve}$$
$$V_{system} = \left(\left(\frac{\pi * 0.45^2}{4} - \frac{\pi * 0.37^2}{4} \right) * 0.03 + \frac{4}{3} \pi * 0.03^3 \right) + \left(\frac{\pi * 0.0127^2}{4} \right) * (1.872 + 1)$$
$$V_{system} = 0.00166 + 0.00024 + 0.00013 = 0.00203 m^3$$



Setting the pressure battery to 500 bar one can calculate the separation pressure after the trigger system is initiated and before the SL has started to separate with the ideal gas law. In this calculation the small change in gas temperature is neglected.

Separation pressure:

$$\frac{P_1 * V_1}{T_1} = \frac{P_2 * V_2}{T_2}$$
$$P_2 = \frac{P_{battery} * V_{bottles}}{V_{system} + V_{bottles}} = \frac{50 * 10^6 * 0.01289}{0.01289 + 0.00203} = 43.197051 MPa \approx 432 bar$$

As the pressure increases the loading on the bolts increase until the bolts fail and the SL separates. The criterion for the separation pressure was set to 400 bars. This calculation shows that this criterion is fulfilled with a margin of 32 bars. During the flooding of the system one will certainly experience more pressure loss then calculated here. To cope with this, the margin of 32 bars will probably be enough to compensate unforeseen pressure loss. If tests show that the pressure gets too low, the immediate solution will be to increase the battery volume. This will decrease the pressure loss in the system due to the filling of the system volume.

As the SL separates from the triggered separation pressure, it is important to check that the increased volume the gas has to fill does not become too big. If the inside pressure becomes smaller then the hydrostatic pressure, the pressure will make the SL function as a suction cup. This means that the suction cup effect of the SL could stop the SL from separating completely and inflict damage to the well components as the surface vessel drifts off. To ensure that this unwanted effect does not occur, the pressure change as the SL separates has been calculated and illustrated in a graph using MatLab calculation software. The effect is shown in figure 23. The applied MatLab code is given in appendix C.

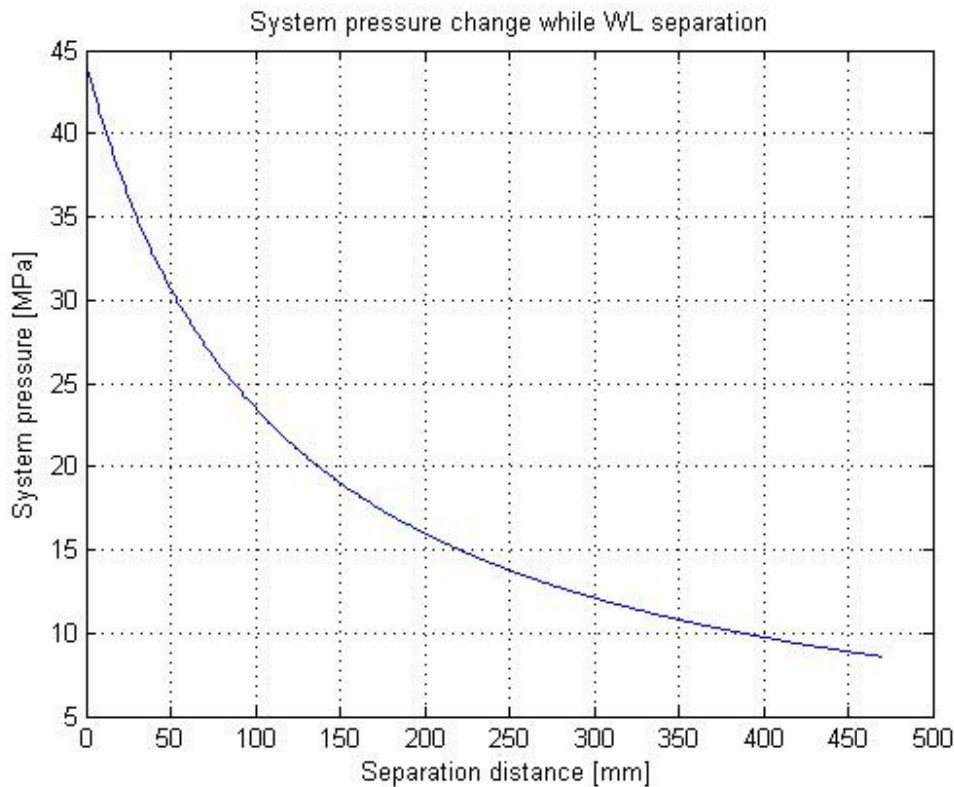


Figure 23: System pressure is decreasing as the SL separates.

As shown in figure 23, just before the separation of the SL is complete, the system pressure will be approximately 8.59 MPa. At this stage, disregarding the top tension from the surface vessel, the hydrostatic pressure will try to hold the SL together, acting as a counter force to the separation pressure. As shown in figure 24, the surface area that the separation pressure and the hydrostatic pressure act on in axial direction is approximately the same. Since the hydrostatic pressure is set to 6.06 MPa (maximum depth set to 600m water depth), the SL will be forced to separate within some margin.

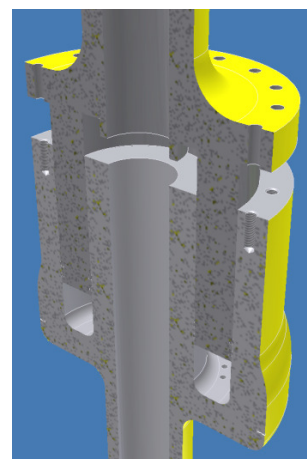


Figure 24: The separation pressure is acting on nearly the same surface area as the hydrostatic pressure when separation is initiated.

The separation speed of the SL is a function of the gas flowing speed, the hindrances of the pneumatic flow path, hose and valve diameter, friction of seals and total force applied to the



separation. Since all these parameters and their influence on each other are difficult to predict, the separation speed should be measured in scale testing. But it is expected that the build-up of pressure required to break the bolts could take some time. As the differential pressure between the pressure battery and the whole system gets smaller, the pressure build-up speed will decrease. When the bolts are broken off, the separation should be finished in seconds. To ensure the required pressurizing speed, the hoses, connectors and valve geometry could be adapted and optimized.

A complete drawing of the pressure bottle is presented in appendix A.

4.4.3.2 Bottle rack, pressure battery and control valve

As stated in the design criteria, welds are to be avoided. Because of this, all necessary components have been designed to clamp on the main SL structure. The first component which was made was the bottle rack. This rack is designed to hold in place the pressurized cylinders and the main control valve. An example of how this could look like is presented in figure 25.

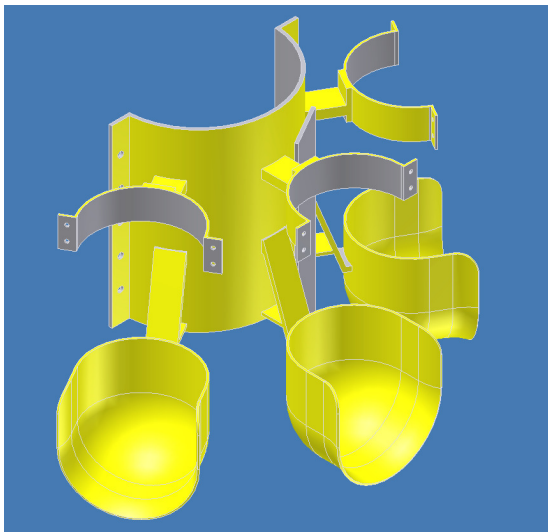


Figure 25: The bottle rack, holding the pressure battery. The rack is designed to allow easy handling of the bottles



Figure 26: The multi directional electronically actuated valve, also called the control valve, mounted on the bottle rack along with hoses, bottles and connectors.

While in operation, the SL maintenance procedures could demand that the bottles need to be changed periodically. This design is shaped to allow easy handling of the bottles. The back plate is dimensioned to fit around the bottom connector, clamping the equipment to the SL. An identical

rack is set adjacent, holding the backup bottles and valves. In figure 26, the multi directional control valve is shown mounted on the bottle rack along with bottles, hoses and connectors. Through the multi directional valve, all bottles are connected to the SL. The calculations done in chapter 4.4.3.1 shows that one stand-alone system is capable of separating the SL on its own. Thus, each system contains the necessary power to initiate the SL and disconnect the riser. By designing the system in such modules, also more efficient maintenance procedures are expected.

To better understand how the system is meant to function, a sketch of the multi directional, control valve design is presented in figure 27. Of course, the valve sketch seems highly simple, but the sketch indicates the main valve functions of the multi directional valve. All valves and gauges are electrically controlled from a micro controller that also communicates with the operator.

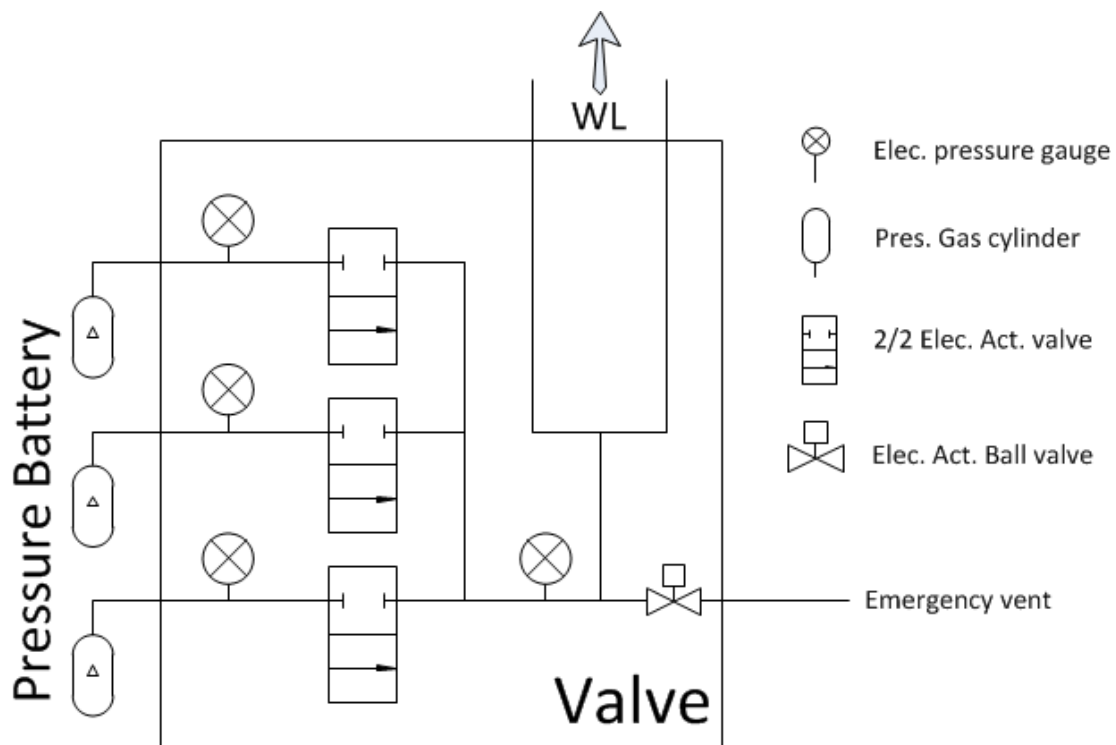


Figure 27: Schematic presentation of the multi directional electronically actuated control valve.

It has been chosen three 2/2 electrical actuated valves, one for each bottle. This could increase the possibility of error in the system, and should be assessed further. By designing the system like this,



one can isolate a faulty bottle in the pressure battery if necessary. Electrical pressure gauges are set to monitor the initial pressure of the battery for each bottle, and also the pressure of the system at all times. This is important to monitor because a leak can be detected at an early stage, preventing unwanted separation. If the pressure should become too high in the system for any reason, the emergency ventilation valve is set to automatically ventilate the pressure to sea. This valve is also operable by the operator.

4.4.3.3 Control rack

Directly underneath the bottle rack is the control rack located. The control rack houses the power supply, the positioning system and the system controller. In the Autodesk Inventor model, the dimensions are approximate. It is possible that the dimensions needed for the systems are too small or too big. But the model indicates a preliminary study design. Further study and selection of components will reveal what kind of changes that would have to be made to the control rack. The control rack housing is intended to be flooded or pressure balanced. The control rack and housing is presented in figure 28, and an explosion view of the contents is presented in figure 29.

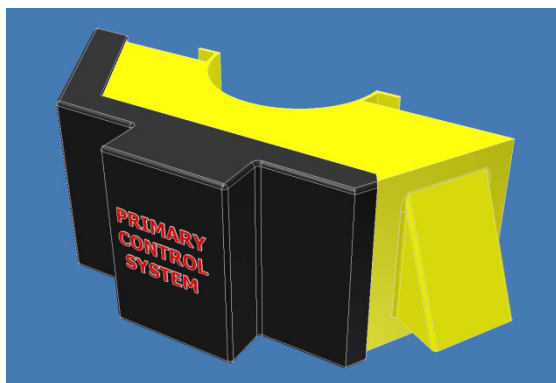


Figure 28: The control rack housing with cover. The opening on the right allows the transducer to signal the transponder on the well stack for position monitoring.

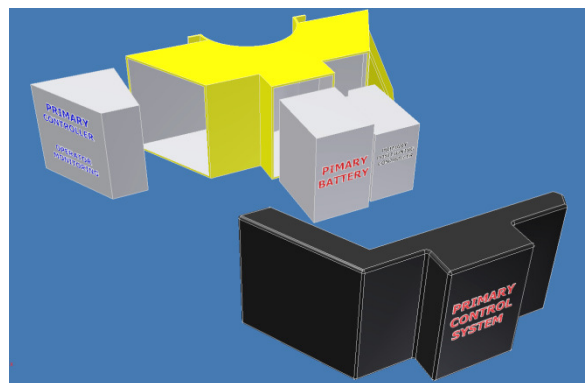


Figure 29: Control rack housing, exploded view. From the right; Primary Controller and Operator Monitoring systems, primary battery and positioning system.

On adjacent side of the SL, a secondary control system is placed. This system controls the secondary trigger system and pressure battery.



4.4.4 BOLTS

The SL bolts have a complicated load scenario. Their main purpose is to completely fail under a given load. But they should also cope with the operation loads, fatigue loading if present and ensure a tight seal at all times. After evaluating all parameters which dimension the bolts and also their behavior, a special design was chosen. In a regular bolt design, the weakest part of the bolt when loaded in tension is at the thread root.⁽¹³⁾ The threading gives the bolt weak properties because of the sudden change in geometry and also represents a notch where a crack can easily be developed.⁽¹⁴⁾ Since the break load is of such importance, the need of precision is great. Ideally the bolt has to perform as designed and has to be possible to test multiple times with high grade of repeatability. To ensure this effect the decision was made to use over-dimensioned bolts which could be able to cope with all load scenarios. This will make the threads and bolt head over-sized so that any unwanted non-repetitive results are prohibited. To ensure the bolt to fail, the bolt diameter is changed slightly midway up the bolt shaft between the threads and the bolt head. By high precision material technology the bolt will be designed to fail at a given tension load within a small margin.

4.4.4.1 Bolt material

Since the SL has a very special set of design criteria and functions, a normal set of bolt data has not been found suitable to the bolt design. Therefore, it was decided to produce a specially designed bolt from scratch. The first step in designing the bolts was to decide on a material to use. The program which was used for this was CES EDUPACK. When the SL bolts are loaded at break load, it is considered important to make the bolts fail suddenly, almost in a brittle manner. If the bolt behaves too much ductile when loaded at break load or close to break load, other effects could occur like partial separation or the SL may fail to function as intended. Regular riser bolt steel, AISI 4340, was the first material which was assessed. The problem with this material was the ductility. As a measurement of the ductile behavior CES EDUPACK state the elongation as a percentage of the total length of the test specimen as the test specimen reaches plastic deformation. For brittle materials this percentage is given to be under two percent. For AISI 4340 this value is set to be 9-15%, giving an elongation behavior which could be threatening for the SL functions. Also, as the elongation percentage generally gets high in the material data, the distance in stress level from yield strength to tensile strength gets high. This allows the bolt to plastically deform a long way before failing which is not the desired property for the SL bolts. In further study the criterion of selecting a material with elongation percentage close to 2% was prioritized. With this in



mind along with the environmental criterions a list of suggestions to materials was generated from the program.

From this list several titanium alloys were suggested. The first selected material to be studied was an alloy called **Ti-20%TiC**. This is a Titanium alloy with 20% Titanium Carbide. The elongation percentage for this alloy was 0.3-0.31%, which is a great improvement from regular riser bolts. Yield strength is set to $991\pm 48\text{MPa}$ and mean tensile stress is set to $1004\pm 45\text{MPa}$. This gives definitely an improved brittle behavior and looks suitable for the task at hand. The titanium alloy possesses excellent properties with respect to the environment affecting the bolts. When assessing potential corrosion problems, the difference in electrochemical potential between AISI 8630 (SL material) and Ti-20%TiC makes the SL and most likely the whole riser the anode. The SL has a much larger surface than the bolts, but if the SL is surface protected with paint, small pits and openings in the paint could lead to potentially dangerous unwanted local corrosion. This normally occurs in the area where the bolts are in contact with the SL material. So if Ti-20%TiC is to be used as bolt material in this design, treating the SL surfaces with paint is not recommended. A bare metal surfaced SL will lead to general and not local corrosion, which is much safer. Still, having the SL material AISI 8630 in open salt water will eat the sacrificial anodes fast and is not a very tempting way to design a critical component.(15)

Further study of many materials using CES EDUPACK was done. Since Titanium adds galvanic corrosion to the equation, it was prioritized to try to find a material which was more similar to the SL material. This implies the use of steel, because the galvanic corrosion problem would be minimized. After two days of searching and investigation, the search for a material that will fulfill all demands was terminated. Either the criterions have been too strict or the parameters need to be altered in order to get useful results. When deciding on which material parameter to change, the thesis suddenly started to look like a master's degree from another department. Therefore it was considered wise to list the search parameters set to the material selection process in table 2, and instead of selecting a specific bolt material; values that are presentable for an imaginary bolt material were selected. The data used for the imaginary bolt material "*Im01*" is given in table 3.

The data sheets for material AISI 4340, Ti-20%TiC and AISI 8630 is given in appendix D.



Table 2: Selected search parameter used in material selection.

<i>Bolt material criterion</i>	<i>Value</i>
Steel	Fe- main alloy component
Carbon	More than 0.29%, brittle steels
Yield strength	More than 900 Mpa
Tensile strength	No limits
Difference between yield and tensile strength	As small as possible, brittle failure
Elongation	Less than 2%, from zero loading to break load.
Toxicity	Non-toxic
Operational temperature rating	-50 to +150 degrees Celsius
Flammability	Non flammable
Durability: Fresh water	Limited use is acceptable
Durability: Saltwater	Limited use is acceptable



Table 3: The imaginary bolt material data.

<i>Im01, Bolt material data</i>	<i>Value</i>
Yield strength	900±50 MPa
Tensile strength	1000±50 MPa
Yield difference from tensile strength	Is set to 10%
Elongation	0.5 to 1 %
Operational temperature rating	-50 to +150 degrees Celsius
Flammability	Non flammable
Durability: Fresh water	Acceptable
Durability: Saltwater	Limited use
Toxicity	Non-toxic

4.4.4.2 Standard Summary: ISO 13628-7:2005

The standardization for WL design is limited to one page in ISO 13628-7:2005. In this section, the most relevant parts are presented.

- *“The yield and ultimate tensile strength values applicable for weak-link assessment shall be the maximum specified values. The maximum strength values to be used shall be the mean strength plus two standard deviations or equivalent.”*

The data for Im01 material is given as the maximum and minimum values of the empirical test data. It has been considered conservative to choose the highest value of the yield and tensile strength.



- *“A safety margin of 10% in the weak-link assessment may be applied.”*

Since this is not a demand, it has been considered unnecessary to introduce additional safety margins in this project.

- *“All riser system components shall be capable to safely resist the same loads as generated in the pipe(s) of the riser string when subjected to accidental loads, except safety joints designed into the riser system to fail under specified loads.”*

The SL will be designed to cope with the normal operational and accidental loads. If the SL detects that the riser string applies high moment loading on the well stack, it will separate. If the axial tension in the SL exceeds the specified value from AKSO of 300 Mg, it will separate.

For further reference, the complete standard section regarding SL design is presented in appendix E. (16)

4.4.4.3 Bolt dimensions

To ensure the flange connection to be leak tight under normal operation, the bolts need to be pretensioned. The load data is provided by AKSO and is presented in table 4.

Table 4: Load data provided from AKSO.

<i>Load type</i>	<i>Magnitude</i>
Operation maximum pull (While installation)	35Mg (WCP)+25Mg (EDP)+4.25Mg (SJ)+3*3.266Mg (RJ) Static = 75Mg ±10% due to heave motion while installation
Constant operational pull	20-30 Mg ≈ 25 Mg
Operational cycle load	10-20 Mg ≈ 15 Mg



Max pull, break load	300 Mg
Torsion load in SL	0, Swivel joint will compensate
Lateral load on connection	0, Bolts does not block this DOF. Geometry does.

As the load data shows, there are two types of loading scenarios. The first and critical scenario is while the SL is used to run the WCP and EDP to connect the surface vessel to the well. In this case, the two modules are hanging from the SL and exert a static load. Because of the small phase difference in heave compensating systems and the actual movement of the surface vessel, it is normal to experience some cyclic axial acceleration and movement in the riser which will give cyclic loading on the SL bolts.(17) The exact cyclic load is hard to measure, but from AKSO the maximum has been defined as approximately 10% of static load where 100% of this should be dimensioned to tension. The other scenario is while the SL is in normal operation. In this scenario the SL experience significantly less loading.

When a connection like the flange connection is bolted together, and the bolts are pretensioned, the connection will act as a unit. This means that the applied external loading will not only be supported by the bolts but also the joint itself. By studying a bolt-joint diagram one can dimension the pretension of the bolts so that the bolt will ensure a tight fit regardless of the loading. The bolt-joint diagram is shown in figure 30. The figure shows how the joint acts as a unit, dividing the external load mostly into the joint but also a fraction is directed into the bolt. In the figure, green line shows the bolt elongation as a function of tension in the bolt. Red line shows the deformation of the joint material as a function of the compression from the joining force. The black line shows the increasing bolt load as a result of the applied external load. Blue line shows the external loading and how it affects the joint. As the external load forces the joint to separate, the blue line reaches the point where there is now joining force in the joint. Beyond this point the joint will leak, and in this case, the SL could be set off from sensor signal or be damaged. All applied bolt data is taken from standard NS 5720.

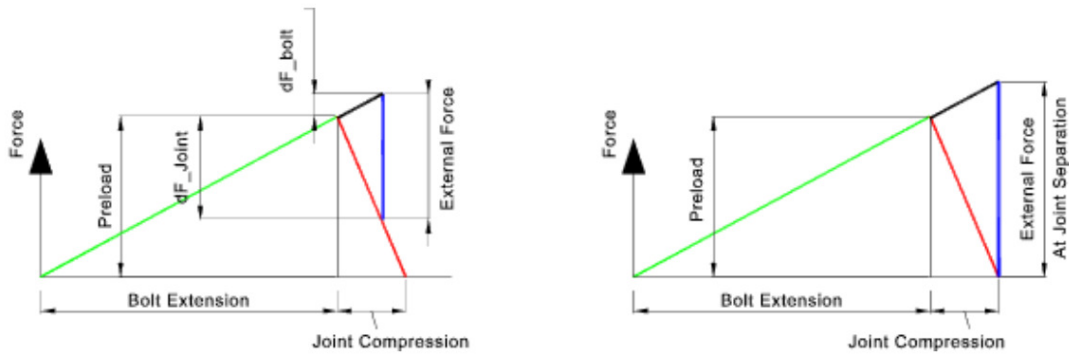


Figure 30: The bolt-joint diagram. The diagram shows how the joint acts as a unit where the forces are transferred mostly into the joint and a fraction is transferred to the bolts.(18)

The relation between the deformation of the bolt (δ_1) and the compression of the flange (δ_2)

should be for thick flanges: No sealing, thick flanges: $\frac{\delta_1}{\delta_2} = 4 - 10 \Rightarrow \frac{\delta_1}{\delta_2} = 6$

To ensure that the sealing remains tight, a squeeze safety factor for the flange is defined.

$$\text{Squeeze safety factor: } n_k = \frac{F_i}{F_i - F_k} = 1,5 - 2 \Rightarrow n_k = 2$$

The pretension is defined by utilizing the shape similarities of triangles shown in figure 30. A more detailed picture is presented in figure 31.

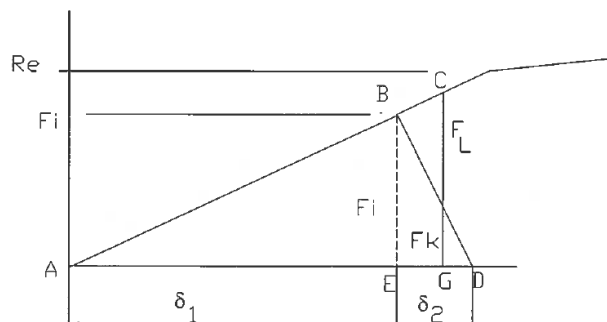


Figure 31: The shape similarities of the triangles made in the bolt-joint diagram.



From figure 31 we get:

$$1. \Delta ACG \approx \Delta ABE$$

$$2. \Delta DEB \approx \Delta DGH$$

From similarity number one:

$$i) \quad \frac{F_l + F_k}{F_i} = \frac{\delta_1 + (\delta_2 - x)}{\delta_1}$$

From similarity number two:

$$ii) \quad \frac{F_i}{F_k} = \frac{\delta_2}{x}$$

$$iii) \quad \delta_1 = 6\delta_2$$

$$n_k = \frac{F_i}{F_i - F_k} = 2 \quad \Rightarrow \quad F_i = 2 * (F_i - F_k)$$

$$iv) \quad F_k = \frac{1}{2} F_i$$

From equation i) and iii):

$$\frac{F_l + F_k}{F_i} = \frac{6 * \delta_2 + \delta_2 - x}{6 * \delta_2} = \frac{7 * \delta_2 - x}{6 * \delta_2} = \frac{7}{6} - \frac{x}{6 * \delta_2}$$

From equation i), ii) and iv):

$$\frac{F_l + \frac{1}{2} F_i}{F_i} = \frac{7}{6} - \frac{1}{6} * \frac{F_k}{F_i} = \frac{7}{6} - \frac{1}{6} * \frac{F_i}{F_i} = \frac{7}{6} - \frac{1}{6} = \frac{6}{6} = 1$$

Thus:

$$F_l = \frac{13}{12} F_i - \frac{1}{2} F_i = \frac{7}{12} F_i \quad \Rightarrow \quad F_i = \frac{12}{7} F_l$$



F_l , is the maximum work load on each bolt which requires no leakage:

$$F_l = \frac{(W_{WCP,EDP,SJ,RJ} + W_{10\%}) * 10^3 * g}{n_{bolts}} = \frac{(75 + (75 * 0.1)) * 10^3 * 9.81}{16} = 50583N$$

This sets the minimum pretension for each bolt:

$$F_i = \frac{12}{7} * 50583N = \underline{\underline{86.714kN}}$$

By pre-tensioning the bolts the equivalent stress in the bolts would be affected by the torsion stress from the make-up torque applied to the bolt when assembled. The make-up torque is calculated by:

$$M_v = F * r_m * \tan(\varepsilon_1 + \varphi) = 86714N * 0.013 * \tan(13.00391 + 1.40263)$$

$$M_v = \underline{\underline{300.547 Nm}}$$

where

$$\varepsilon_1 = \tan^{-1}\left(\frac{\mu}{\cos(\alpha)}\right) = \tan^{-1}\left(\frac{0.2}{\cos(30^\circ)}\right) = 13.00391$$

$$\varphi = \tan^{-1}\left(\frac{P}{\pi * d_2}\right) = \tan^{-1}\left(\frac{2}{\pi * \frac{27 + 25}{2}}\right) = 1.40263$$

M_v = Torsion moment

F = The pretensioned force

r_m = The middle radius

ε_1 = The friction angle : $\tan \varepsilon_1 = \frac{\mu}{\cos \alpha}$

φ = The thread rate of climb : $\tan \varphi = \frac{P}{\pi * d_2}$

μ = Friction coefficient in thread

2α = The thread profile angle

P = The climb per thread

d_2 = The threads middle diameter

The thread surface is assumed to be lubricated. To represent this, a friction coefficient for the threads is set to 0.2. The climb per thread was set to 2, as for a standard large M-type bolt.



When the make-up torque is applied, the contact between the bolt head and the top connector surface creates friction resistance. By applying a washer one could better control this friction force and also its ability to hold the bolt in place. The washer is assumed not to be lubricated, and is given a friction coefficient of 0.35. The total make-up torque on each bolt yields:

$$M_s = \mu' * F * r'_m = \mu' * F * \frac{s + d_h}{4} = 0.35 * 86714 * \frac{0.041 + 0.028}{4} = 448.745 Nm$$

$$M_{tot} = M_s + M_v = \underline{\underline{749.292 Nm}}$$

Where :

μ' = Friction coefficient bolt head

F = The pretension force

r'_m = Middle radius

s = Bolt head representative diameter

d_h = Diameter of the hole

This is what the assembler needs to apply of make-up torque to the bolt with the wrench. But, for further analysis the torque needed to overcome the threads resistance is the most interesting. Now, calculating the cross section diameter needed at adjusted diameter to be able to withstand the loading and also breaking at tension load limit:

Equivalent stress in the bolt is given by:

$$\sigma_{eq} = \sqrt{\sigma_d^2 + 3\tau_v^2}$$

By solving this equation with respect to the diameter needed to hold the load at exactly 300 Mg tension in the SL, an adjusted diameter dimension is set.



$$\sigma_{eq} = \sqrt{\sigma_d^2 + 3\tau_v^2} = \sqrt{\left(\frac{F_{break}}{A_{adj.}}\right)^2 + 3\left(\frac{M_v}{W_v}\right)^2} = \sqrt{\left(\frac{F_{break}}{\pi * d_{adj.}^2}\right)^2 + 3\left(\frac{M_v}{\pi * d_{adj.}^3}\right)^2}$$

$$\sigma_{eq}^2 = \frac{F_{break}^2 * 16}{\pi^2 * d_{adj.}^4} + \frac{3 * M_v^2 * 256}{\pi^2 * d_{adj.}^6}$$

Solving for the adjusted diameter needed:

$$d_{adj.}^2 * (d_{adj.}^4 * \sigma_{eq}^2 * \pi^2 - 16 * F_{break}^2) = 768 * M_v$$

Which gives:

$$d_{adj.} = \underline{\underline{15.31mm / -15.31mm}}$$

where:

$$M_v = 300.547 \text{ Nm}$$

$$\sigma_{eq} = 1000 \text{ MPa (Im01 material)}$$

$$F_{break} = \frac{F_{break}}{n_{bolts}} = \frac{300000 \text{ Kg} * 9.81}{16} = 183938 \text{ N}$$

With the pre-tension of 86.7 kN in each bolt, the total squeeze force in the SL connection is:

$$F_s = F_i * n = 86714 * 16 = 1387.4 \text{ kN} \Rightarrow 141.4 \text{ Mg}$$

This squeezes the SL connection together, securing a tight seal at all times with a squeeze safety factor of 2.

When using this dimensioning technique, the bolts should **not** break from fatigue failure because the cyclic loading affecting the bolts will be minimal if not zero. Still, if a fatigue failure should happen the SL should disconnect the riser and shut down operations. If the well's safety and SL systems function as intended, the greatest concern is economically related. This is naturally unacceptable and cannot happen. Further study should be made with respect to the selected material for the bolts. Since the bolt is over-dimensioned at bolt head and threads, and the failure will be at the adjusted diameter area on the shaft, the adjusted area should be specially treated. By polishing this area and thoroughly checking it, cracks which may accelerate a fatigue failure will be as small as possible. This will increase the fatigue life expectancy making the bolt more capable of handling any cyclic loading which may occur.



This diameter has been used as an estimate on what to start with when entering the Abaqus analysis model. It is expected some stress concentrations in the bolt geometry due to the sudden change in diameter. To limit this effect, the changes need to be as smooth as possible. The effect is discussed in more detail in the Finite Element Analysis (FEA) chapter.

4.4.4.4 Bolt design

The calculated dimensions have been used to model the bolt. As mentioned before, the bolt gets an adjusted diameter section half way up the bolt shaft. This is where a controlled failure will be achieved. In this thesis, the bolt is modeled as a M27 bolt, regardless of how it will perform under the assumed loading. This is because the bolt is thought to be over-dimensioned to cope with the loading in a most secure way. The adjusted cross-section gets a diameter of 15.31 mm, as calculated. It is important to state that the bolt is intended to fail in the adjusted cross section, not in other places.

How the bolt performs is described in the FEA section of this thesis, but to cope with the stress concentrations, the sharp changes in geometry has been rounded off to make the transition from a thick to a slender bolt shaft as soft as possible. This is of course parameters which could be studied in a separate thesis, but it indicates the designs purpose. The bolt design is presented in figure 32. It could show to be important that the bolt is surface treated as polished or similar in the adjusted area. This is to enforce the bolt with respect to fatigue. Surface cracks are impossible to completely avoid, but a strict control should be done to ensure that any critical surface cracks are removed.

It has been inspiring for the candidate and also considered interesting to mention to the reader that this bolt design was designed with no help from the supervisors at NTNU or AKSO. A discussion with the supervisor at AKSO at a later stage in the project revealed that today's weak-links, designed to cope with excessive tension, have the same bolt design.



Figure 32: The Bolt design for the SL.



4.4.5 THE ASSEMBLY OF THE SL

The SL is meant to be installed into the riser string as a riser joint on site. The assembly of the top and bottom connector should be done on shore, securing clean environment and proper tools. The trigger system should be mounted on the SL on site, installing the pressure battery as a last event. Then the SL systems should be tested to ensure right values on control parameters. To protect the trigger system and its vital components from falling debris, a protection grating is installed. The final design of the SL installed in the C/WO riser is presented in figures 33 and 34. Also, drawings which show the final design in more detail are presented in appendix A.



Figure 33: The final design of the SL

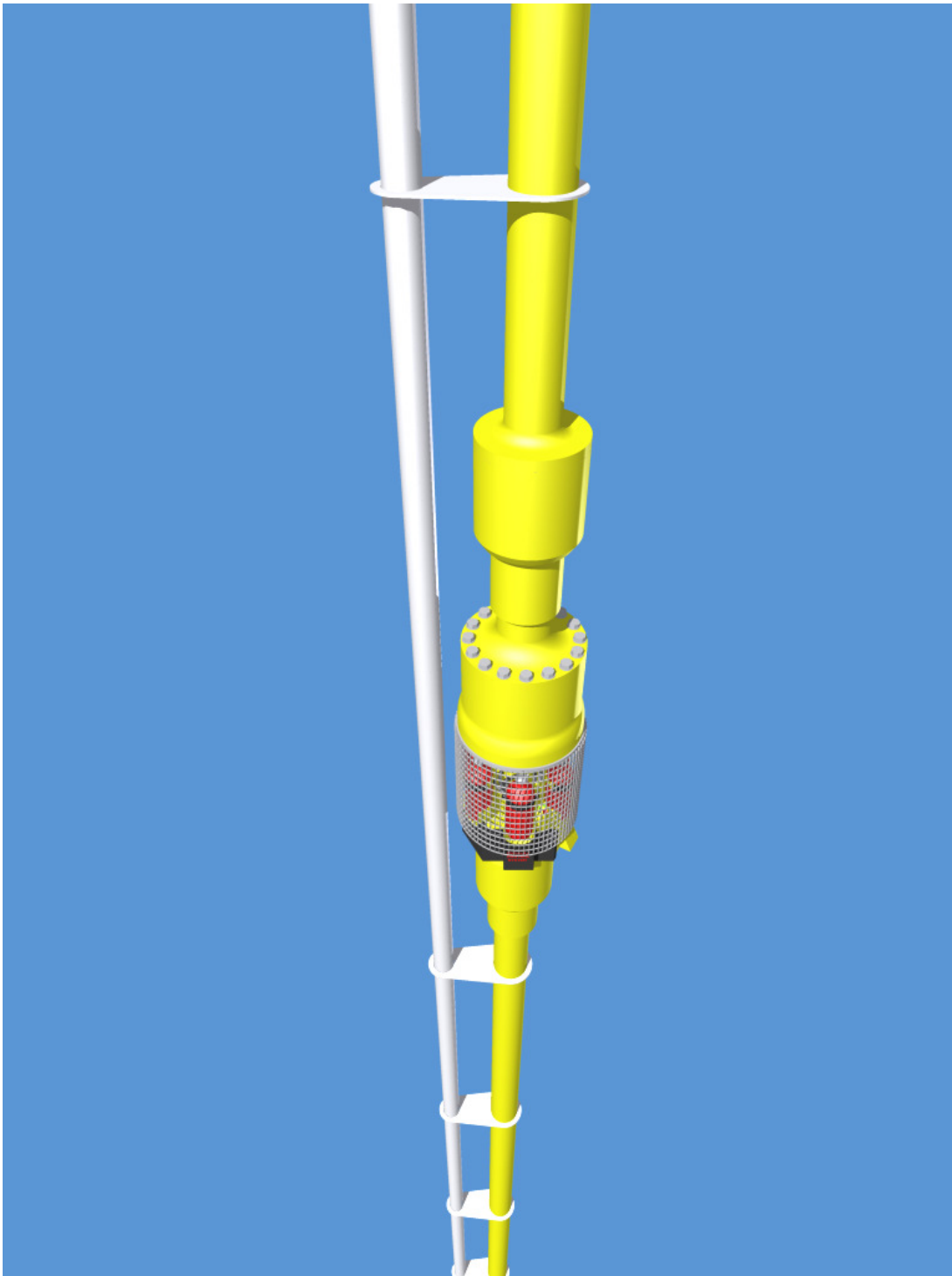


Figure 34: Final design of the SL installed in the C/WO riser string.



5.0 FINITE ELEMENT ANALYSIS

In this chapter, the FEA of the SL structure is presented. The analysis was first planned to be done as a total analysis of the assembled SL, then a more detailed analysis of the parts were to be done. The only problem was that during the FEA work, some difficulties arose when analyzing the whole model. Due to large geometry differences from bolts to the connectors, Abaqus experienced discontinuities, elements with zero volume and failed to converge in calculations. One could spend a lot of time adjusting meshes and searching for errors, so the matter was discussed with the supervisor. The result of the discussion was that it was considered sufficient to study the model parts instead. Loading them with the given loads from AKSO, setting functional boundary conditions, which represent the scenario from the global data as detailed as possible.

The whole SL has been first of all modeled in Autodesk Inventor. This is to easier have control of the dimensions and functions of the SL when designing. As mentioned earlier, the most convenient procedure should have been to export the Inventor model to a *.SAT file, and then import it in Abaqus. The problem with the export/import procedure is that when imported in Abaqus, the model is a solid, with no sketches and other geometry details. So to save time and ease the work load, the model was modeled fully in Abaqus, using the Inventor model as a template. This allows the Abaqus model to get trimmed much faster and eases the work load in the long run, especially when optimizing dimensions. Because the model is not stress analyzed at all in Inventor, the need of trimming the dimensions as the analysis progressed was a matter of course. This could also slightly affect the figure presentations in this report because a lot of small dimensional changes have been done to the Abaqus model as the analysis progressed.

5.1 LOADING SCENARIO

The SL is subjected to various forces, and most of them are dynamic. Mainly this is because almost all the loads on the riser string are generated from the ocean movement. The surface vessel, which is constantly moving in waves and wind, is exerting various pull loads and moment loads to the riser string. In between the surface and the bottom, also called the pelagic zone, various changing loads from current and temperature is acting on the riser string. This calls for an analysis where one has to try to resemble the reality as best as can be in a global analysis, and then go locally with the results afterwards. Of course, this would have made the workload of this project all too big. The loading data given from AKSO is therefore treated as a static loading scenario, checking the SL in



the ranges of maximum operational loading. To cope with the dynamical loading, the SL has been given geometry which should be the same or better as the regular AKSO riser joints. The riser joints have been thoroughly checked by AKSO and are in service today. The SL is also planned produced without welds, making the SL more fatigue resistant according to necessary calculations and safety margins.

On the inside of the SL, various loads caused by the well flow gives other challenges. Well pressure will be varying and also the temperature of the well will vary. With the pressure varying, the SL will also have varying deformations causing the SL diameters to change. Also, the temperature variation inside the SL will cause varying thermal expansion and compression of the SL. Basically, both these effects could cause the SL to become a shrink fitted connection, and if not accounted for, make the SL fail to function properly in an emergency situation. Proper tolerances should be able to cope with all these effects. This dimensioning of tolerances is not dealt with in this project but should be done in further work.

For reasons of better presenting the SL loading and boundary conditions, it has been considered informative to show the global boundary conditions and loading scenarios affecting the SL assembly. As described in chapter 4.2, the loading of the SL has been set. In the Abaqus model, the general boundary condition is set to the bottom connector. This is modeled as encastréd (clamped) and is presented in figure 35. Due to symmetry, the model is split in half at a vertical plane. This is presented in figure 36.

The pull from surface vessel is modeled as a negative pressure force on the surface where the top connector is bolted to the next riser joint. Of course, this is a simplification because the bolts will affect the top connector more detailed than this. But the effect is assumed to be evenly distributed on the cross section of the top connector as the force reaches the geometry of interest. This is presented in figure 37, and has a magnitude of 300 Mg tension.

The operational moment is assumed to be 59 kNm at maximum, which is the maximum operational moment load at node 61 given in appendix F, “*Maximum Bending Loads on Riser System for Connected Mode Operations*”. This is modeled to act at a reference point in the model. Between the reference point and the top connector bolted surface there is modeled a kinematic coupling, locking the degrees of freedom between the point and surface. The reference point and the kinematic coupling are presented in figure 39. The inside pressure of the riser is set to the



maximum inside pressure of 10 ksi, approximately 690 bar. The inside pressure loaded surface is presented in figure 38.

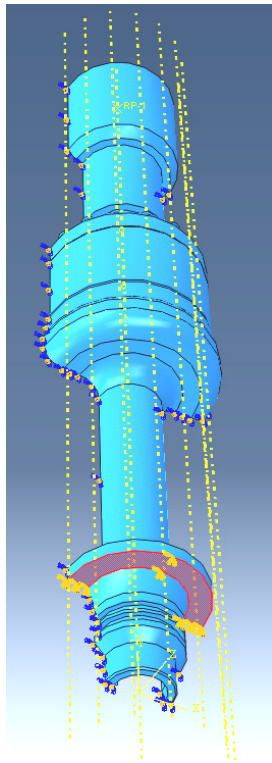


Figure 35: The bottom connector is encastred to resemble the riser fastening point.

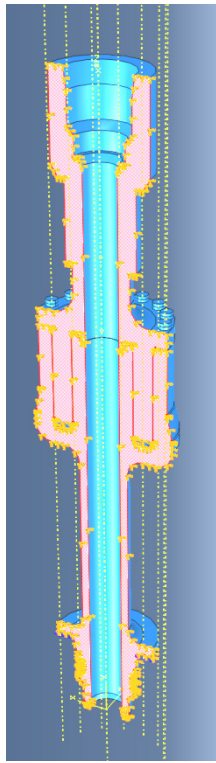


Figure 36: A vertical symmetry plane split the model in half.

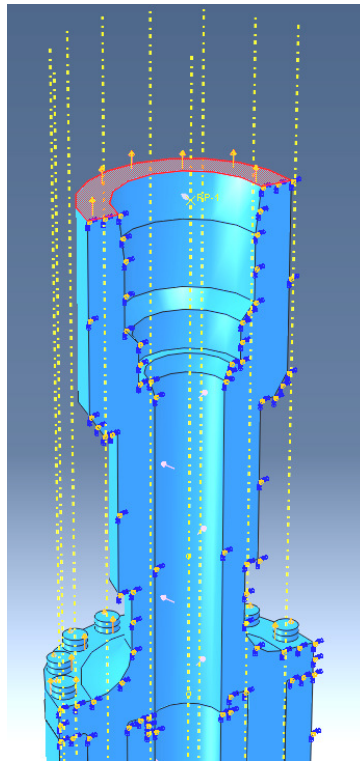


Figure 37: The top tension is modeled as a vertical pulling force.

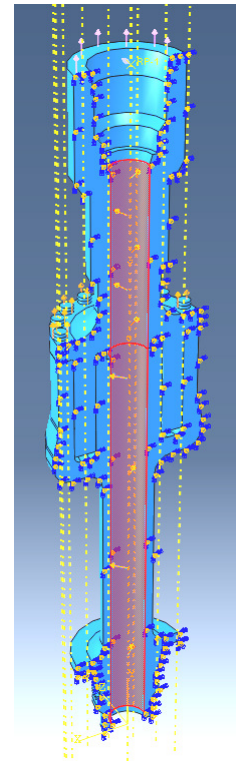


Figure 38: The well pressure is set to an inside pressure force.

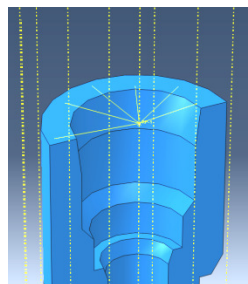


Figure 39: A kinematic coupling locks a centered reference point in all degrees of freedom to the top surface. The moment load is then put to work in this point.



The last loading which was accounted for is the separation pressure delivered from the pressure battery when the SL is initiated from the trigger system. How the loads are affecting the SL during separation is studied in more detail in chapter 5.5, Parameter study.

From all potential situations, the situation where the SL is separated by the SL trigger system is lightly to give the highest loading on the SL structure. In this situation, the surface vessel has drifted off, the EDP has failed to disconnect and the SL has been activated by the trigger system because of too large offset from reference position directly above the well.

The other situation where the SL has to function is when the SL is only subjected to the maximum tension from the surface vessel. In this situation the surface vessel system fails to compensate the heave motion excited on the vessel from waves. The function criterion is that the bolts has reached their maximum capacity and is failing from high stresses.

There are many situations where the SL should reach its maximum loading. Either it is because of compensator lockup or critical drift-off, or the two combined. For both these tests it is important that the SL structure cope with all forces with minor problems. It is the bolt's performance which is the critical element and should be of most concern in this analysis.

5.2 THE TOP CONNECTOR

Since the two joining components, the top connector and the bottom connector, behave as a unit when subjected to the global loads, it is difficult to simulate exactly how the two will inflict on one another when analyzing one component at a time. Because of this, the components have been loaded more heavily by concentrating the boundary conditions to areas in the geometry which is considered important. This makes the loading in these areas conservative. But since it is important that the connectors are designed to cope easily with the riser loads, this way of testing them has been considered wise.

As a precaution, the boundaries which prohibit the top connector from moving are set to the area which the bolts are affecting. This is done by surface partitioning the contact area of the bolt heads in Abaqus. The loads which are acting are the riser moment, the inside pressure and the separation pressure. In the previous chapter it is shown how the symmetry plane are set as boundary. When this loading is applied to these surfaces, the bolts will fail and the separation will complete.



5.2.1 ELEMENT TYPE

For the analysis of the top connector it has been chosen quadratic tetrahedron elements. The name of the element type is C3D10, which is a 10-node quadratic tetrahedron. The Tetrahedron element is preferred in this model because the self generating mesh function makes the analysis easier for the rather complex geometry. However, the use of this element needs to be cautious. Strict control of how the automatic meshing tool performs has been done. This is to prevent distorted elements and uncontrolled behavior. Sensitivity studies show that the quadratic TET mesh ousts the linear TET mesh in most cases of 3D-body geometries. This is because the linear TET mesh misrepresents the shear stresses. This extraneous shear “absorbs” strain energy and the element reaches equilibrium with smaller nodal displacements. Consequently, the element does not predict the bending displacements accurately and will have overly stiff behavior. When using quadratic HEX mesh, which cannot be used for this model because the geometry is too advanced, one should get the best result. Especially when using high node numbered elements. To get a more accurate feeling on how the model behaves when using the C3D10 element, one has to take in account many effects and judge as generally as possible.(19)

5.2.2 RESULTS- TRIGGERED SEPARATION

As a part of the analysis it has been done a stress convergence evaluation. By reducing the mesh size multiple times and recalculating the stresses, checking the most loaded areas for any changes in stress level, it has been selected an appropriate general element size of 20 mm. This generates 33490 elements representing the top connector. After checking the model in Abaqus monitor, there were very few distorted elements and no conflicting degrees of freedom in the nodes. Also the calculation was completed after two iterations, which implies a stable model. As figure 40 shows, the highest stresses are located in the sealing lip which is in reality backed up by the geometry inside of the bottom connector, thus making this highest value not very interesting. It is apparent that it is the inside pressure level of 10 ksi which gives the highest stresses. Also, the 40 MPa separating pressure acting on the bottom surface of the piston gives the largest compression forces on the bolt head contact surfaces.

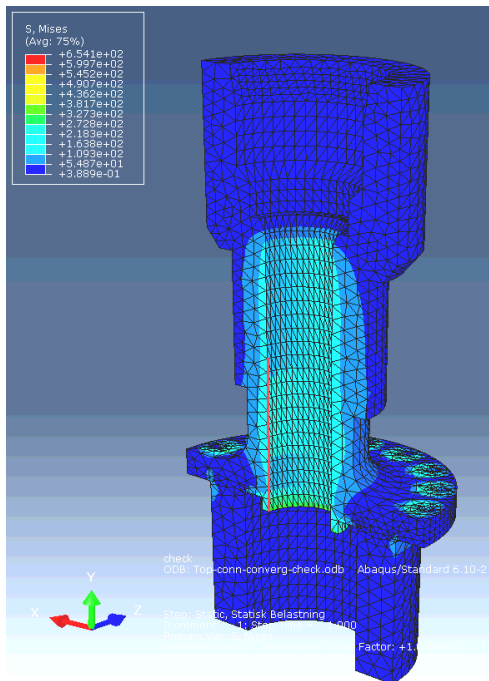


Figure 40: The top connector Abaqus model, loaded by triggered separation forces. Red line shows the nodal path of highest stresses.

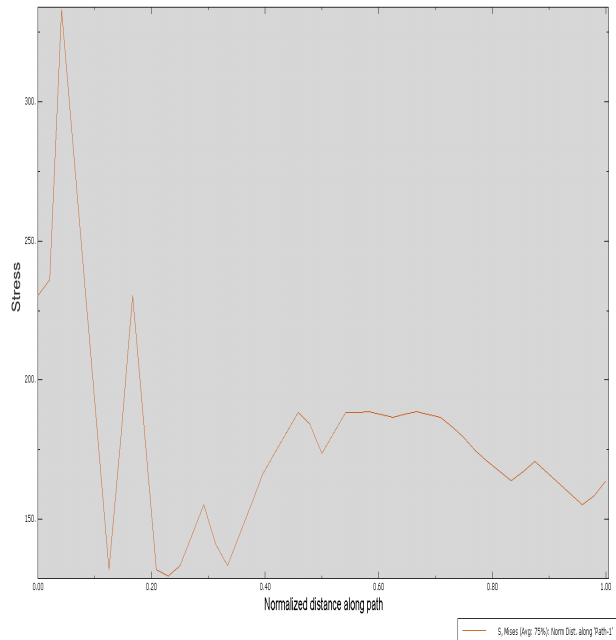


Figure 41: Von Mises Stress along the path of interest. Highest value of interest is below 200 MPa.

The analysis shows that the top connector will hold the maximum load well. Neglecting two very high loaded noise elements in two very separate places, the highest von Mises stress of interest is shown in figure 41, where the stress variation along the red edge in figure 40 is shown. As the curve is showing from bottom to the top of the red line, the highest load of interest is below 200 MPa, safely below the yield limit set for AISI 8630. Yield limit for the SL material AISI 8630 is set to 508 ± 26 MPa. Highest deformation is given to be less than $1/10^{\text{th}}$ of a millimeter, which is considered acceptable everywhere.

5.2.2.1 Checking the model

- When looking at the stress given from the separation pressure, the stresses lie in vicinity off 40 MPa at the piston cross section. This is behaving as expected.

- Checking the hoop stress of the same path as the von Mises stress was given, calculations show the stress given from inside pressure is similar to calculations done by hand. The Abaqus model result is given in figure 42.

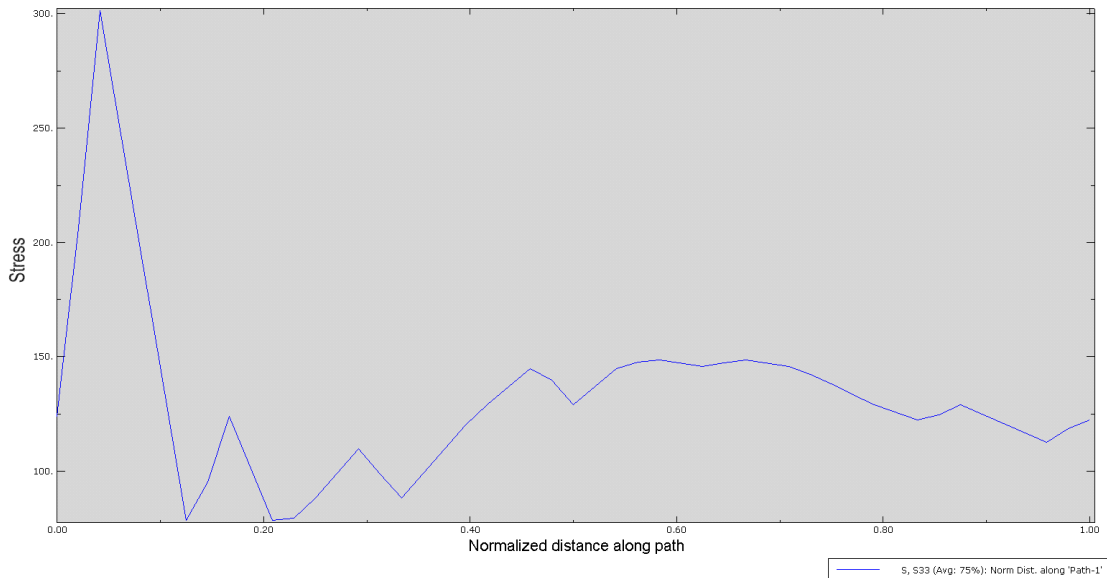


Figure 42: Hoop stress inside the SL, varying along the path shown in figure 40.

The figure shows by printing the Second Piola Kirchhoff force, that the general hoop stress is at its maximum for the pipe section at approximately 0.58 of normalized distance from the sealing lip and is just below 150 MPa of hoop stress. Calculating the hoop stress expected for thick walled pipes yields:

$$\sigma_c = \left[\frac{(p_i r_i^2 - p_o r_o^2)}{(r_o - r_i)^2} \right] - \left[\frac{r_i^2 r_o^2 (p_o - p_i)}{r^2 (r_o^2 - r_i^2)} \right] = 145 \text{ MPa}$$

where:

σ_c = stress in circumferential direction (MPa)

r = radius to point in tube or cylinder wall (mm, in)

maximum stress when $r = r_i$ (inside pipe or cylinder)

The slight difference in stresses is probably because of the other forces affecting the pipe section and contributing to the horizontal stress tensor. The result is considered acceptable.



It has been considered other effects that could be calculated numerically to further check the model. Due to the separation pressure, the moment from the riser and the inside pressure, it is considered difficult to resemble the effects in calculations done by hand. When analyzing the model with smaller loading, the hand calculations get more accurate. This is because the deformations get smaller and so the Green strain stresses resembles better the hand calculations above.

As a final check, all the stress directions and expected behaviors are checked to be satisfying. The Abaqus model result is probably representing the deformations and stresses in the top connector well, provided the load case which was set. Neither is the model showing significant stress concentrations, which probably gives a good fatigue resistance.

5.2.3 RESULTS- ACCIDENTAL PULL

This analysis test the SL for the forces acting when the surface vessel fails to compensate for its heave motion from waves. For this analysis it was chosen a general element size of 10, generating 43397 quadratic tetrahedron elements. A quick check in Abaqus monitor shows 15 distorted elements sporadically distributed in the mesh and no conflicting degrees of freedom in the nodes. The calculation was completed after 4 iterations, which implies a stable model. All forces have converged as is. To control the degrees of freedom in some nodes, the top face of the top connector was partitioned. This makes some elements distorted. The distortion is very local so the stresses here have been neglected.

The forces which are applied to this analysis are the maximum top pull of 300 Mg and the maximum moment from the global analysis. The moment is set to 59 kNm and is acting on the top surface of the top connector.

Viewing the model as a whole, the largest von Mises stresses is located again at the sealing lip. This is neglected as before, leaving the pipe section which has the smallest cross section. The von Mises stress is presented in figure 43.

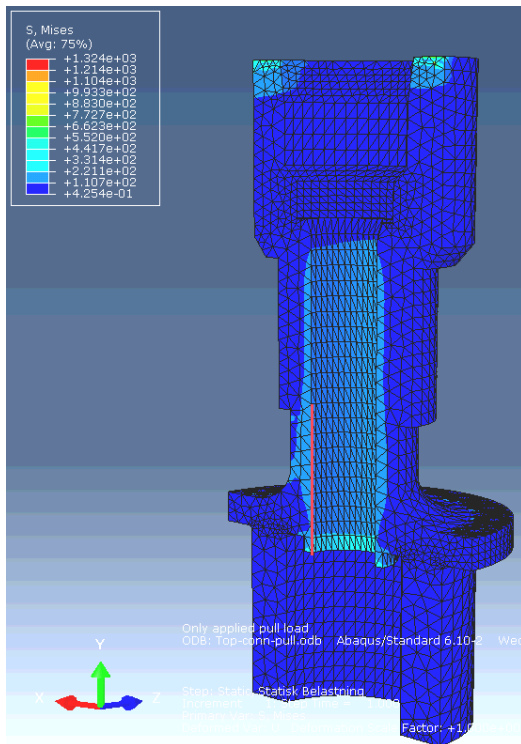


Figure 43: The top connector Abaqus model, loaded by maximum pull forces. Red line shows the path of highest stresses.

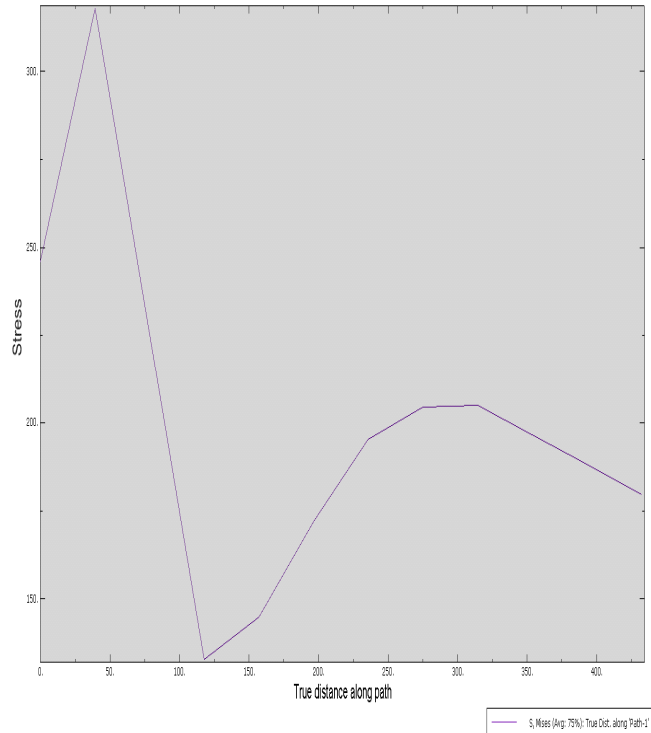


Figure 44: Von Mises Stress along the path of interest. Highest value of interest is directly above 200 MPa.

The analysis shows that the top connector will hold the maximum load well. The highest von Mises stress of interest is shown in figure 44, where the stress variation along the red edge in figure 43 is shown. As the curve is showing from bottom to the top of the red line, the highest load of interest is approximately 215 MPa, safely below the yield limit set for AISI 8630. Yield limit for the SL material AISI 8630 is set to 508 ± 26 MPa. Highest strain is given to be less than $1/10^{\text{th}}$ of a millimeter, which is considered acceptable everywhere.

5.2.3.1 Checking the model

- When plotting the stress in vertical direction of the cross section from Abaqus, it is possible to check the result with hand calculations to some degree. Figure 45 presents the 2nd Piola Kirchhoff stress tensor (S22) along the same path shown in figure 43.

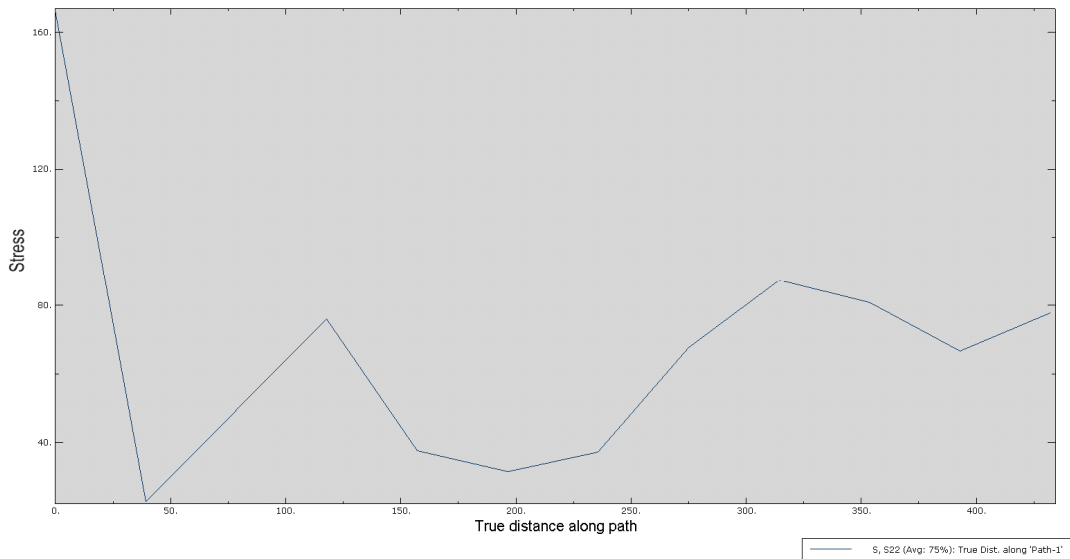


Figure 45: Vertical stress component along the path of interest.

The peak which represents the evenly distributed load on the cross section is evaluated to be in vicinity of 315 mm from the sealing lip. This peak shows a maximum of approximately 85 MPa. The geometry which affects the stress distribution in this area is important to be aware of. Hand calculating the pull and moment affecting the cross section gives:



Pull, inside surface stress:

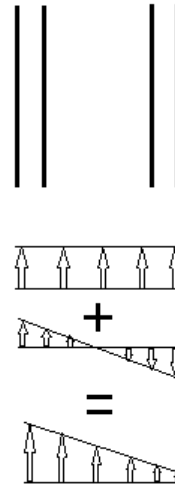
$$\sigma_{pull} = \frac{F_{pull}}{A_s} = \frac{1471500}{\frac{\pi(285^2 - 170^2)}{4}} = 71.6 \text{ MPa}$$

Moment, inside surface stress:

$$\sigma_M = \frac{M * y}{I_z} = \frac{2.95 * 10^7 * 85}{\frac{\pi(142.5^4 - 85^4)}{4}} = 8.9 \text{ MPa}$$

Total vertical stress, inside:

$$\sigma_{S22} = \sigma_{pull} \pm \sigma_M = 71.6 + 8.9 = 80.5 \text{ MPa}$$



This result is considered to be quite close. Comparing the two calculations directly is quite difficult because geometry in this area is changing. Also, the hand calculations suggest nominal strain in the model while the Abaqus model calculates the result from Green strain. The effect of this is that as the material is loaded, the strain produced in other directions affects the total strain, thus making the stress higher. This gives a better result than using the nominal strain. The hand calculations show that the model probably is giving reasonable results, the model is considered to be sufficient.

5.2.4 COMPARING THE MODEL

To get an indication of the accuracy of the mesh types and mesh sizes, a comparison of the 20 node hexahedron mesh, which should be the best element for this solid structure, and the 10 node tetrahedron mesh has been done. To do this, a model of the pipe section which has been subjected to analysis has been made. The length of the pipe section was decided to be 3 m. This was more than enough length to achieve a uniform and stable stress situation. The pipe was loaded with an inside pressure of 70 MPa (≈ 10 ksi), bending moment of 59 kNm and a pull of 300 Mg. The first test was done with 20 node **hexahedron** element. The mesh was made very dense to get an accurate result. The second test was done with the 10 node **tetrahedron** mesh with a global element size of 20. The test result is given in table 5.



Table 5: Test result of the comparison model.

Loading type	Element type	Highest mean stress from inside of pipe	Stress value[MPa]	Test model
Pull =300 Mg Moment=59kNm P_inside=10ksi	TET mesh	von Mises	199.5	
		S22	107.3	
	HEX mesh	von Mises	198.3	
		S22	107.2	
Pull=300 Mg Moment=59kNm	TET mesh	von Mises	107.2	
		S22	107.2	
	HEX mesh	von Mises	107.2	
		S22	107.2	

As the test show, the elements are describing the model response very similar. This means that the 10 node tetrahedron is probably describing the stresses accurately in the top-connector model.

Again, stresses as isolated as these, gets higher results then the stress calculated by hand calculations. This is because Abaqus is using Green strain which consider material deformations.

5.2.5 CONCLUSION- TOP CONNECTOR

The top connector has passed all checks done in this analysis. This does not mean that the top connector will function one hundred percent as intended. Further study should be made, especially with respect to the total assembly response of the SL.

5.3 BOTTOM CONNECTOR

As for the top connector, a totally accurate model is not easy to make without doing an analysis of the total assembly. Contact forces between the top and bottom connector will have to be treated with reasonable assumptions when modeling and assessing the results.

To simulate the forces acting on the bottom connector, special considerations has been taken to how the forces affect this part. Since the bolt is the upper limitation on how the SL shall perform while trigger separated, the surfaces which were encastréd was the bolt cross section surface, modeled as a partition face on the top surface of the bottom part. This is shown in figure 46. This is because when loading the SL with separation pressure on the inside of the annular floor, the forces will be balanced in a way which resembles the true assembly, shown in figure 47. Also, the pulling force from surface vessel is now acting as a downward pulling force as if the surface vessel pulled the SL from beneath, shown in figure 48. Inside pressure is modeled as normal. The riser moment has been modeled to act on a reference point constrained with a kinematic coupling to the connection surface which is bolted to the next lower riser joint. This is shown in figure 49.

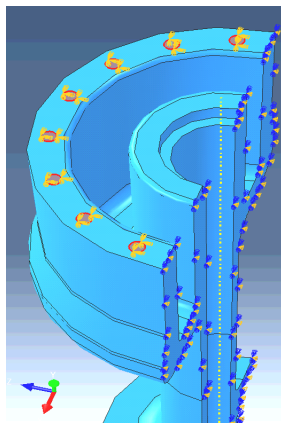


Figure 46: The encastréd, resembling the bolts effect.

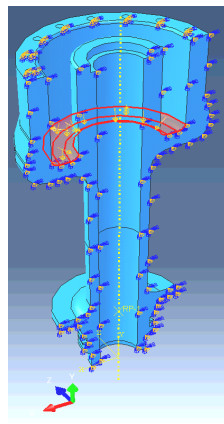


Figure 47: The separation pressure acting as a downward force to the SL, balanced by the bolts.

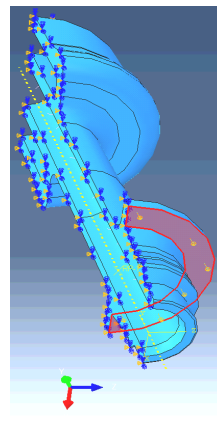


Figure 48: The pulling force of 300 Mg is modeled as a negative pressure force on the bolted surface.

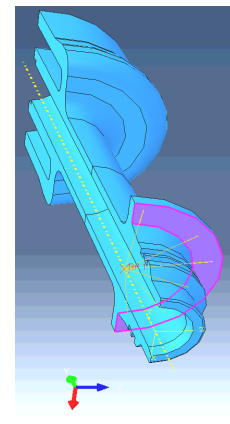


Figure 49: The moment is acting in the reference point which is kinematically coupled to the bolted surface.

For this analysis, the same element type as for the top connector is used. This element proved to be giving good results for the top connector, and seems to suit the purpose as the geometry type is much the same.



5.3.1 RESULTS- TRIGGERED SEPARATION

The stress convergence test showed to give stable results at the same element size as the top connector analysis, a global size of 20. This generated 73730 elements representing the bottom connector. Five elements were reported as distorted. Of these, two elements were located in the connector head and three were located on the inner rim at the top of the SL geometry. They had quite some distance between them; therefore these were neglected but kept in mind. Abaqus reported in Monitor that 18 nodes may have conflicting degrees of freedom because of the kinematic coupling to the reference point. This was checked out and was found not to be conflicting. Also, the calculation was completed after three iterations, which implies a stable model.

As figure 50 shows, the highest stresses are located at the encastréd bolt section, which is of course expected. Again, a path has been selected to evaluate the highest stresses. This is indicated by the red line in the figure. In figure 51, the stresses along the path are plotted. Largest von Mises stress on this path does not exceed 250 MPa, which is acceptable. At the curvature of the annular bottom where the separation pressure is acting there is a stress level of 190 MPa. This is considered acceptable. Highest deformation is given to be less than 1/10th of a millimeter, which is considered acceptable everywhere. It is important to notice that this analysis is loading the part in a way which is beyond the possible load scenario. With maximum separation pressure from the trigger system and the maximum allowed pulling force, the bolts will definitely fail. But this ensures that the bottom connector will keep its integrity at all times. Actually, the result may imply that the SL is over-dimensioned.

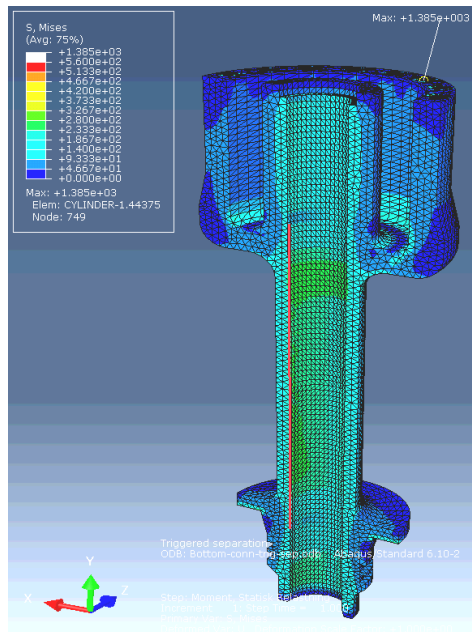


Figure 50: The bottom connector Abaqus model, loaded by all forces. Red line shows the path of highest stresses.

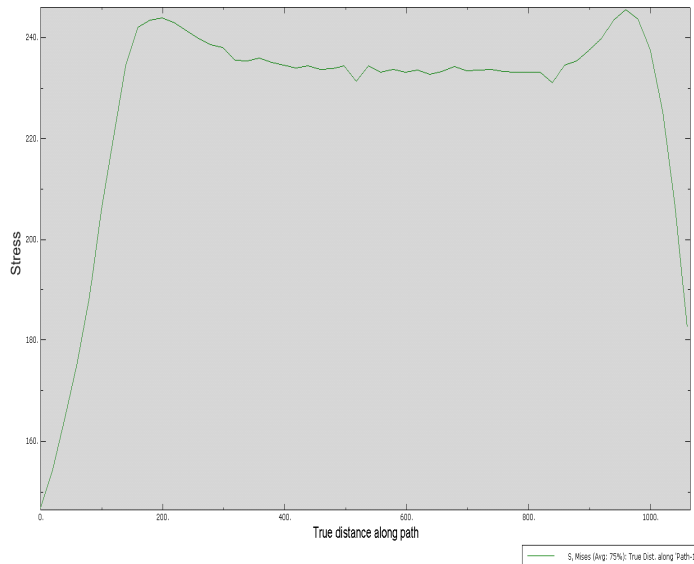


Figure 51: Von Mises Stress along the path of interest. The mean stress along the pipe section is approximately just beneath 240 MPa.

5.3.2.1 Checking the Model

The best way to check this model was found to make a similar pipe section as the one traveling from the SL pressurized separation geometry to the bottom interface, using 20 node hexahedron elements and compare the results.

In figure 52, the test geometry is presented. The mesh used in this model is very dense to get accurate results. As the stresses along the path shows, in figure 53, the mean value is stable at 243-244 MPa. Compared to the SL geometry, this implies that the model is showing reasonable results.

Since the geometry of the bottom connector and the top connector is quite the same, the same amount of checks is considered unnecessary. The effects which were studied in the check of the top connector have been generally continued in the analysis of the bottom connector.

The model has been checked for any unnatural behavior in loading response by adjusting and studying isolated stresses in different directions and controlling the response directions and signs. The model is behaving as expected.

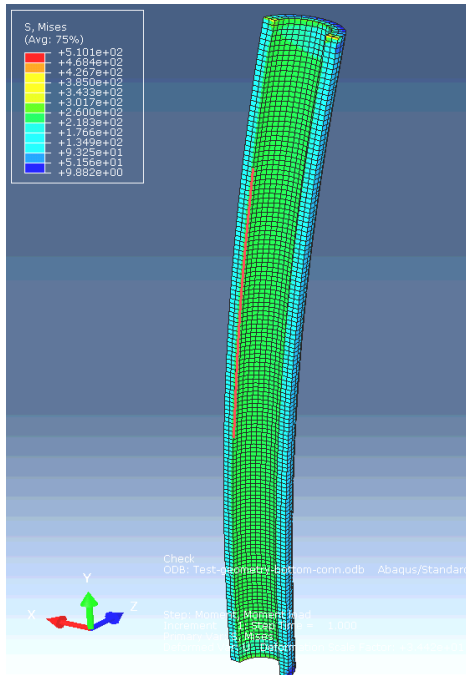


Figure 52: The test geometry made from the pipe section in the bottom connector. Red line indicates the path of interest.

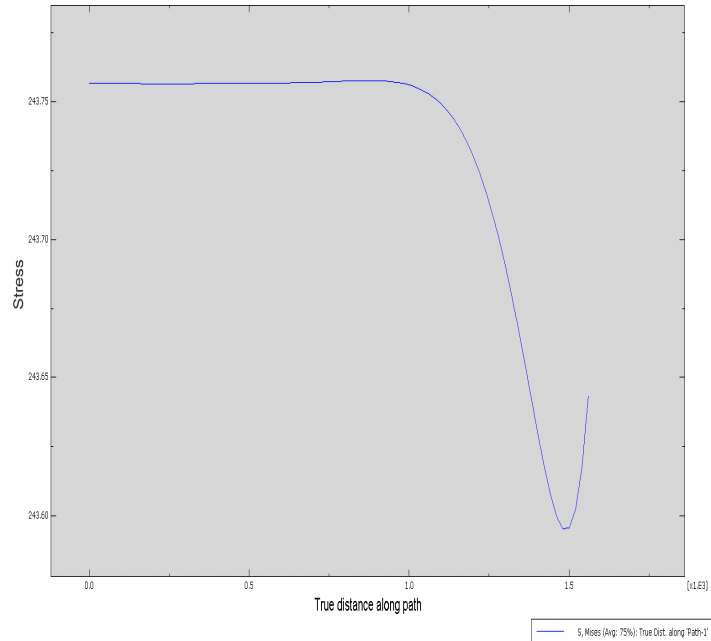


Figure 53: Von Mises Stress along the path of interest. The mean stress along the pipe section is 244 MPa. NB: Please notice the vertical axis variation from 243.575 MPa to 243.755 MPa.

5.3.2 CONCLUSION- BOTTOM CONNECTOR

The bottom connector analysis has been carried out with acceptable results. Both the SL geometry and test geometry with different kind of element type seems to get same results. The highest stresses are below critical stresses with clear margin.

One can always discuss whether the boundary conditions and loading configuration is set correct compared to the real behavior. This result should be checked against the full assembly. If the results of the full assembly resemble the result got here, the assumptions made here is probably correct.

5.4 BOLT

As a first model of the bolt, the dimensions which were calculated in chapter 4.4.4.3 were used. As Abaqus took into account the deformations, which are large with respect to the bolt size, the stress



which was calculated in Abaqus was much too high compared to the hand calculations as expected. Therefore the bolt diameter at the adjusted section was increased, until the stress levels were acceptable. The bolt was loaded with the break load of 300 Mg pull from surface vessel. This was looked upon as a limit load where the bolts capacity regarding tensile stress should be 1000 MPa. In this analysis the torque from the pre-tensioning of the bolt was set to 300.547Nm.

Only one load scenario was checked in this analysis. This was the scenario where the SL is protecting against excessive tension from e.g. compensator lock-up. This scenario is suspected to be the SL's most delicate situation where the range between break and hold need to be tightest. In the scenario where the SL has a triggered separation, the bolt loading will be much higher, resulting in definite failure.

5.4.1 RESULTS- BOLT

This test was performed with a very dense mesh. A global element size of only 3 mm, generated 61572 elements representing the bolt. No elements were reported as distorted and the model reached equilibrium in only one iteration, which implies that the model was stable. This model is only suitable for the tetrahedron mesh in Abaqus when using automated meshing. From using the TET mesh in several models during the preliminary project and master's thesis, the 10 node element is probably giving reasonable results for this geometry. Some care was given to the distribution of the elements by manually seeding some edges, but nothing complicated.

As mentioned in chapter 4.4.4.3, "*Bolt dimensions*", the dimensions have been subjected to change while analyzed in Abaqus. The bolt's main dimension of M27 has not been changed, but the adjusted diameter has. From testing in Abaqus the diameter of the adjusted section was finally chosen to be 20 mm. When loaded with pretension, the critical load of 300 Mg and the make-up torque, this yields stress of about 975 MPa, which is close to the breaking point for Im01 material. In this case the bolt has started to yield and will break or have already broken. In figures 54 and 55, the bolt model, nodes of interest and the plot describing the nodal stresses is presented.

When modeling the bolt in Abaqus, the part of the bolt which is threaded was encastréd. This is an inaccurate way of describing the threads influence on the bolt behavior. The highest stress in the threads will be at the thread root, as the threads get deeper into the material the stresses will decrease in the bolt gradually as the threads are gripping deeper into the part. When modeling the boundary condition like this, stress concentrations get unnaturally high at the thread root. This is

why this stress is neglected in the analysis. The loading is modeled as a bolt head bottom surface load which is causing the tension force in the bolt.

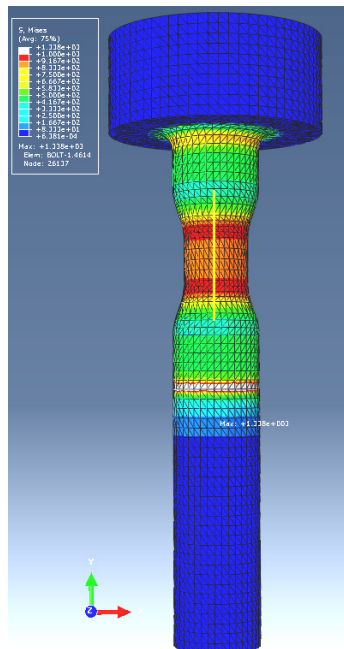


Figure 54: The bolt from Abaqus analysis model. The von Mises stress level is reaching the tensile limit of 1000 MPa. Yellow line indicates nodes of interest.

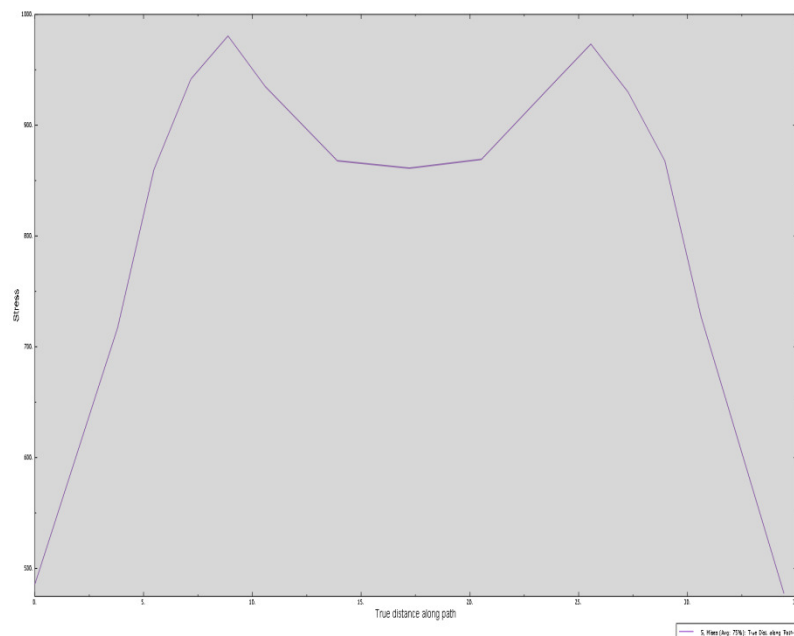


Figure 55: Von Mises stress at nodes following the yellow line in the figure from bottom to top. Stress levels are reaching the tensile stress limit of 1000 ± 50 MPa.

Stress concentrations are located in the transition between big diameter and small diameter on the bolt shaft. This is expected, because this is consistent with theory describing the effect of notches and geometry change in a loaded part. It is possible to influence this effect by altering the transition between the two diameters, giving the rounded surfaces even bigger diameters. After some research and altering of the diameters, this effect does not disappear completely, but has been softened greatly. The dimensions chosen for the analyzed bolt has been considered to represent a satisfying result.(13)

5.4.2 CONCLUSION- BOLT

This result of choosing bolt dimensions has to be carefully reconsidered when more information on a specific bolt is to be tested. The stress concentration shows that the bolt is likely to break off at



the point where the geometry reaches the smallest diameter. Still, the design indicates that this design could work as the SL bolt.

5.5 PARAMETER STUDY- SL SEPARATION

When the SL is separating the loading get less complicated. This is because the bolts have broken off, no longer supporting the pull and (or) the separation pressure. This means that the force which is directly transferred through the SL as the separation process is ongoing is the moment. In this situation, the area which the moment is transferred through as contact forces is decreasing fast. This means that there is potential danger for wedging effects and forces which make the material plastically deform. In a worst case scenario this could mean that the SL will not be able to separate completely. To simulate exactly what is happening is difficult. But, to get an indication of how the forces are distributed as the SL separates, a parameter study has been done.

The SL has been modeled as an assembly, with no bolts holding the two parts together. As a general contact, regular steel to steel lubricated surface friction coefficient of 0.25 has been used. This coefficient represents a somewhat treated surface where the surface is more or less lubricated or designed to slip. (13)The SL has been run in Abaqus only loaded by the moment. The moment is kept constant as the separation distance is increasing.

For this analysis a global element size of 30 mm is used, creating 24057 elements representing the top connector and 32809 elements representing the bottom connector. In the bottom connector there was detected no distorted elements. In the top connector there were detected three distorted elements. All these elements were located more than 400 mm apart causing no special problems. Also, their location was in no vicinity of interesting geometry. They were mainly located in the riser interface geometry of the top connector, not in the piston geometry or where stress concentrations from the moment may form. Some warnings from the kinematic couplings were detected in the message file, but as before, the nodal degrees of freedom were checked to be causing no problems.

First, a model where the SL has not been initiated was done to get an overview of the response and stress distribution. Then several models of the SL separating by 100, 200, 300, 400, 430,450,460 and 465 mm were done.



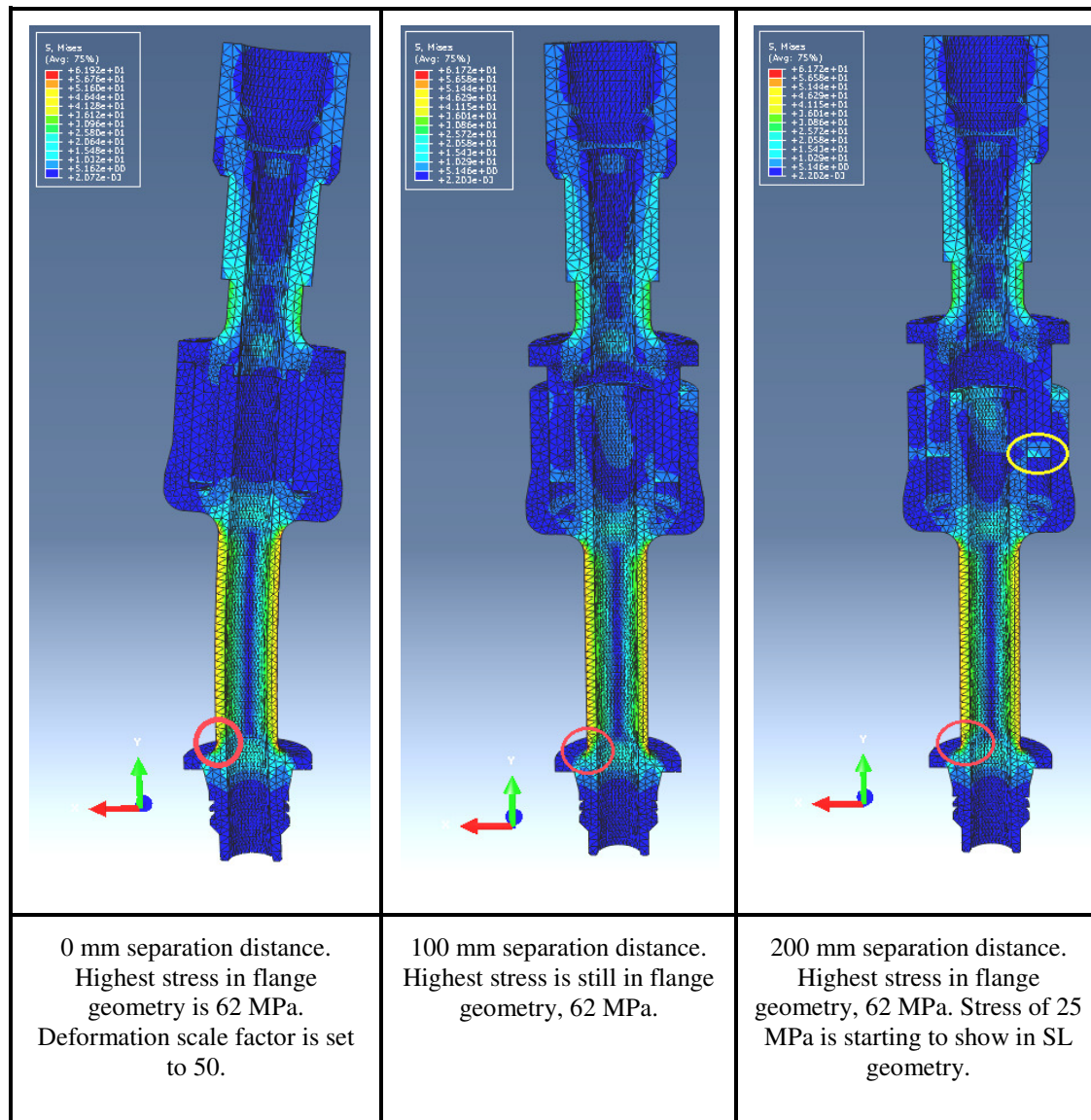
In this study, the element which was used was changed from C3D10 to C3D10M. Because of the new situation with contact between the parts, it was decided to search for some help on element selection. After searching for literature describing the problem without result, one had to turn to internet forums and Abaqus user's manual. C3D10M is a modified 10 node quadratic tetrahedron. The "M" element is more expensive, that is, requires more memory to run so the computational time increases a bit. The element has hourglass control, which ensures the element shape not to deform causing faulty results when response is entering plastic zone of the material. Using C3D10 or C3D10M on a solid part with no contact forces, the result will be the same. The user 's manual states more exact that C3D10M are more accurate for high-strain plasticity then C3D10, but for relatively low strain in ballpark $< 5\%$, both should give similar results for no contact. But when introducing multiple part assemblies with contact, the C3D10 fails to represent correct results at contact surfaces. The C3D10M on the other hand represent the contact situation well and is chosen for this analysis.

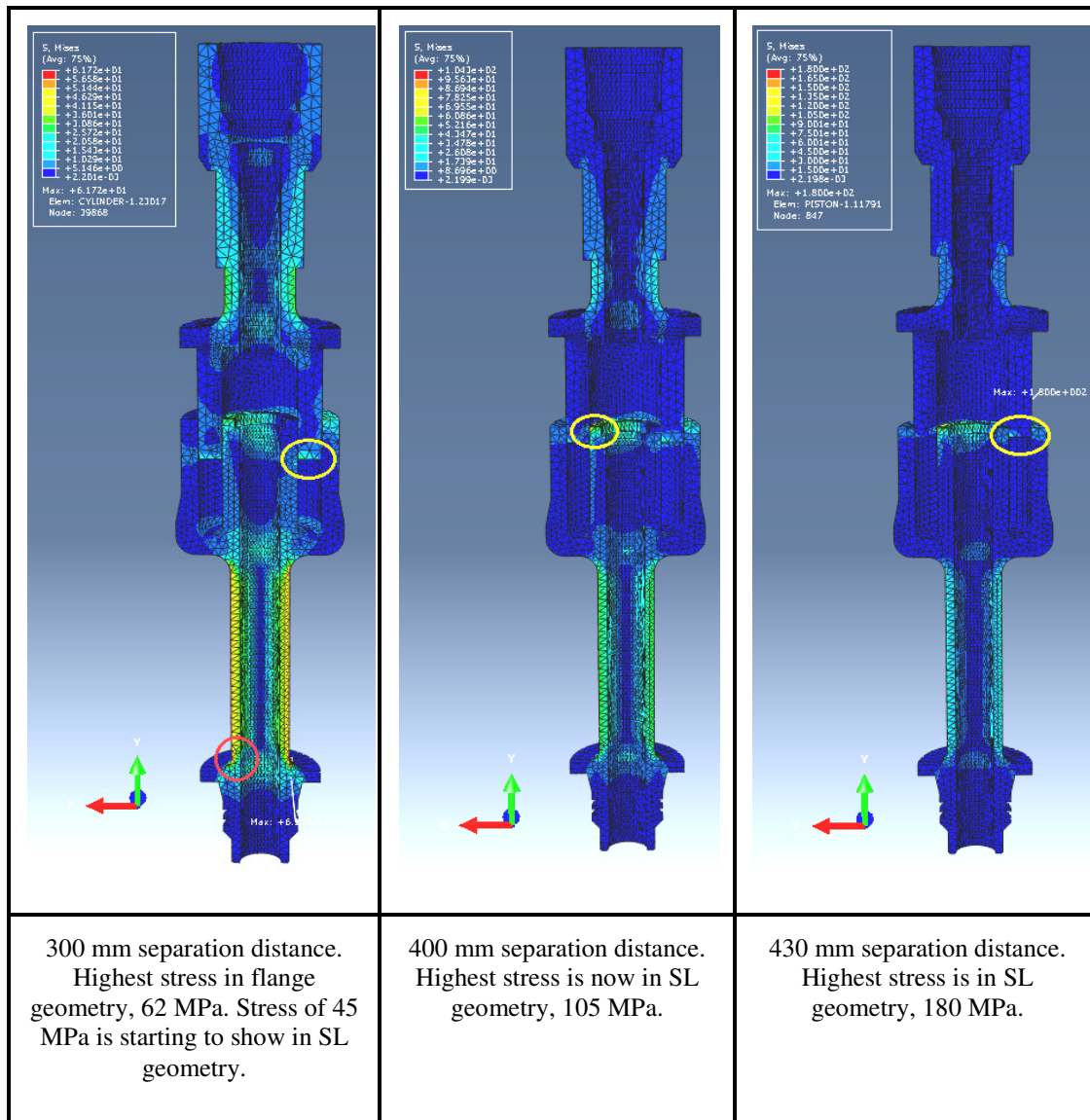
5.5.1 RESULTS

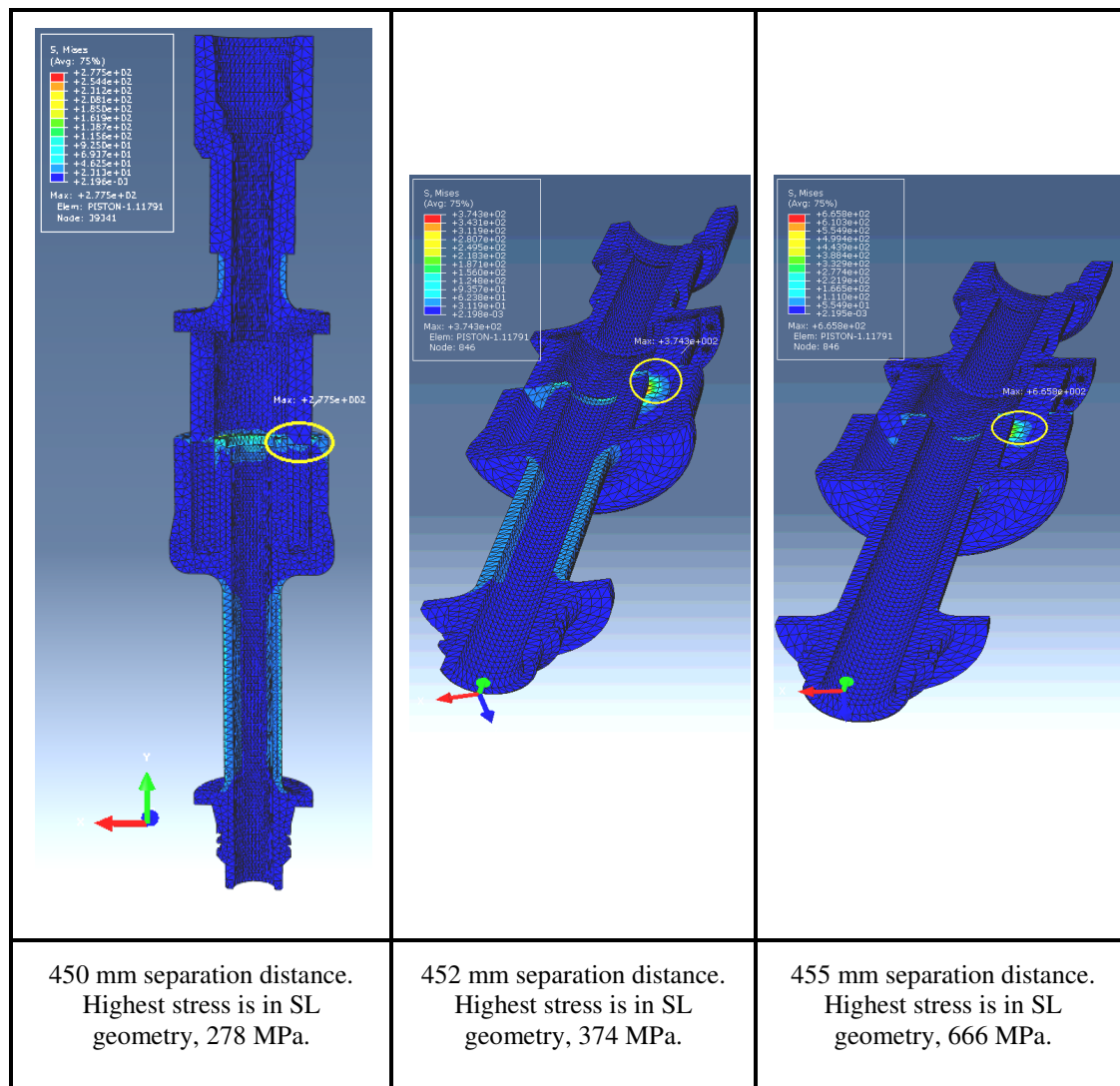
Total separation distance is 470 mm. In table 6 over the next few pages, the highest stress in the model and its location is given as the SL separates. The red circles indicate the stress level in flange geometry. The yellow circle indicates the highest stress in SL geometry. The first figure, with no separation distance, have a deformation scale factor of 50, the rest are scaled to true deformation.



Table 6: Change in stress level as the SL separates.







As the figures show, critical stresses does not arise until the separation distance passes 450 mm for this geometry and moment load. Of course, the geometry is very important when studying these effects and will probably be altered in later designs. Also, the moment is kept constant in this analysis, something that will not be the case in real life. Because it is easy to imagine that the moment could be higher than 59 kNm when the SL is separating from uncontrolled drift off.

From this analysis it is natural to conclude that the SL behaves as expected. As the SL separates and the contact surfaces decrease in area the stresses get locally high. In the last 20 mm of separating distance, the stresses reaches yield limit for AISI 8630. This indicates that the material probably will deform and the contact forces between surfaces will get very high.



When assessing wedging effects, it is difficult to conclude anything without any scale test data. But since the stresses is not that high until 450 mm separation distance, and the surfaces is designed to be lubricated, the friction will probably not allow the surfaces to wedge enough to lock the parts together.

A problem which arises when assessing the results are the stored energy (moment) in the SL connection just upon release. This energy will most likely be suddenly released in a snapping manner, transforming the energy into a horizontal motion in the stationary riser string. In particular if the moment loads get higher than the one used in this analysis. Of course, the acceleration in water will most likely be affected by added mass and drag forces, thus removing the energy which is released quite fast, but this effect could be transferred into the well stack through the riser string and cause damage. This recoil effect should be assessed in more detail in further study.

As the bolts break from excessive top tension or separation forces, it is natural to assume a recoil effect in the tensioned riser string. Exactly how this is dampened in the system is difficult to estimate, but some dampening effect is assumed to be present. This should be assessed in further study.

5.5 FEA CONCLUSION

From the finite element model it has been gained a lot of knowledge on how the SL performs under loaded conditions. The best way to prove the results have shown to be the evaluation of similar geometries with the same loads. Then the deformations are taken care of in both models giving representative results to compare as it has been done for this model.

The Abaqus model shows that the SL geometry tested, probably will withstand the loading in a satisfying way. Von Mises stresses show to be well beneath the yield stress for the component analysis. When separating, the detail geometry get very important and should be decided upon before another analysis is done, but in general, there was not found any immediate problems with respect to wedging effects. More research should be done on this subject and also scale testing should be done.



6.0 CLOSING OF THE WELLBORE

In the process of developing the system that should close and secure the well after separation is finished, multiple concepts has been studied. Most of them are directly connected to how the SL separates. When designing a closing-function which should work with the SL as it is designed, it was tempting to try to make a solution where the riser was closed by two special valves. These valves where to be located in the top and bottom connector. The valves should be designed to close by utilizing the forces which separate the SL, either by connecting them to each other, or some kind of adjacent geometry. This sketching and idea generating process was stopped. This was because no matter what the idea was, the solution always got too complex. Like it has been shown many times in history, the most reliable systems are often very simple. This is why the focus was directed on how to make the most of the present systems.

6.1 UTILIZING THE EXISTING SYSTEMS

The well stack, which consist of the X-mas tree (XMT), Well Control Package (WCP) and Emergency Disconnect Package (EDP) for the Kristin W/CO riser system, hold many safety functions. For the development of this system some of them have been considered to be of use. The XMT and WCP possess fail-safe functions. Basically this means that if a safety issue arises, the system will automatically set the system to the least threatening state. One of the main fail-safety functions is the hydraulically actuated valves. These valves open and close the wellbore and are spring loaded to be fail-closed, not fail-open. This means that when the tree has an undisturbed and stable hydraulic pressure and signal connection from the surface vessel, the valves are forced open and in operational mode. On the other hand, if the communication signal suddenly disappears for some reason, no force is holding the valves open and the well is closed automatically. This could potentially happen in any operational state. Therefore, to cope with situations where there is drill pipe, coil tubing, wire line or tooling passing through the well stack at the time of emergency, a special valve is introduced. This valve is placed in the WCP and is called a Shear-Ram valve. The shear ram valve is designed to cut any obstruction in the well bore and seal of the well. The WCP also contains gate valves which could seal the well. So, if any safety issues arise, the operator has time to identify the problem, because the WCP is a fully enclosed pressure housing with no dynamic seals between the wellbore and the surrounding environment.(20)



Utilizing the well-stack safety functions are considered to be the smartest way of closing the wellbore in case of a SL separation. Not only does this imply a small and simple system, but also a cost efficient system. This means that the SL will have to cut the hydraulic and signal connection between the surface vessel and the well control systems as it separates. This signal is transferred through an umbilical line which could contain electrical power, hydraulic supply line, fiber optics and hydraulic signal lines. The design of the umbilical line is based on what kind of well control system which is used. For the Kristin field, an electro-hydraulic system is used. This means that in the umbilical runs hydraulic supply pressure, electrical power and fiber optic signals. On the seabed, hydraulic accumulators supply the valves inside the XMT and WCP with high speed hydraulic pressure signals, controlled by a control module. The control module is communicating with the operator through fiber optic signals.(7)

To be able to close and secure the well, the SL need to cut the umbilical which runs beside the C/WO riser at separation. This will force the well system to run in safety-mode and close the well.

6.2 CUTTING THE UMBILICAL

Inspiration from the Shear-Ram cutting mechanism resulted in a shear-cutting system which is driven by the SL's separation pressure. As calculated in chapter 4.4.3.1, the maximum pressure right before separation is set to 432 bars. When adding some extra hose, connectors and a pneumatic cylinder the pressure will decrease to:

$$V_{system} = [WL + Hoses and connectors + Control Valve] + shear-ram hose + actuator$$

$$V_{system} = [0.00203 \text{ m}^2] + \left(\frac{\pi * 0.0127^2}{4} \right) * (1.2) + \left(\frac{\pi * 0.07^2}{4} \right) * 165$$

$$V_{system} = 0.00203 + 0.00079 = 0.00282 \text{ m}^2$$

$$\frac{P_1 * V_1}{T_1} = \frac{P_2 * V_2}{T_2}$$

$$P_2 = \frac{P_{battery} * V_{bottles}}{V_{system} + V_{bottles}} = \frac{50 * 10^6 * 0.01289}{0.00282 + 0.01289} = 41.024824 \text{ MPa} \approx 410 \text{ bar}$$

This result is still considered satisfying with respect to the SL separating functions. The system still has a pressure reserve of 10 bars. This calculation is done with the actuator at full travel giving the

largest volume. At initiation of the cutting sequence, the pressure will be slightly higher. The actuator is not planned to be balanced with hydrostatic pressure so one has to consider the decreased shear force due to hydrostatic pressure in the shear-cutting mechanism. Balancing the cutting force by assuming a cutting pressure of 400 bars:

F_{cut} = Force from separation pressure - Force from hydrostatic pressure

$$F_{cut} = 40MPa * \left(\frac{\pi * 70^2}{4} \right) - \frac{1030 * 9.81 * 600}{10^6} MPa * \left(\frac{\pi * 70^2}{4} \right)$$

$$F_{cut} = \left(\frac{\pi * 70^2}{4} \right) * (40 - 6.06258) = 130.6 kN$$

This is the shear-force which will cut the umbilical and is planned to work as shown in figure 56. The shear-force could prove to not be great enough to cut the umbilical. If this is the case, a redesign of the system could be inescapable. Exactly how the cutting mechanism could alternatively be powered, should be assessed in further study if the system proves unreliable .

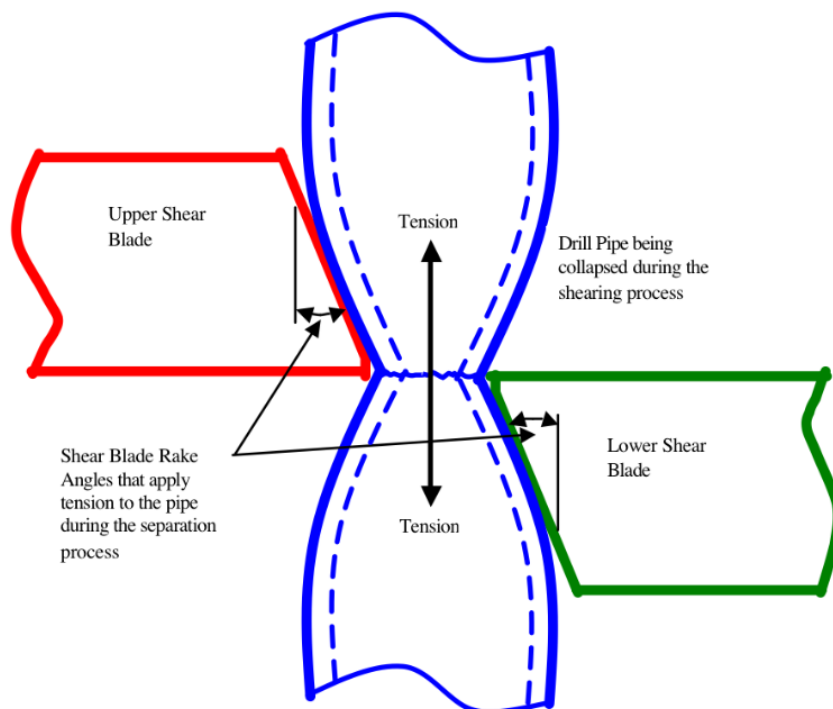


Figure 56: The Shear-ram cutting mechanism used for cutting standard drill pipe.(21)

6.3 THE DESIGN OF THE CUTTING SYSTEM

In figures 57 and 58, the cutting mechanism is shown. A simple system model is applied, but it shows the main features. The ring which mounts the system to the SL is thought to be made from light weight composite material only holding the system in place. The cutting function of the system is self supported while cutting; only transferring some torsion force to the mounting plate because of the moment created while cutting the umbilical. When not operated, the actuator is set inside its cylinder housing, protecting it when not used.



Figure 57: The mounting ring with the cutting system attached.

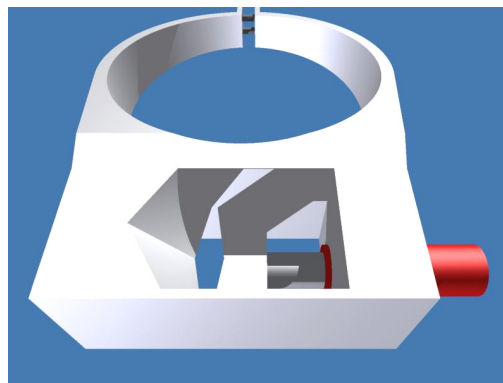


Figure 58: The actuator pushes the cutting block towards the adjacent cutting geometry, creating large shear forces which cut the umbilical.

The cutting system is mounted on the bottom connector of the SL, utilizing the tension which increases for the umbilical as separation is in progress. The SL with the mounted cutting system and the umbilical which runs along the riser string is presented in figure 59.



Figure 59: The cutting system mounted on the bottom connector. The umbilical line passes through the cutter.

From the main separation pressure it has been drawn a line which power the cutting actuator. This is shown, highlighted in red, in figure 60.

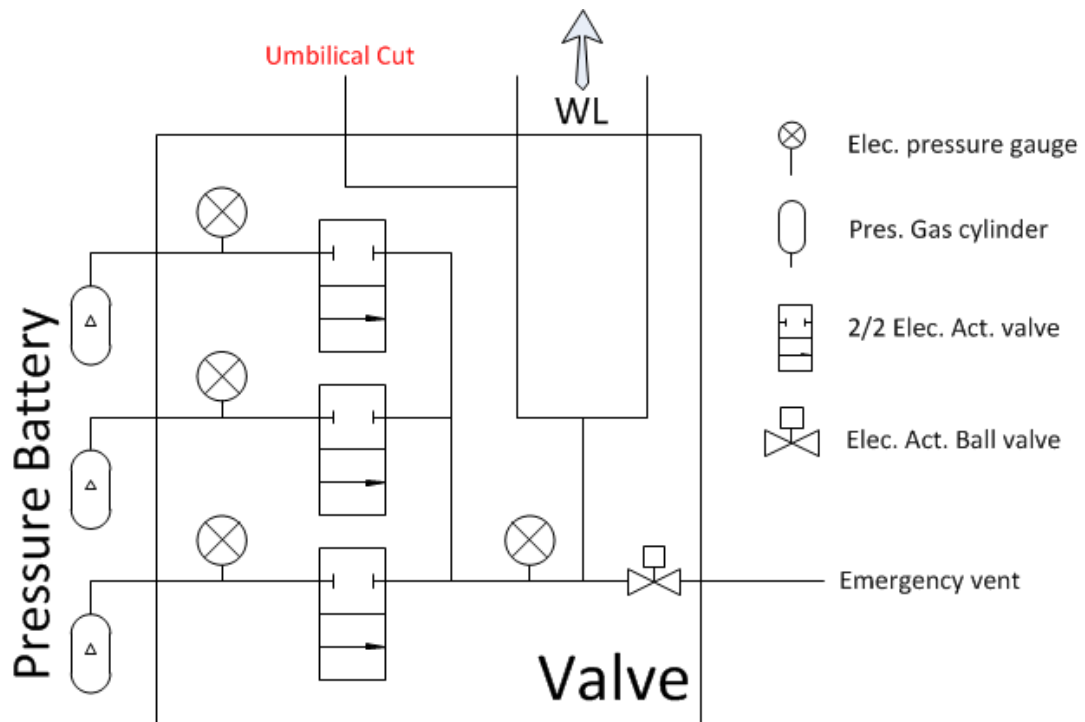


Figure 60: Valve schematic showing the line which is planned to power the umbilical cutting actuator.



7.0 RELIABILITY STUDY

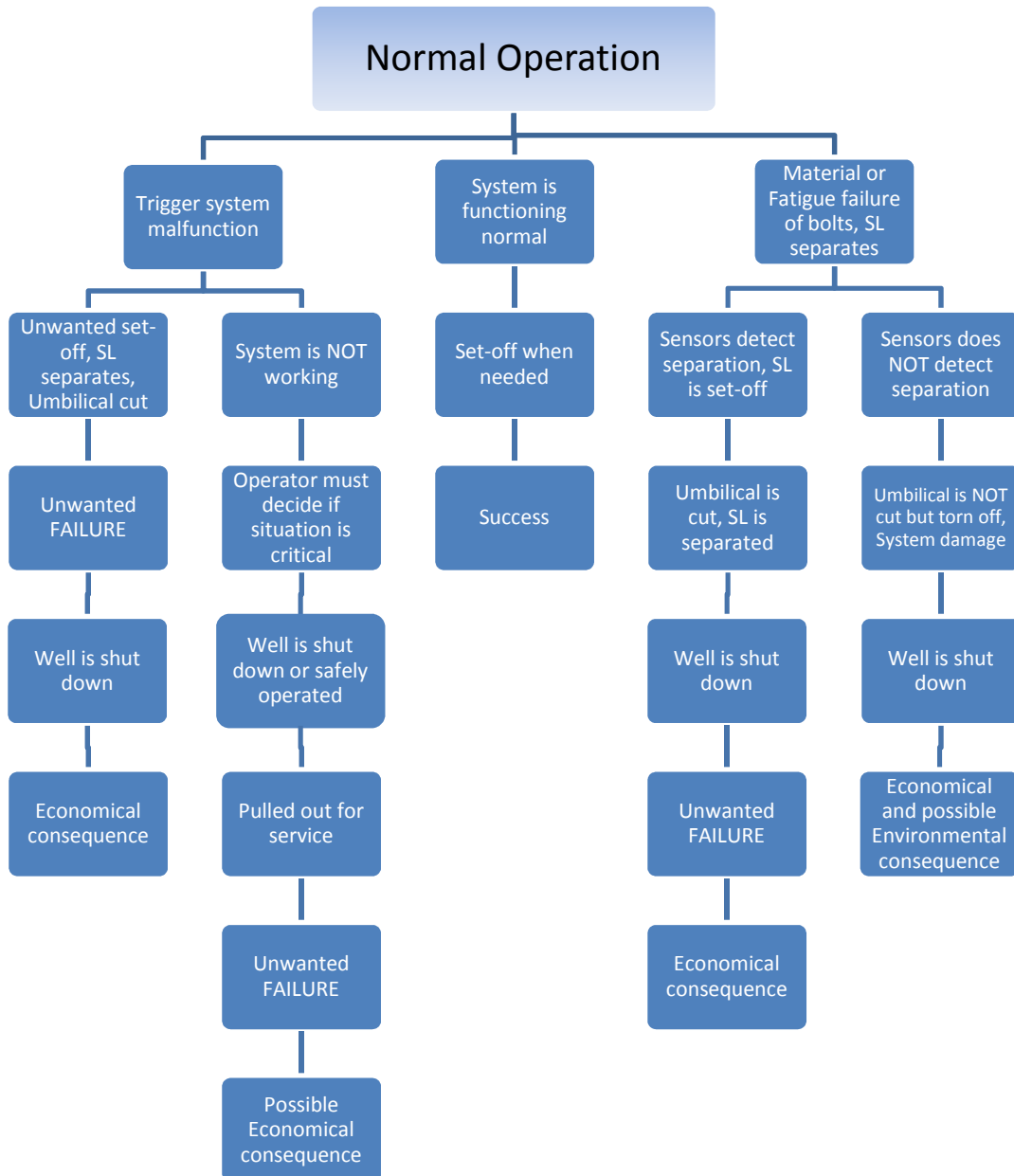
This study has been done mainly to identify critical aspects regarding the SL functions and design. By producing a block diagram from four different operational states, the SL functions have been evaluated. Of course, there are a lot of unknowns in the system and all of them cannot be accounted for until the design of all systems are complete, but the study indicates which components and functions that could be most critical. For illustrative purposes, a picture of the final design from a different angle is presented in the figure below.





7.1 NORMAL OPERATION

The first operational state is the Normal Operation mode. This is where the SL copes with a normal loading scenario and shall easily cope with the riser response and behavior.



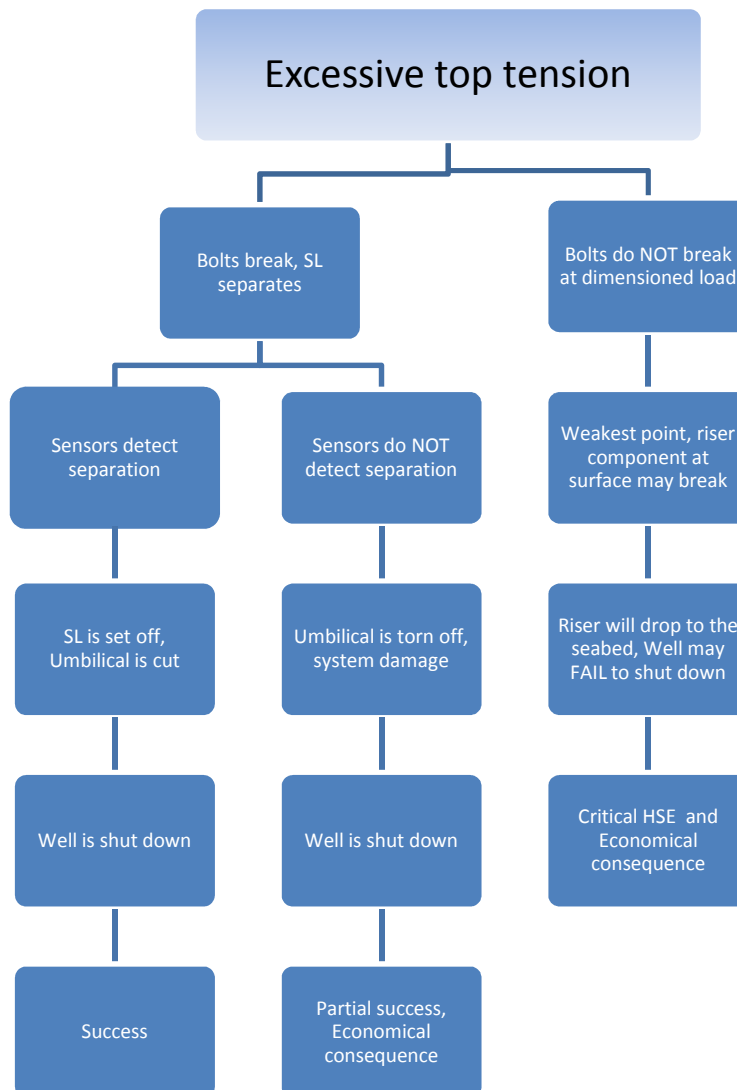
When assessing the normal operation block diagram, the different scenarios studied here ends up with the well in shut off mode and riser disconnected. This is somewhat satisfying with respect to the prevention of major accidents, but is still a non-operative and unwanted condition. A critical



component for the SL is of course the bolts but also the separation sensors. It is highly important that these function properly. Therefore study should be made to ensure the sensors reliability is satisfying so that the economical and environmental consequences could be minimized if some failure should happen.

7.2 EXCESSIVE TOP TENSION

In this scenario, the riser string is experiencing top tension up to and above the tension breaking point of 300 Mg. This high level of top tension is typically experienced when the heave compensating system at surface vessel is malfunctioning. At this loading condition the SL is designed to break and separate.

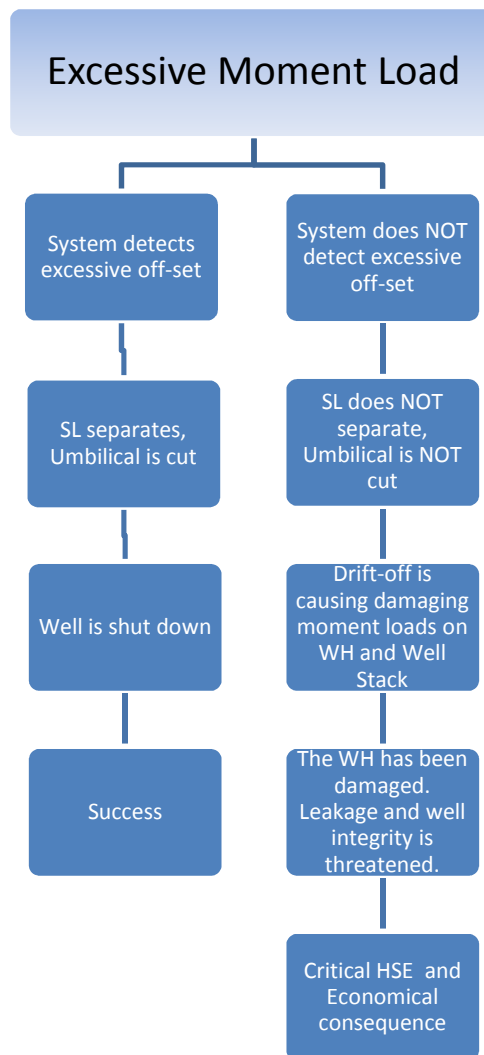




The scenario with the most critical consequence is surely the scenario where the bolts do not break at the dimensioned load. This is unlikely to happen if bolts are dimensioned properly but worth mentioning. Again, the sensor functionality proves to be important. In both cases where the bolts break because of excessive tension, the well is expected to shut down.

7.3 EXCESSIVE MOMENT LOADING

When the Well Stack is subjected to high moment loads because of surface vessel drift-off, the SL is designed to separate when EDP does not work. The SL measures the offset position from the Well Stack and operates in accordance to specified maximum horizontal offset values. When the maximum values are breached, the trigger system is initiated and separates the SL.





It is assumed that the excessive moment loading is more damaging for the well integrity than the situation where the top tension exceeds 300 Mg. Uncontrolled high moment loading could damage the WH and well stack to the extent of total collapse of well barriers. This could result in huge environmental contamination and HSE consequences. The SL is a third barrier protection against this kind of situations, but the moment detection is very important if all other systems fail.

7.4 COMBINED LOADING

In the preceding chapters of this reliability study, the loading is treated as they were acting alone. This is of course far from reality. The loading will act simultaneously, creating stress from both tension and moment. The riser string will react to the surface vessel motions and also the pelagic forces like current in different layers and temperature changes. In normal operation, it has always been vital for safe operations that the operator make safe decisions with respect to weather and sea conditions. Exactly how these effects could affect the SL functions needs to be investigated further by doing dynamical analysis of the riser string with the SL in place. Then one can detect any normal operation problems regarding the SL functions. The result of a SL which misinterprets the situation could lead to an unwanted separation, which could cause serious equipment damage and unwanted down-time.

When DP and EDP have stopped working and the surface vessel is experiencing uncontrolled drift off, it is natural to expect high tension and moment loads. The SL trigger system with acoustic inclination monitoring should be tested thoroughly to ensure that either the top tension safety mechanism separates the riser or that the off-set system ensures the separation.

7.5 RELIABILITY STUDY CONCLUSION

The bolts, separation sensors and off-set measurement system prove to be very important parts of the trigger system as expected. Should any of these fail to function properly, the SL may represent a serious HSE and economical risk. Reliability testing should be done to the trigger system, to ensure the operational safety of the SL at all times. The study shows that by making the umbilical cutting system dependant of a fully functioning trigger system, the system get vulnerable. Designing a system which is more mechanically reliable, e.g. not powered by the trigger system, the umbilical could be successfully cut even if a major system error separates the SL. An example of such a system could be a system which is powered by the geometry itself as the SL is separating.



The redundancy of the systems proves to be important for the SL, as for all critical subsea systems. This should be assessed in more detail in further study.



8.0 CONCLUSION

Considering the scope of work which was given for this thesis, the candidate is pleased with the result. The thesis has been very educative and a better understanding of riser components, analyzing and development of such has been gained.

The first task was to decide where to place the new developed SL in the riser string. Placing the SL in the well stack will only make the entire system more vulnerable, more expensive and geometrically larger to cope with much higher loads and also give an increased fatigue loading on the wellhead. As study showed, the best place to install such a SL is in the riser string. This yields a slimmer design, which is geometrically smaller, lighter, more cost effective and represent less loading on other vital components.

The second task was to decide upon the interface to adjacent riser components. This has been done in collaboration with AKSO and modeled in Inventor. The SL was also to be designed in extent in Autodesk Inventor. A design of the whole assembly has been modeled in inventor and reviewed by AKSO and the supervisor from NTNU. Relevant design calculations regarding the SL functions were to be done to ensure that the SL will work as intended. As the design moved forward, relevant geometry calculations have been done and dimensions have been adapted to the results. Due to the favorable placement location which was chosen for the SL, the SL has been dimensioned to replace the existing link which is solely based on tension response, enabling the SL to protect the system from excessive moments and tension.

Task number three was to do a static analysis of the whole SL design in Abaqus. Due to time consuming errors in the mesh generator because of advanced geometry, it was decided to do an analysis of each part making use of special boundary conditions resembling the real life situation as best as possible. The design was modeled from scratch in Abaqus to be able to easily trim the design for optimal dimensions. All geometries showed acceptable results with respect to stress and deformations. As the analysis progressed, dimensions of the SL geometry and the Inventor assembly were adjusted, making the Inventor model up to date.

The fourth task was to look at the local response of the SL geometry as the SL separates in Abaqus. For this analysis it was decided to look at the loading which was considered dangerous for the SL geometry at separation. This was the moment load, since this is the only loading which still gets



transferred through the SL one hundred percent. As the SL was separated bit by bit, the stresses from contact forces inside the SL were monitored, resulting in the identification of a critical range where the material reaches yield stress. This range of separation distance was limited to the last twenty millimeters of separation. Since the contact surfaces should be polished and lubricated, wedging effects is unlikely to happen, also because of the rather small contact and friction surface left of the separation. Of course, the absolute final design of all details is to be set in later study, but the analysis has helped gathering information on how the SL will behave under the applied load case.

The last task was to develop an outline and more specific design of the system which closes the well bore after SL initiation. With some inspiration from the Shear-ram valves normally placed in BOP's and WCP's, a similar system has been developed. This specially designed cutting mechanism is activated when the SL separates. The cutting mechanism cuts the umbilical line, disrupting the command signal from the operator to the well. The cutting of the umbilical line will result in a total utilization of all fail-safe features in the well stack, cutting nearly any obstacle in the well bore and securing the well.

To sum up the system which has been developed during this thesis, a simple reliability study has been performed. This study helped illustrate some problems with the SL design. In general, the greatest challenges seem to be located in the trigger and closing systems. This is highly expected since the system has not been tested and is only developed on paper.

This thesis has been most educative for the candidate. The mixing of different program structures, designing and analyzing at the same time and the continuously control calculations to ensure the functional aspects of the system, has been highly interesting.



9.0 FURTHER WORK

Since the concept and systems has only been designed by one person, all systems and design geometry would gain from a total and detailed design review done by a team of qualified engineers. The probability of defining more critical issues regarding operation and functioning design increases drastically by involving fresh thinking heads. This chapter has been written as a pointer to where the further work of the SL concept should continue.

9.1 TRIGGER SYSTEM

The trigger system is developed mainly with its functions in mind in this thesis. Detailed design work is yet to be developed. Possible vendors and specialists on the positioning system designed for the SL should be involved to conclude to some degree if the system could function as intended. This is important if one should continue with the further design. Also, the measured off-set parameter, functioning as a moment control, should be assessed further. This is to ensure that the off-set monitoring would be able to actually monitor the right parameter in a satisfying way.

It is possible that the room which is made for the trigger system in the SL geometry is not sufficient. This could result in a major redesign of the SL. This should be assessed as the work progresses.

The system is designed with redundancy. The level of redundancy should be assessed further and evaluated. Should the system for some reason not possess the right level of redundancy for all components, the system could be redesigned in extent.

9.2 UMBILICAL CUTTING MECHANISM

The umbilical cutting mechanism functions should be assessed further in a design review. In the preliminary design done in this thesis, the shear ram function is powered by the trigger system. As the reliability study implies, designing a system which cuts the umbilical by utilizing forces from the two separating connectors, could make the cutting function more reliable. This could result in a special geometry which could be less effective with respect to geometry size and weight. More design work should be able to come up with more concepts which could lead to a more reliable result.



9.3 THE GEOMETRY OF THE SAFETY LINK

The geometry of the SL made in this thesis has been proven to give satisfying results. A detailed design review is likely to generate comments and improvements to the geometry. This will generate more design work.

In this thesis, the loading is highly simple compared to real life loading. More detailed information on the expected loading scenario is needed. The more detailed loading will result in further work in Abaqus. The SL should be tested with dynamic loading. Especially the accidental and extreme loading scenarios should be tested. Combined dynamic loading from moment and tension could also give implications to the total SL geometry and functions. This should be analyzed in extent to prevent any surprises when scale testing is commenced.



10.0 REFERENCES

1. **James Brekke, Subrata Chakrabarti, John Halkyard.** *Handbook of Offshore Engineering-Volumes 1-2.* Huston : Elsevier Ltd., 2005. ISBN: 978-0-08-044381-2.
2. **Hays, Kirsten.** Update 1- Shell starts production at Perdido. *REUTERS.* Wed. Mar 31, 2010, Vol. 2010.
3. **Robertson, Campbell.** Search continues after oil rig blast. *The New York Times.* Internet article, April 21, 2010, Vol. 2010.
4. **The Daily Telegraph.** Deepwater Horizon oil spill stopped, says BP. *Telegraph.co.uk.* Internet article, 15 Jul 2010, Vol. 2010.
5. **Whipple, Tom.** Deepwater Horizon: The Aftermath. *Post Carbon Institute.* Internet article, Aug 5, 2010, Vol. 2010.
6. **Yong Bai, Qiang Bai.** *Subsea Pipelines and Risers.* s.l. : Elsevier, 2005. ISBN: 978-0-080-4456-63.
7. **Sangesland, Sigbjørn og Golan, Michael.** Introduction to subsea production technology. Trondheim : Lecture notes from TPG4200, Subsea Production Systems, Okt. 1994.
8. **Bai, Yong og Bai, Qiang.** *Subsea Pipelines and Risers.* Great Britain : Elsevier Ltd, 2005. ISBN: 0-080-4456-67.
9. **Kongsberg Maritime.** <http://www.km.kongsberg.com/>. *Alt:* http://en.wikipedia.org/wiki/Dynamic_positioning. [Internett] 2011. [Siteret: 12 February 2011.] <http://www.km.kongsberg.com/ks/web/nokbg0240.nsf/AllWeb/14E17775E088ADC2C1256A4700319B04?OpenDocument>.
10. **Karlsen, Ludvig et. al.** *Fishing Technology, Part 2: Hydro Acoustics.* s.l. : Landbruksforlaget, 2001. ISBN:9788252923872.
11. **Jahn, Frank, Cook, Mark og Graham, Mark.** *Hydrocarbon Exploration and Production.* Amsterdam : Elsevier BV, 2008. ISBN:978-0-444-53236-7.
12. **Green Tweed.** <http://www.gtweed.com>. [Internett] 27 04 2011. [Siteret: 27 04 2011.] <http://www.gtweed.com>.
13. **Dahlvig, Christensen, Strømsnes.** *Konstruksjonselementer.* Malmö : Gyldendal Norsk Forlag, 2000 2nd. edition. ISBN: 82-585-0100-1.



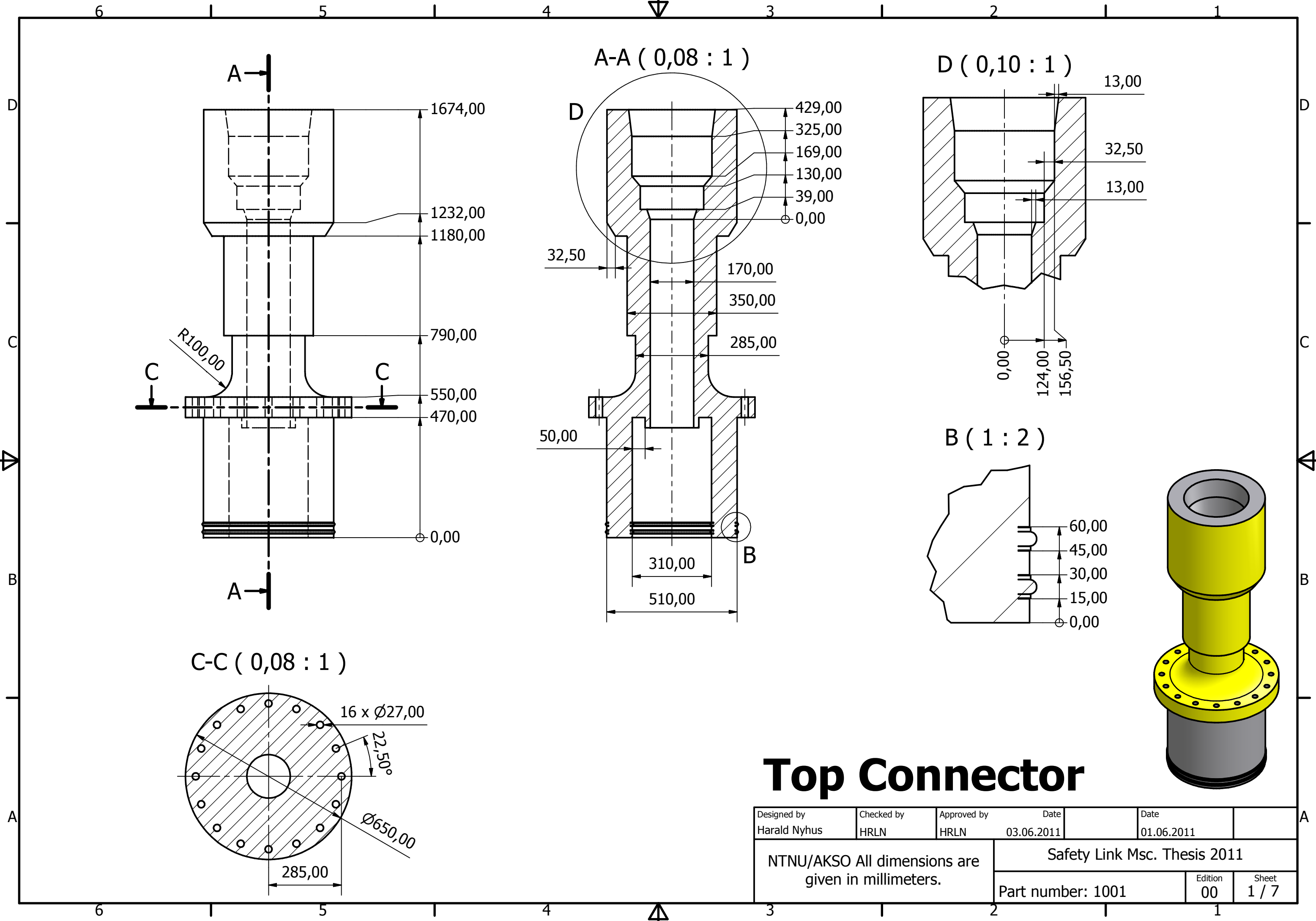
14. **Anderson, T.L.** *Fracture Mechanics, Fundamentals and Applications. 3rd. edition.* s.l. : CRC Press, 2005. ISBN:0-8493-1656-1.
15. **Schweitzer, Philip A.** *Fundamentals of corrosion : mechanisms, causes, and preventative methods / Philip A. Schweitzer.* s.l. : CRC Press, 2010. ISBN:9781420067712.
16. **NORSOK.** Design and operation of subsea production systems -- Part 7: Completion/workover riser systems. *ISO 13628-7:2005.* Geneva, Switzerland : ISO copyright office, 2005. Vol. 2005.
17. **Faltinsen, O.M.** *Sea Loads on Ships and Offshore Structures.* Cambridge : Cambridge University Press, 1990. ISBN:0-521-45870-6.
18. **Roy Beardmore.** RoyMech. [Internett] 23 12 2009. [Sisert: 05 04 2011.] http://www.roymech.co.uk/Useful_Tables/Screws/Preloading.html.
19. **Moan, Torgeir.** *Kompendium: TMR4190- Finite Element Modelling and Analysis of Marine Structures.* Trondheim, Norway : Department of Marine Technology, 2003. U K-03-98.
20. **NORSOK.** Design and operation of subsea production systems---Part 4: Subsea wellhead and tree equipment. *ISO 13628-4:2010.* Geneva, Switzerland : ISO copyright office, 2010. Vol. 2010.
21. **Wikipedia.** en.wikipedia.org. [Internett] December 2004. [Sisert: 1 6 2011.] http://en.wikipedia.org/wiki/File:MMS463a_shear_ram_forces.png.
22. **National Ground Water Association.** *Illustrated Glossary of Ground Water Industry Terms: Hydrogeology, Geophysics, Borehole Construction, and Water Conditioning.* s.l. : National Ground Water Association, 2003. ISBN: 978-1-56034-103-1.
23. **Johannesen, Kjell.** *Konstruksjonsteknikk.* Bergen : Fagbokforlaget, 2001. ISBN: 82-7674-636-5.
24. **Nardone, Paul J.** *Well Testing Project Management - Onshore and Offshore Operations.* s.l. : Elsevier, 2009. ISBN: 978-1-85617-600-2.

10.1 FIGURE REFERENCE

All figures are made by the candidate, unless otherwise is described.

Appendix A

Drawings of developed SL components and systems.

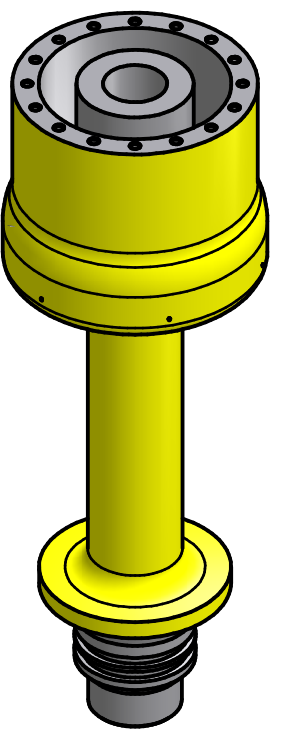
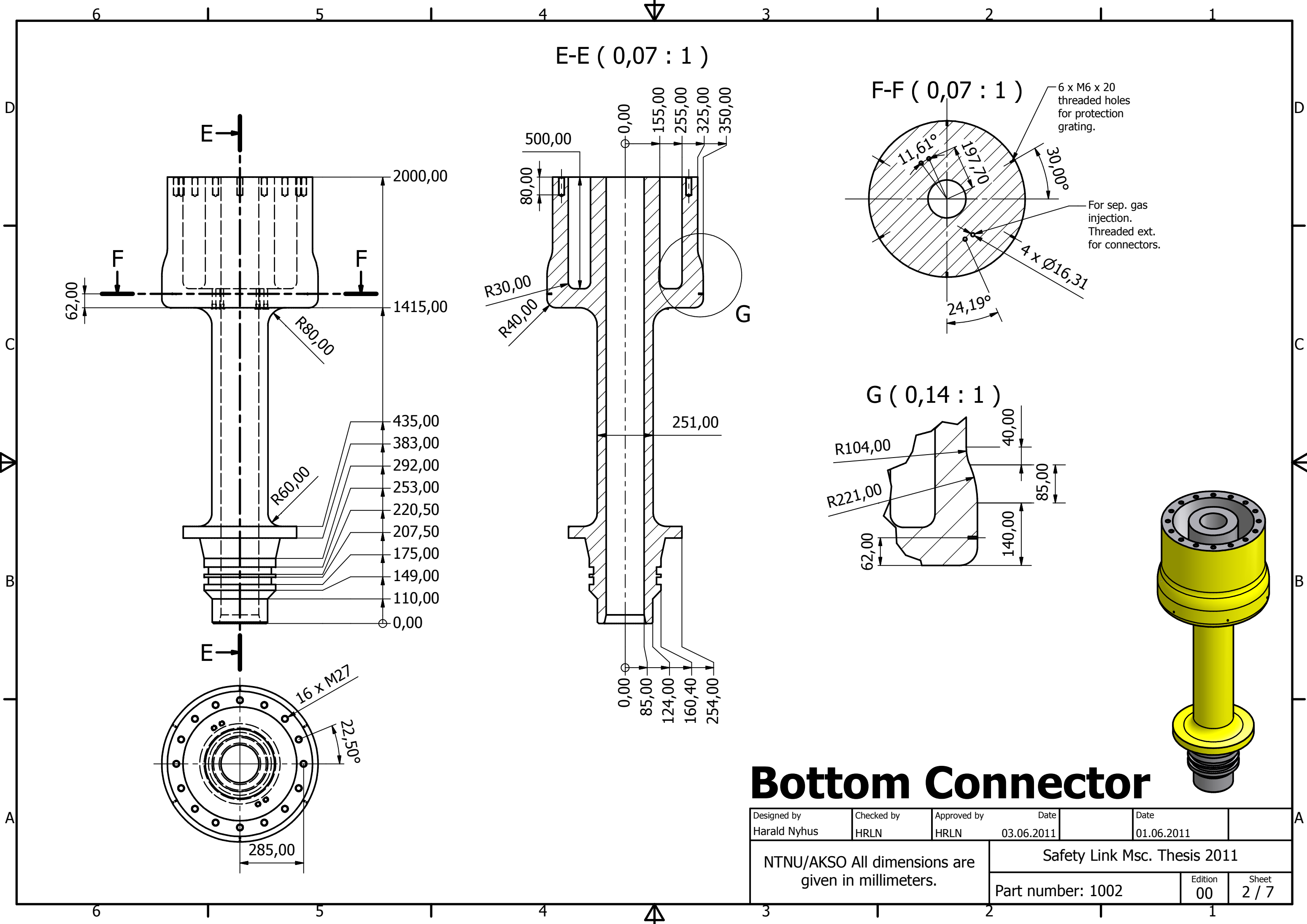


Top Connector

Designed by Harald Nyhus	Checked by HRLN	Approved by HRLN	Date 03.06.2011	Date 01.06.2011
NTNU/AKSO All dimensions are given in millimeters.			Safety Link Msc. Thesis 2011	
Part number: 1001			Edition 00	Sheet 1 / 7

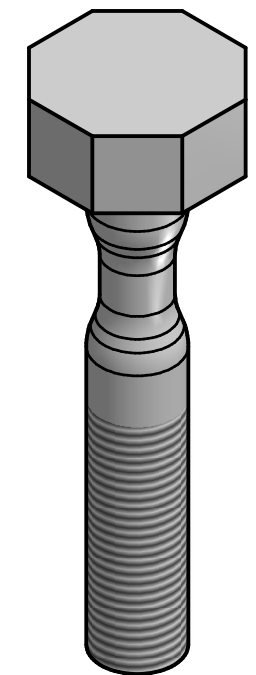
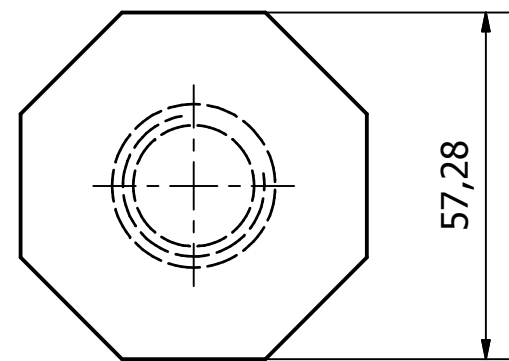
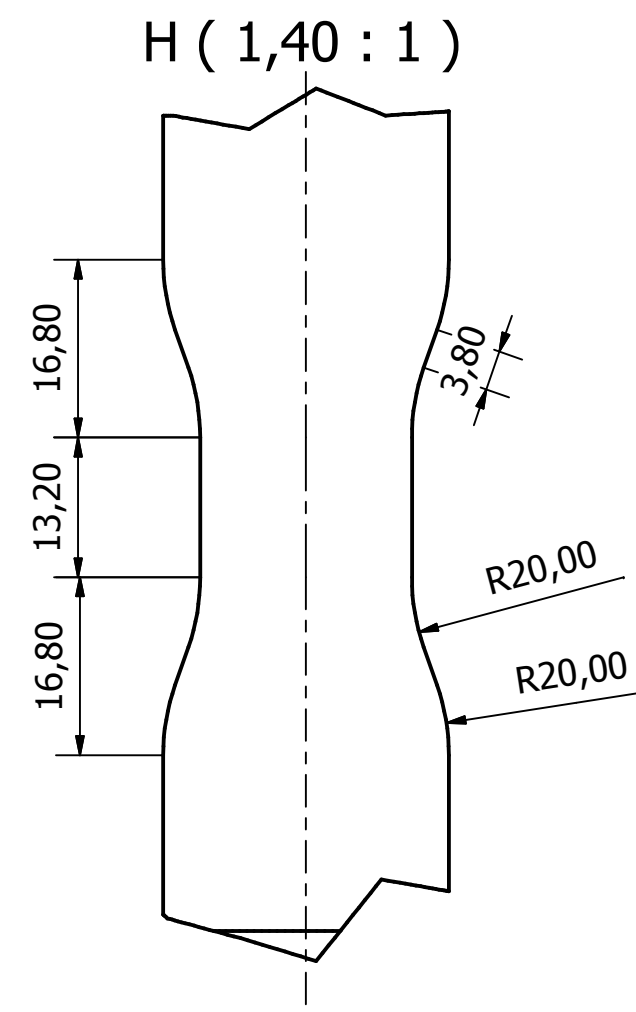
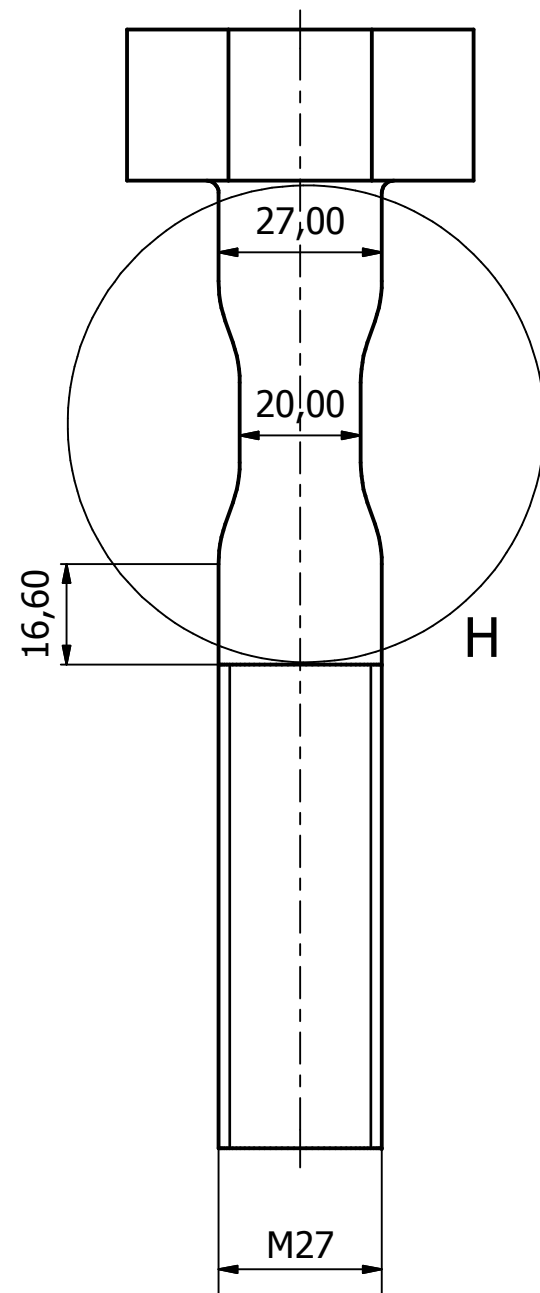
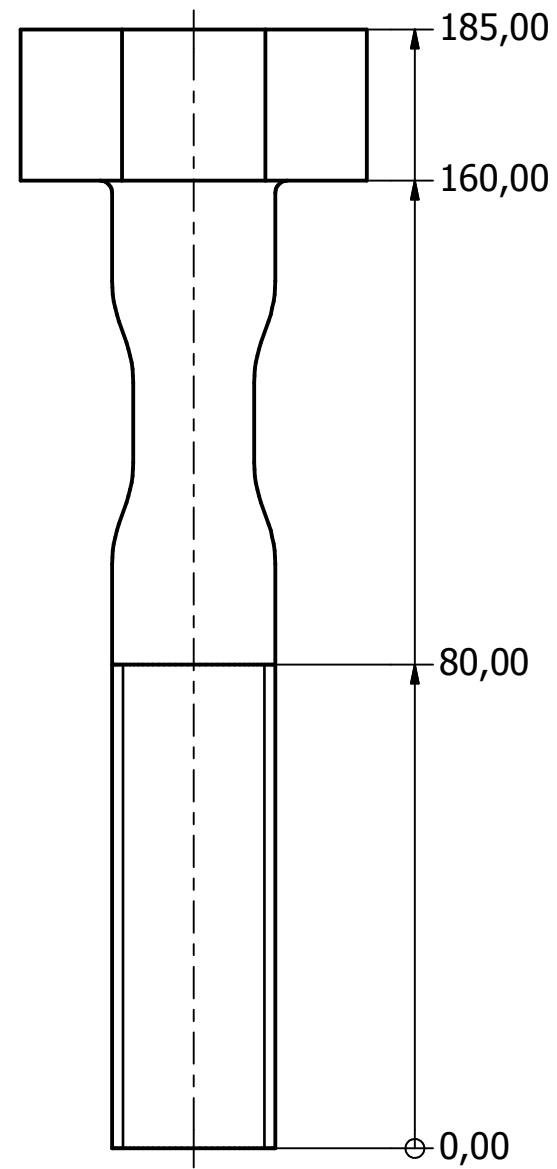
PRODUCED BY AN AUTODESK EDUCATIONAL PRODUCT

PRODUCED BY AN AUTODESK EDUCATIONAL PRODUCT



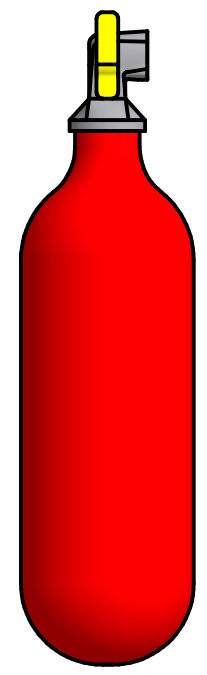
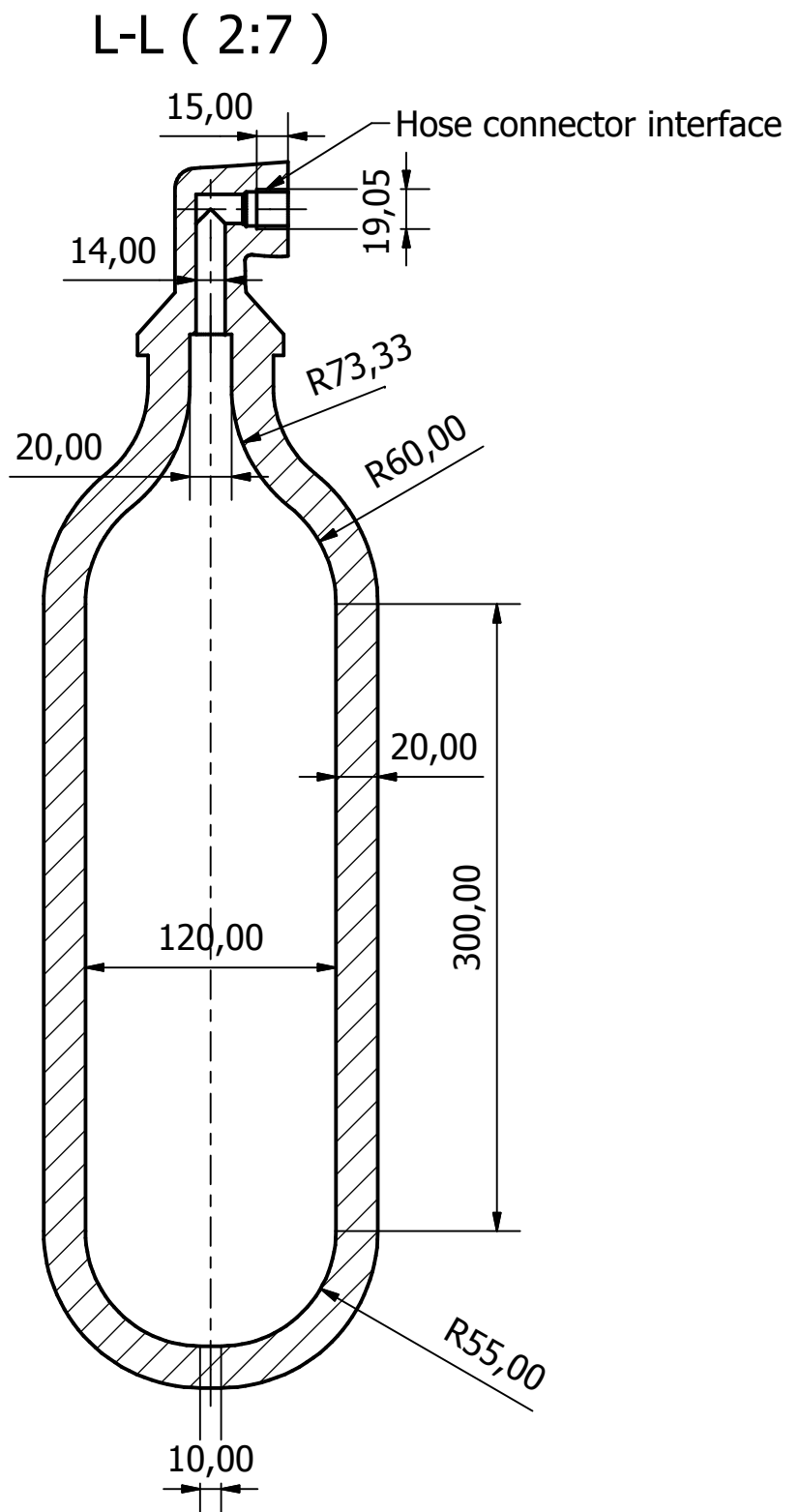
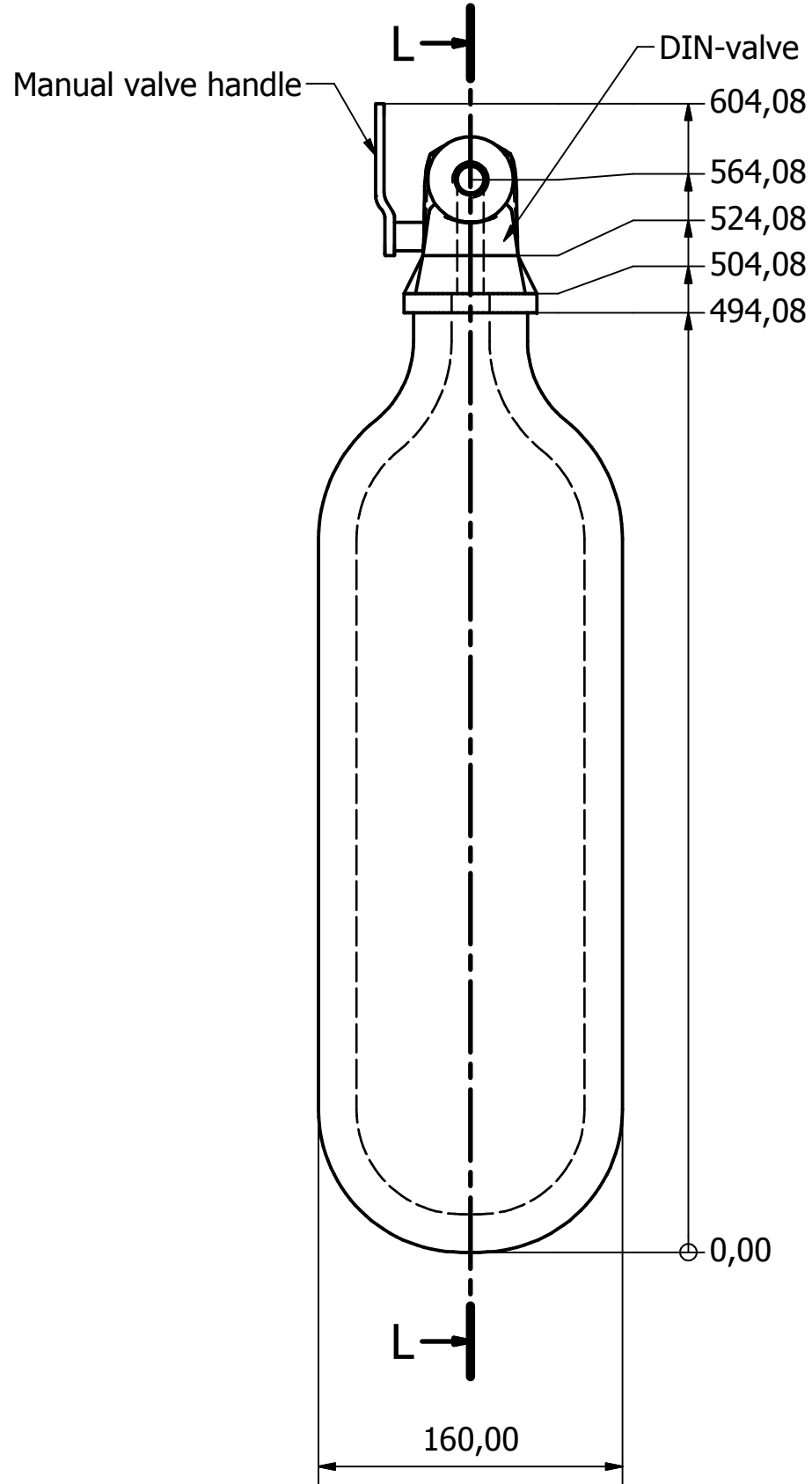
Bottom Connector

Designed by Harald Nyhus	Checked by HRLN	Approved by HRLN	Date 03.06.2011	Date 01.06.2011
NTNU/AKSO All dimensions are given in millimeters.			Safety Link Msc. Thesis 2011	
Part number: 1002			Edition 00	Sheet 2 / 7



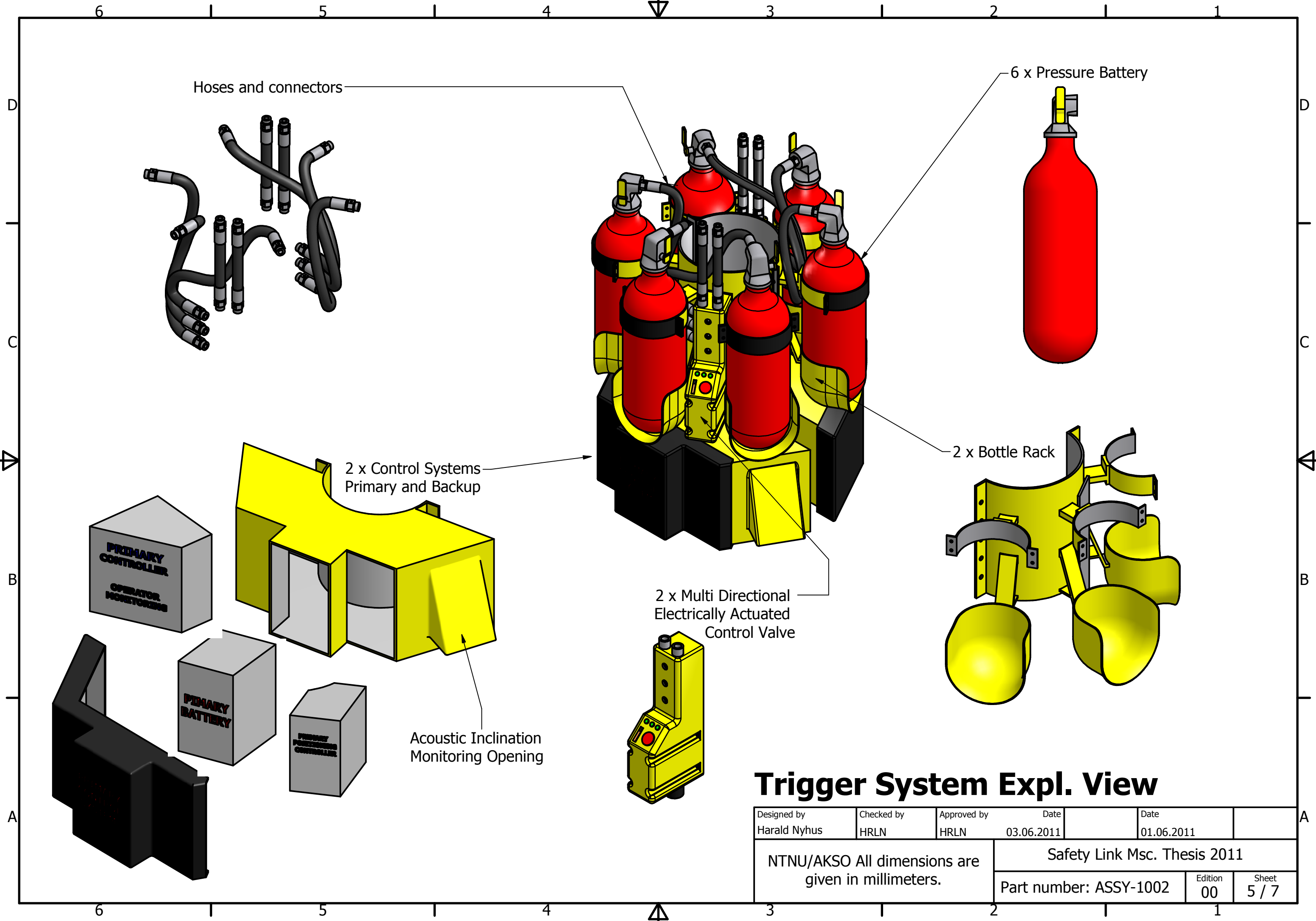
Safety Link Bolt

Designed by Harald Nyhus	Checked by HRLN	Approved by HRLN	Date 03.06.2011	Date 01.06.2011
NTNU/AKSO All dimensions are given in millimeters.			Safety Link Msc. Thesis 2011	
Part number: 1003			Edition 00	Sheet 3 / 7



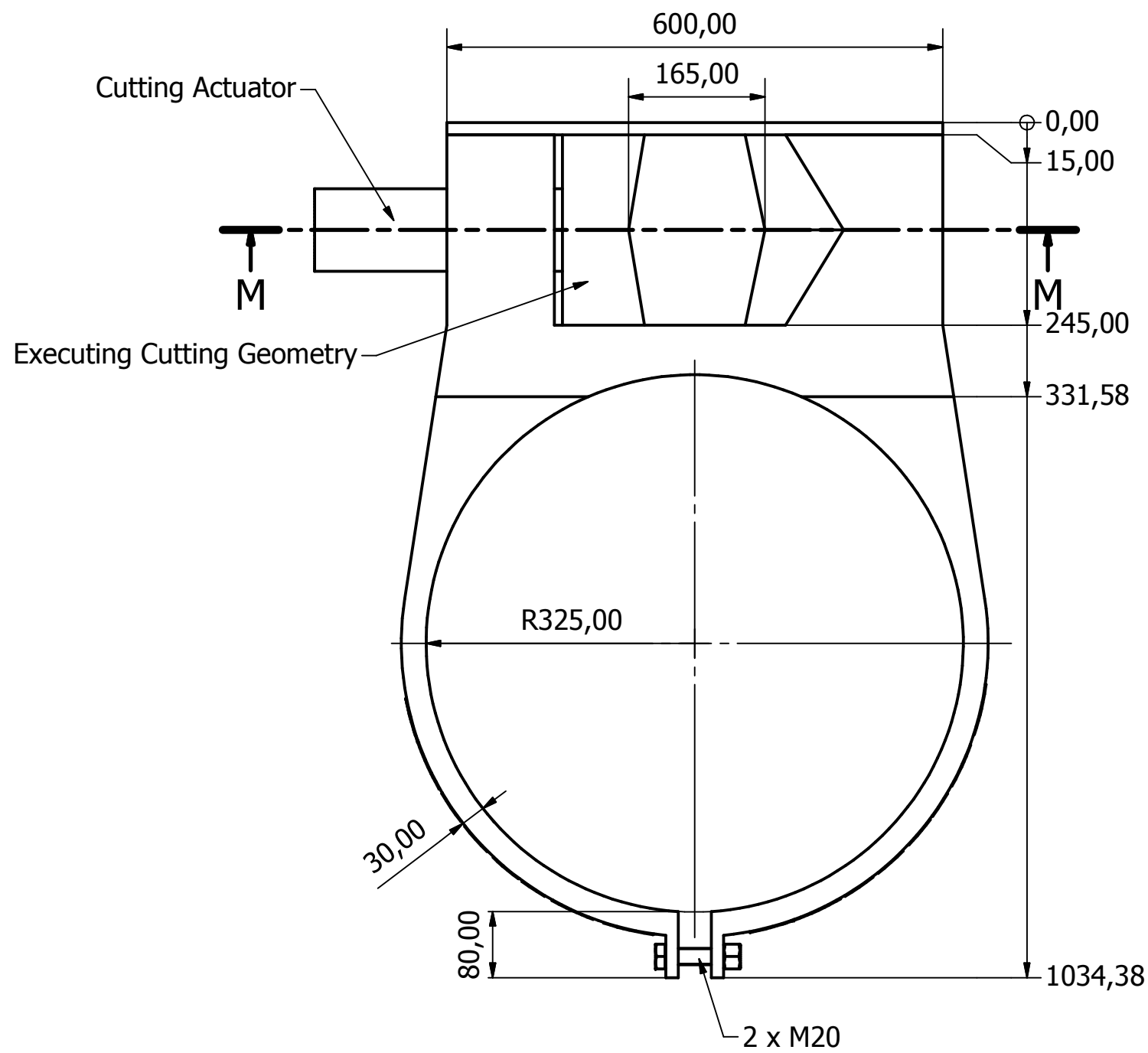
Pressure Battery

Designed by Harald Nyhus	Checked by HRLN	Approved by HRLN	Date 03.06.2011	Date 01.06.2011
NTNU/AKSO All dimensions are given in millimeters.			Safety Link Msc. Thesis 2011	
			Part number: ASSY-1001	Edition 00
				Sheet 4 / 7

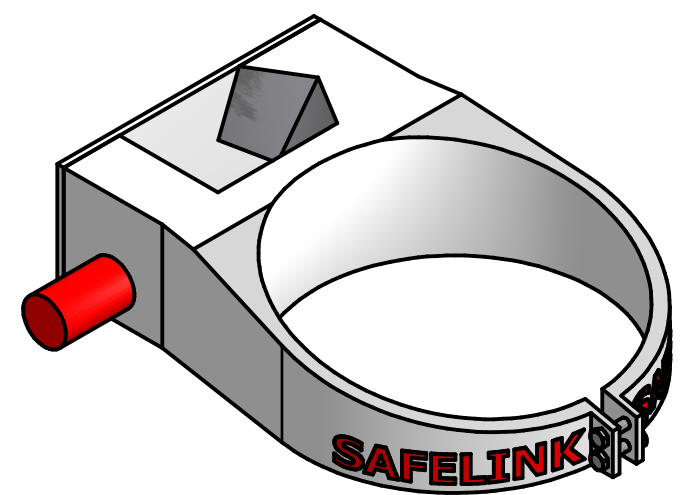
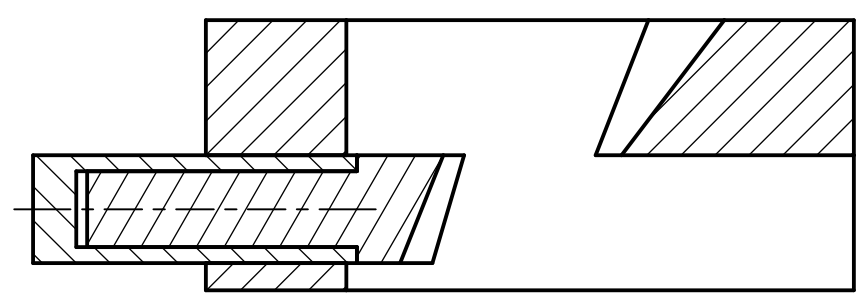


Trigger System Expl. View

Designed by Harald Nyhus	Checked by HRLN	Approved by HRLN	Date 03.06.2011	Date 01.06.2011
NTNU/AKSO All dimensions are given in millimeters.			Safety Link Msc. Thesis 2011	
			Part number: ASSY-1002	Edition 00
				Sheet 5 / 7

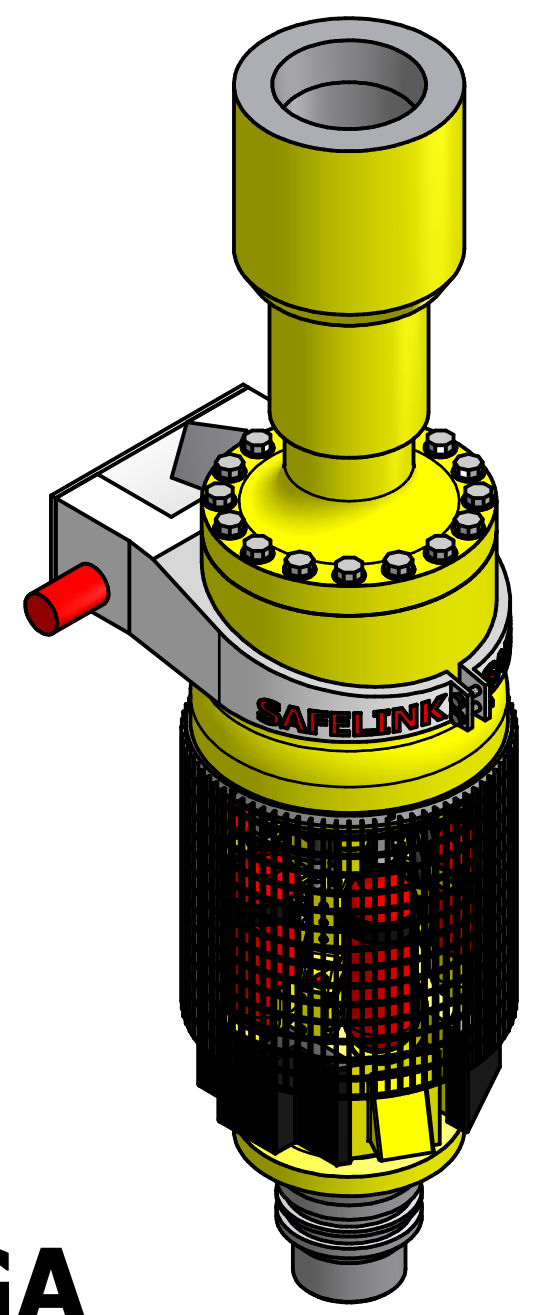
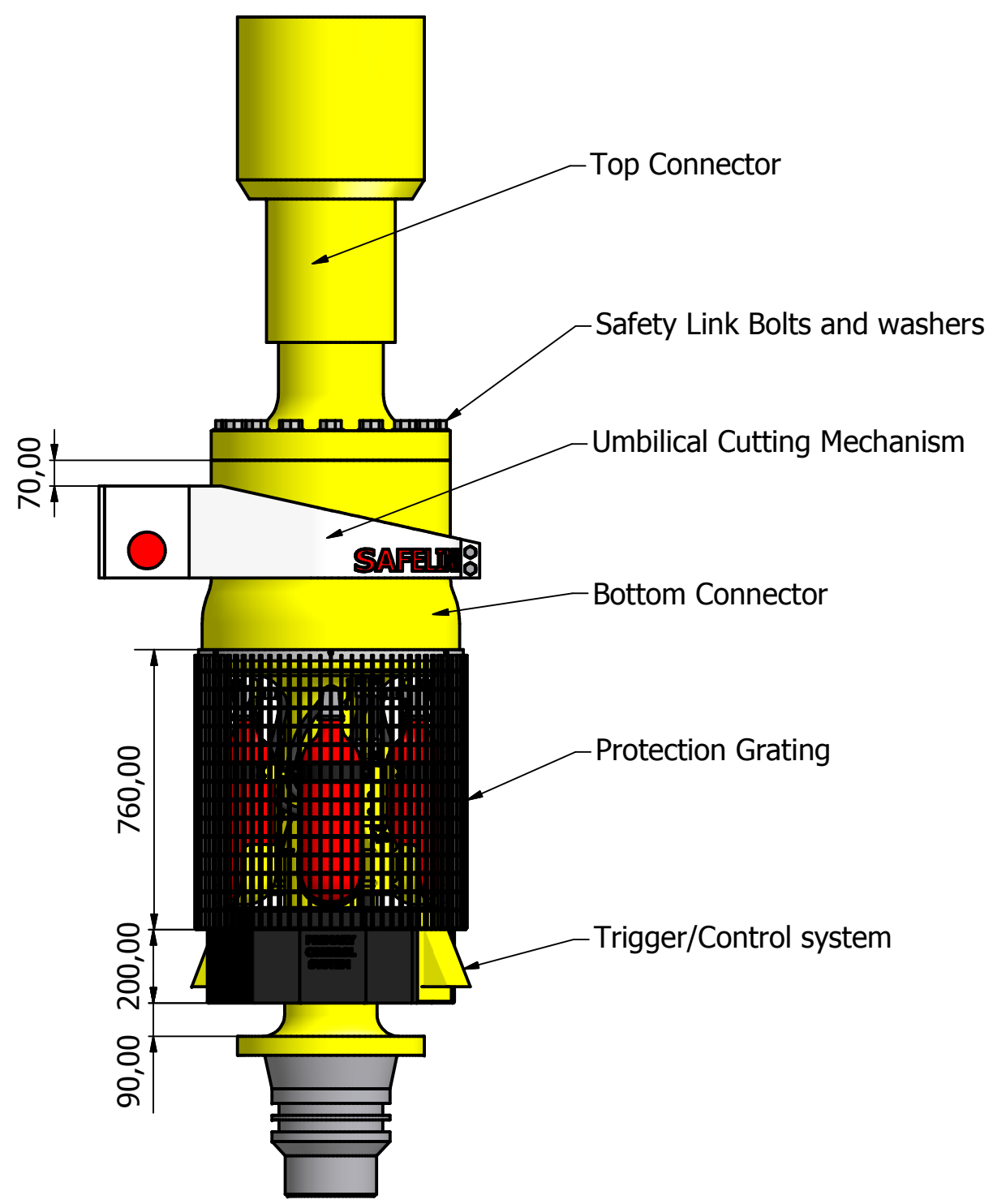


M-M (1 : 7)



Umb. Cutting System

Designed by Harald Nyhus	Checked by HRLN	Approved by HRLN	Date 03.06.2011	Date 01.06.2011
NTNU/AKSO All dimensions are given in millimeters.		Safety Link Msc. Thesis 2011		
		Part number: ASSY-1003	Edition 00	Sheet 6 / 7



Safety Link GA

Designed by Harald Nyhus	Checked by HRLN	Approved by HRLN	Date 03.06.2011	Date 01.06.2011
NTNU/AKSO All dimensions are given in millimeters.		Safety Link Msc. Thesis 2011		
		Part number: ASSY-1004	Edition 00	Sheet 7 / 7

Appendix B

Datasheet; GT-rings 13000-14000 series.



METRIC G-T® RINGS

13,000 & 14,000 Series

COMPACT SEAL

The unique G-T® Ring provides a compact double-acting seal for use in new designs for light or heavy duty applications where a more bulky type of seal had previously been required.

This proven seal combines a tough, resilient, T-shaped sealing element with precisely dimensioned, pressure-activated non-extrusion rings (Figure 1) in applications where pressures may range to 10,000 psi (690 bar) or higher.

The seal eliminates several major sealing problems:

1. Sealing element is protected from extrusion where clearances are large or pressures are high,
2. Prevents spiral failure common to O-Rings, and
3. As non-extrusion rings are radially activated, they may be fabricated of materials with high shear strengths that will successfully bridge large clearance gaps encountered during high pressure cylinder breathing or incidental to use of wear rings. For more than 40 years, the G-T Ring has been used by the Ordnance Department in recoil systems and by Industrial designers to solve their most severe sealing problems encountered in a wide variety of industrial, mobile and oil field requirements.

Utilize related ISO recommendations where appropriate as follows:

1. ISO/R286, tolerances (where suitable),
2. ISO 468, surface roughness, and
3. ISO 3286, Single Point Cutting tools-corner radii.

The sequential range of rod and bore diameters for each cross section are recommended for G-T seal type usage in dynamic applications only. Extension of range of diameters in each cross section group is possible but should be discussed with Greene, Tweed. For example, use of 1.78 mm cross section seal in a 20 mm dynamic piston application would not be recommended in favor of a 2.12 mm Cx seal.

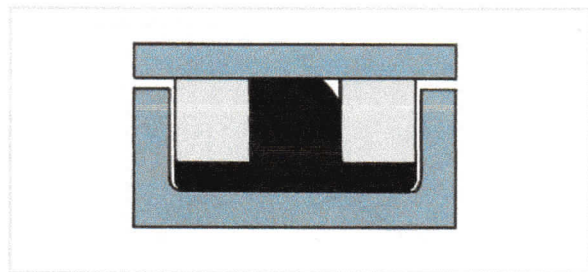


Figure 1

TABLE 1 ELASTOMERIC COMPOUND SELECTOR

Service Conditions	Temp Range	Base Polymer	Durometer Hardness (Shore A)	Compound Designator	Compatible Non-Extrusion Ring Material*
HYDRAULIC FLUIDS					
General purpose hydraulic oils, petroleum base lubricating oils, air	-40°C to 149°C	NBR (Nitrile)	70	173	TFE, NWR
Water, water-glycols, soluble oils	-40°C to 100°C	AU (Urethane)	70	367	TFE
Water-glycol, ASTM oils #1,2,3,5	-40°C to 163°C	NBR	70	173	TFE
Silicone Oils	-54°C to 163°C	Fluoraz® EYPEL Polyphosphazene	75	737	TFE,NWR
Pydraul 10E 29E, Fyrquel	-40°C to 149°C	NBR	70	173	TFE, NWR
	-54°C to 149°C	EPR (Ethylene propylene)	80	952	TFE, NWR
	-54°C to 163°C	Fluoraz (was PNF)	75	737	
	-54°C to 121°C	EPDM (Ethylene propylene diener terpolymer)	70	801	TFE, NWR, P5
	-54°C to 163°C	Fluoraz	75	733	
Pydraul 30E, 50E, 90E, 115E	-29°C to 204°C	FKM	70	731	TFE, P5, P8
	-54°C to 163°C	Fluoraz	75	737	TFE, P4
FUELS					
Gasoline, Kerosene	-54°C to 71°C	NBR	70	160	TFE, NWR
	-29°C to 204°C	FKM	70	731	TFE, P5, P8
BRAKE FLUIDS					
Automotive (SAE-J-1703)	-54°C to 121°C	EPDM	70	813	
Petroleum, Silicone	-54°C to 149°C	EPR	80	952	TFE, P4
ATF fluids, low aniline point oils	-54°C to 163°C	Fluoraz	75	737	
	-40° to 149°C	NBR	70	700	TFE, NWR, P5
	-54° to 163°C	Fluoraz	75	737	
GASES					
Refrigeration gases, freons	-40°C to 121°C	CR	75	156	TFE, NWR, P4
Nitrogen and most inert gases	-54°C to 135°C	NBR	70	160	
	-40°C to 107°C	NBR	70	173	TFE, NWR, P4
	-29°C to 175°C	FKM	70	731	
Chemicals, lubricating oils, solvents	-29°C to 204°C	FKM	70	731	TFE, P8
Well-drilling fluids, petroleum-based fluids, good low temperature service	-51°C to 121°C	CO (Epichlorohydrin)	80	957	TFE, NWR, P8
Steam, amines, H ₂ S (sour gas). (Very low permeability material)	0°C to 230°C	Fluoraz (Tetrafluoroethylene-propylene Elastomer)	52 (Shore D)	790	
			75	797	TFE, NWR, P8
			90	799	

*TFE: Virgin or filled to GT spec.

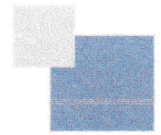


TABLE 2 13,000 & 14,000 SERIES PISTON TYPE DIMENSIONAL INFORMATION

GT CODE	Ød4		Ød3		Ød9	GROOVE WIDTH G (+ 0.25/-0)			RADII		
	Bore ID (mm)	Tolerance H8 (microns)	Gland OD (mm)	Tolerance h8 (microns)	Piston OD (mm)	Tolerance (microns)	b Narrow (mm)	b1 Intermed. (mm)	b2 Wide (mm)	r1 (mm)	r2 (mm)
10800	6.3	+22	3.40	+ 0	6.3	- 25 (e9)	2.39*	3.78	5.26	0.3	0.1
10900	7	- 0	4.10	- 18	7	- 61				0.5	0.3
11000	8		5.10		8						
11100	9		6.10	+ 0	9						
11200	*10		7.10	- 22	10						
11300	11	+27	8.10		11	- 32 (e9)					
11400	*12	- 0	9.10		12	- 75					
21400	*12		7.60		12		3.58	4.65	6.22	0.3	0.1
21500	13		8.60		13					0.5	0.3
21600	*14		9.60		14						
21700	15		10.60		15						
21800	*16		11.61	+ 0	16						
21900	*18		13.61	- 27	18						
22000	*20	+ 33	15.61		20	- 40 (e9)					
22100	21	- 0	16.61		21	- 92					
22200	*22		17.61		22						
22300	23		18.61		23						
32200	*22		15.99	+ 0	22	- 20 (f9)	4.78	5.97	7.72	0.4	0.1
32300	23		16.99	- 33	23	- 72				0.8	0.3
32400	*25		18.99		25						
32500	27		20.99		27						
32600	28		21.99		28						
32700	30		23.99		30						
32800	*32	+ 39	26.00		32	- 25 (f9)					
32900	33	- 0	27.00		33	- 87					
33000	35		29.00		35						
33100	*36		30.00		36						
33200	38		32.00	+ 0	38						
33300	*40		34.00	- 39	40						
33400	42		36.00		42						
33500	*45		39.00		45						
53500	*45		35.78				7.14	8.48	10.77	0.4	0.1
53600	48		38.78		48					0.8	0.3
53700	*50		40.78		50						
53800	55	+ 46	45.78		55	- 30 (f9)					
53900	*56	- 0	46.78		56	- 104					
54000	60		50.79	+ 0	60						
54100	*63		53.79	- 46	63						

*Noted tolerance is not recommended, GT recommends a tolerance of +0.13/-0.

TABLE 2 13,000 & 14,000 SERIES PISTON TYPE DIMENSIONAL INFORMATION

GT CODE	Ød4		Ød3		Ød9		GROOVE WIDTH G (+ 0.25/-0)			RADII	
	Bore ID (mm)	Tolerance H8 (microns)	Gland OD (mm)	Tolerance h8 (microns)	Piston OD (mm)	Tolerance (microns)	b Narrow (mm)	b1 Intermed. (mm)	b2 Wide (mm)	r1 (mm)	r2 (mm)
54200	65	+ 46	55.79	+ 0	65	- 30 (f9)	7.14	8.48	10.77	0.4	0.1
54300	70	0	60.79	- 46	70	- 104				0.8	0.3
54400	75		65.79		75						
54500	*80		70.79		80						
54600	85	+ 54	75.79		85	- 36 (e9)					
54700	*90	- 0	80.79	+ 0	90	- 123					
54800	95		85.79	- 54	95						
54900	*100		90.79		100						
55000	105		95.79		105						
55100	*110		100.79		110						
55200	115		105.79		115						
55300	120		110.79		120						
55400	*125	+ 63	115.80		125	- 43 (f8)					
55500	130	- 0	120.80		130	- 106					
55600	135		125.80		135						
75600	135		122.65	+ 0	135		9.53	12.07	14.71	0.8	0.1
75700	*140		127.65	- 63	140					1.2	0.3
75900	150		137.65		150						
76100	*160		147.65		160						
76300	170		157.65		170						
76500	*180		167.65		180						
76700	190	+ 72	177.65		190	- 50 (f8)					
76900	*200	- 0	187.66	+ 0	200	- 122					
77100	210		197.66	- 72	210						
77300	*220		207.66		220						
77400	225		212.66		225						
77500	230		217.66		230						
77600	235		222.66		235						
77900	*250		237.66		250						
78200	265	+ 81	252.67	+ 0	265	- 56 (f8)					
78400	*280	- 0	267.67	- 81	280	- 137					
78600	300		387.67		300						
78700	*320	+ 89	307.67		320	- 62 (f8)					
78800	340	- 0	327.68	+ 0	340	- 151					
78900	*360		347.68	- 89	360						
79000	380		367.68		380						
79100	*400		387.68		400						

*Noted tolerance is not recommended, GT recommends a tolerance of +0.13/-0.

TABLE 3 13,000 & 14,000 SERIES ROD TYPE DIMENSIONAL INFORMATION

GT CODE	d5		d6		d10		GROOVE WIDTH G (+0.25/-0)			RADII	
	Rod OD (mm)	Tolerance f8 (microns)	Gland ID (mm)	Tolerance H8 (microns)	Housing ID (mm)	Tolerance H8 (microns)	b Narrow (mm)	b1 Intermed. (mm)	b2 Wide (mm)	r1 (mm)	r2 (mm)
10500	4	-10	6.97	+22	4	+18	2.39*	3.78	5.26	0.2	0.1
10600	5	-28	7.97	-0	5	-0				0.4	0.3
10700	6		8.97		6						
10800	6.3	-13	9.27		6.3	+22					
10900	7	-35	9.97		7	-0					
11000	8		10.97	+27	8						
11100	9		11.97	-0	9						
21200	*10		14.50		10		3.58	4.65	6.22	0.2	0.1
21300	11	-16	15.50		11	+27				0.4	0.3
21400	*12	-43	16.50		12	-0					
21500	13		17.50		13						
21600	*14		18.50	+33	14						
21700	15		19.50	-0	15						
21800	*16		20.50		16						
21900	*18		22.50		18						
32000	*20	-20	26.07		20	+33	4.78	5.97	7.72	0.4	0.1
32100	21	-53	27.07		21	-0				0.8	0.3
32200	*22		28.07		22						
32300	23		29.07		23						
32400	*25		31.06	+39	25						
32500	27		33.06	-0	27						
32600	28		34.06		28						
32700	30		36.06		30						
32800	*32	-25	38.05		32	+39					
32900	33	-64	39.05		33	-0					
33000	35		41.05		35						
33100	36		42.05		36						
33200	38		44.05		38						
53300	*40		49.17		40		7.14	8.48	10.77	0.4	0.1
53400	42		51.17	+46	42					0.8	0.3
53500	45		54.17	-0	45						
53600	48		57.17		48						
53700	*50		59.17		50						
53800	55	-30	64.16		55	+46					
53900	56	-76	65.16		56	-0					
54000	60		69.16		60						
54100	*63		72.16		63						
54200	65		74.16		65						
54300	70		79.16		70						
54400	75		84.16	+54	75						
54500	*80		89.16	-0	80						
54600	85	-36	94.15		85	+54					
54700	90	-90	99.15		90	-0					
54800	95		104.15		95						
54900	*100		109.15		100						
55000	105		114.15		105						
55100	110		119.15		110						

*Noted tolerance is not recommended, GT recommends a tolerance of +0.13/-0.

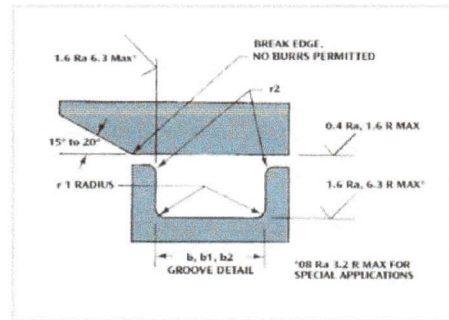
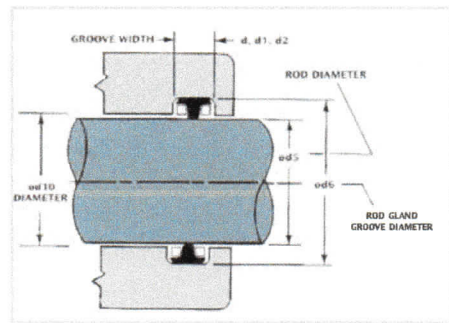
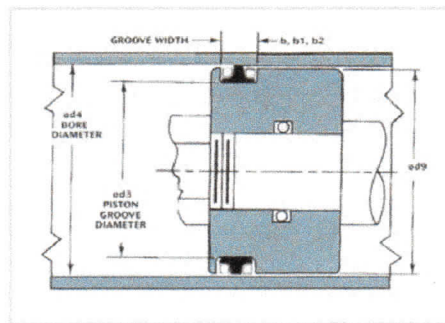
TABLE 3 13,000 & 14,000 SERIES ROD TYPE DIMENSIONAL INFORMATION

GT CODE	Ød5		Ød6		Ød10		GROOVE WIDTH G (+0.25/-0)			RADII	
	Rod OD (mm)	Tolerance H8 (microns)	Gland ID (mm)	Tolerance h8 (microns)	Housing ID (mm)	Tolerance (microns)	b Narrow (mm)	b1 Intermed. (mm)	b2 Wide (mm)	r1 (mm)	r2 (mm)
75200	115	<u>-36</u>	127.12	<u>+63</u>	115	<u>+54</u>	9.53	12.07	14.71	0.8	0.1
75300	120	-90	132.12	-0	120	-0				1.2	0.3
75400	*125	<u>-43</u>	137.12		125	<u>+63</u>					
75500	130	-106	142.12		130	-0					
75600	135		147.12		135						
75700	140		152.12		140						
75800	145		157.12		145						
75900	150		162.12		150						
76000	155		167.12		155						
76100	*160		172.12		160						
76200	165		177.12		165						
76300	170		182.11	<u>+72</u>	170						
76400	175		187.11	-0	175						
76500	180		192.11		180						
76600	185	<u>-50</u>	197.10		185	<u>+72</u>					
76700	190	-122	202.10		190	-0					
76800	195		207.10		195						
76900	*200		212.10		200						
77000	205		217.10		205						
77100	210		222.10		210						
77200	215		227.10		215						
77300	220		232.10		220						
77400	225		237.10		225						
77500	230		242.10		230						
77600	235		247.10		235						
77700	240		252.09	<u>+81</u>	240						
77800	245		257.09	-0	245						
77900	*250		262.09		250						
78000	255	<u>-56</u>	267.09		255	<u>+81</u>					
78100	260	-137	272.09		260	-0					
78200	265		277.09		265						
78300	270		282.09		270						
78400	*280		292.09		280						
78500	290		302.09		290						
78600	300		312.09		300						
78700	*320	<u>-62</u>	332.07	<u>+89</u>	320	<u>+89</u>					
78800	340	-151	352.07	-0	340	-0					
78900	*360		372.07		360						
79000	380		392.07		380						
79100	*400		412.06	<u>+97</u>	400						
79200	425	<u>-68</u>	437.05	-0	425	<u>+97</u>					
79300	450	-165	462.05		450	-0					
79400	475		487.05		475						

*Noted tolerance is not recommended, GT recommends a tolerance of +0.13/-0.

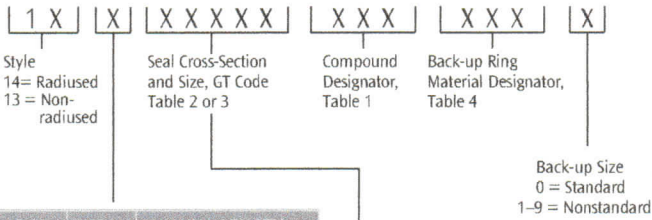
TABLE 4 ANTI-EXTRUSION RING MATERIAL SELECTOR

Pressure (bar)	Clearance Limits (mm)	Recommended Anti-Extrusion Ring Material	Designator
200	Without Wear Rings See Table 3 and 4	Virgin TFE: to MIL-R-8791 NWR: Wear Resistant Nylon to L-P-410a P4: Graphite filled TFE to GT spec. P5: Glass and MoS ₂ filled TFE to GT spec.	005 006 016 021
	With Wear Rings 0.64 diametral clearance for 5.3 mm or 7.00 mm Cx seals	NWR: Wear Resistant Nylon to L-P-410a P5: Glass and MoS ₂ filled TFE to GT spec.	006 021
200-350	Without Wear Rings See Tables 3 and 4	Staged Virgin TFE: to MIL-R-8791 NWR: Wear Resistant Nylon to L-P-410a	050
	With Wear Rings Contact GT Engineering	Staged Virgin TFE: to MIL-R-8791 NWR: Wear Resistant Nylon to L-P-410a P8: Arlon®	070



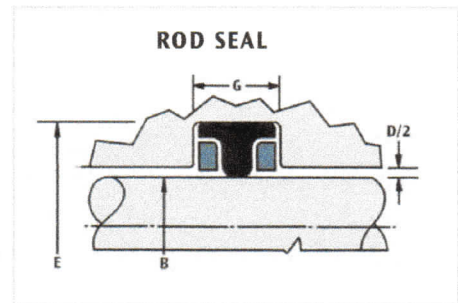
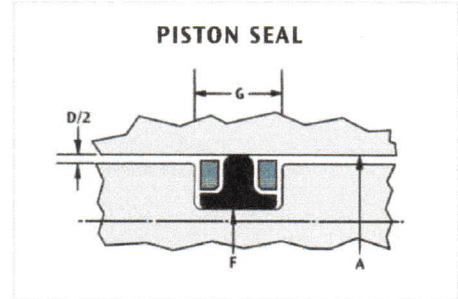
PART NUMBERING SYSTEM

The part numbering system requires the use of the material designator tables found in the above text. For nonstandard designs contact GT engineering.



ROD	PISTON	AXIAL LENGTH
1	2	Narrow Base
3	4	Intermediate Base
5	6	Wide Base
7	8	Narrow Base L-Ring

DESIGNATOR (First digit of Basic Part Number column)	NOM. CROSS SECTION (mm)
1	1.80
2	2.65
3	3.55
5	5.30
7	7.00



Contact Us

Greene, Tweed
Oilfield
Kulpsville, PA, USA

Tel: +1.281.765.4500
Tel: +1.800.927.3301
Fax: +1.281.765.4553

Appendix C

MatLab codes applied for pressure change calculation when SL separates.


```

close all
clear all

g=9.81;

%forspenningskrav, Fra konstr. elem.

Sy_Im01=1000;
F_pull=300000*9.81; % N
n=16;
F1=F_pull/n;
Fa=1.8*F1;
d=15.31;

% Kapasitetsjekk hele sammenstilling
disp('N, hele sammenstillingen i strekk');
F_tot2=(n*Sy_Im01*(pi*d^2/4))/g % N

% Design Separasjonstrykk ASME, flasker må tåle dette
disp('MPa, designtrykk flasker');
P_bottle_design=40*1.5+(40*1.5)*0.1

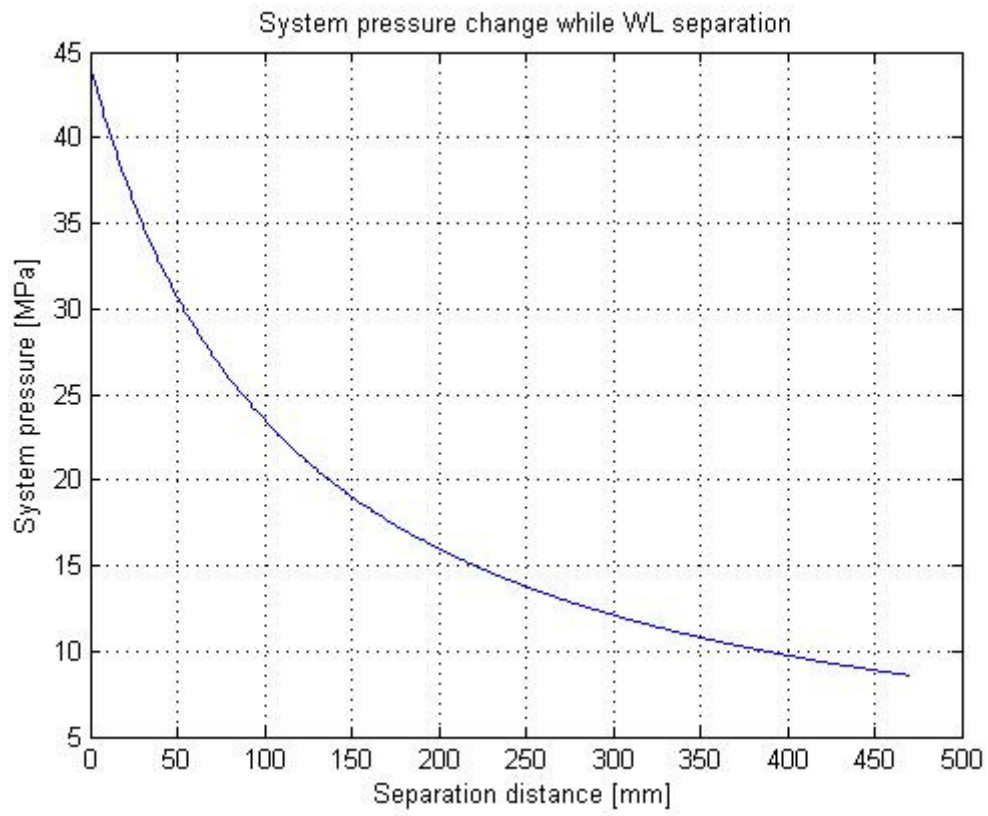
% Volum av flasker
disp('Volum av alle flasker. kubikkmeter, m^3');
v1=((pi*0.12^2/4)*0.3+((4/3)*pi*0.06^3))*3

%Trykkfallet etter initiering ved 500 bar trykk

p1=50000000;
P_decrease=zeros(470,1);
for i=1:470;
    dist=(i/1000);
    v2=v1+(((pi*0.450^2/4)-
(pi*0.370^2/4))*(0.030))+((4/3)*pi*0.030^3)+(((pi*0.510^2/4)-
(pi*0.310^2/4))*dist);
    format long g
    p2=(p1*v1/(v2))/10^6;
    P_decrease(i)=P_decrease(i)+p2;
end;

plot(P_decrease)
grid
title('System pressure change while WL separation');
xlabel('Separation distance [mm]');
ylabel('System pressure [MPa]');

```



Appendix D

Material datasheet; AISI 8630, AISI 4340 and Ti-20%Ti.

General properties

Designation

AISI 8630

UNS number	G86300		
Density	7.79e3	-	7.87e3 kg/m ³
Price	* 4.69	-	5.16 NOK/kg

Tradenames

P11, Pelton Casteel, Inc. (USA); P10, Pelton Casteel, Inc. (USA);

Composition overview

Composition (summary)

Fe/.28-.33C/.4-.6Cr/.4-.7Ni/.7-.9Mn/.15-.3Si/.15-.25Mo/<.035P/<.04S

Base	Fe (Iron)
------	-----------

Composition detail


C (carbon)	0.28	-	0.33	%
Cr (chromium)	0.4	-	0.6	%
Fe (iron)	96.8	-	97.9	%
Mn (manganese)	0.7	-	0.9	%
Mo (molybdenum)	0.15	-	0.25	%
Ni (nickel)	0.4	-	0.7	%
P (phosphorus)	0	-	0.035	%
S (sulfur)	0	-	0.04	%
Si (silicon)	0.15	-	0.3	%

Bio-data

RoHS (EU) compliant grades? 

Toxicity rating Non-toxic

Mechanical properties

Young's modulus	200	-	210	GPa
Flexural modulus	* 200	-	210	GPa
Shear modulus	76	-	79.9	GPa
Bulk modulus	185	-	195	GPa
Poisson's ratio	0.32	-	0.333	
Shape factor	46			
Yield strength (elastic limit)	483	-	534	MPa
Tensile strength	621	-	686	MPa
Compressive strength	483	-	534	MPa
Flexural strength (modulus of rupture)	483	-	534	MPa
Elongation	6	-	15	% strain
Hardness - Vickers	173	-	213	HV
Fatigue strength at 10 ⁷ cycles	* 294	-	339	MPa
Fatigue strength model (stress range)	* 192	-	233	MPa
Parameters: Stress Ratio = 0, Number of Cycles = 1e7 				
Fracture toughness	* 72	-	114	MPa.m ^{0.5}
Mechanical loss coefficient (tan delta)	* 7.2e-4	-	8.9e-4	

Thermal properties

Melting point	1.46e3	-	1.51e3	°C
Maximum service temperature	445	-	496	°C
Minimum service temperature	* -73	-	-48	°C
Thermal conductivity	47	-	50.9	W/m.°C
Specific heat capacity	461	-	480	J/kg.°C
Thermal expansion coefficient	12.4	-	13.1	µstrain/°C
Latent heat of fusion	* 265	-	280	kJ/kg

Processing properties

Carbon equivalency 0.278 - 0.417

Electrical properties

Electrical resistivity * 23 - 35 μohm.cm

Optical properties

Transparency Opaque

Durability: flammability

Flammability Non-flammable

Durability: fluids and sunlight

Water (fresh) Acceptable
 Water (salt) Limited use
 Weak acids Limited use
 Strong acids Unacceptable
 Weak alkalis Acceptable
 Strong alkalis Limited use
 Organic solvents Excellent
 UV radiation (sunlight) Excellent
 Oxidation at 500C Acceptable

Geo-economic data for principal component

Principal component Iron
 Typical exploited ore grade 45.1 - 49.9 %
 Minimum economic ore grade 25 - 70 %
 Abundance in Earth's crust 3.9e4 - 4.31e4 ppm
 Abundance in seawater 2.38e-4 - 2.63e-4 ppm
 Annual world production 1.14e9 - 1.26e9 tonne/yr
 Reserves 7.51e10 - 8.3e10 tonne

Main mining areas

China, Brazil, Australia, India, Russia.

Primary material production: energy, CO2 and water

Embodied energy, primary production 32 - 38 MJ/kg
 CO2 footprint, primary production 2.01 - 2.22 kg/kg
 NOx creation * 12.6 - 13.9 g/kg
 SOx creation * 21.5 - 23.8 g/kg
 Water usage 36.9 - 111 l/kg

Eco-indicators for principal component

Eco-indicator 95 110 millipoints/kg
 Eco-indicator 99 198 millipoints/kg

Material processing: energy

Casting energy * 4.06 - 4.49 MJ/kg
 Forging, rolling energy * 2.65 - 2.93 MJ/kg
 Metal powder forming energy * 37.8 - 42 MJ/kg
 Vaporization energy * 25.1 - 27.7 MJ/kg
 Conventional machining energy (per unit wt removed) * 5.3 - 5.86 MJ/kg
 Non-conventional machining energy (per unit wt removed) * 47 - 52 MJ/kg

Material processing: CO2 footprint

Casting CO2 * 0.244 - 0.269 kg/kg
 Forging, rolling CO2 * 0.212 - 0.234 kg/kg
 Metal powder forming CO2

	* 3.02	- 3.36	kg/kg
Vaporization CO2	* 2.01	- 2.22	kg/kg
Conventional machining CO2 (per unit wt removed)	* 0.424	- 0.469	kg/kg
Non-conventional machining CO2 (per unit wt removed)	* 3.76	- 4.16	kg/kg

Material recycling: energy, CO2 and recycle fraction

Recycle	✓		
Embodied energy, recycling	* 9.28	- 10.3	MJ/kg
CO2 footprint, recycling	* 0.562	- 0.621	kg/kg
Recycle fraction in current supply	39.9	- 44	%
Downcycle	✓		
Combust for energy recovery	✗		
Landfill	✓		
Biodegrade	✗		
A renewable resource?	✗		

Possible substitutes for principal component

Iron is the least expensive and most widely used metal. In most applications, iron and steel compete either with less expensive nonmetallic materials or with more expensive materials having a property advantage. Iron and steel compete with lighter materials, such as aluminum and plastics, in the motor vehicle industry; aluminum, concrete, and wood in construction; and aluminum, glass, paper, and plastics in containers.

Notes

Typical uses

General construction; general mechanical engineering; automotive; Pressure vessels; pipework;

Warning

Some rare heat treatments of certain alloys may produce values for mechanical properties outside the given ranges, e.g. AISI 9255. tempered at 205C

Reference sources

Data compiled from multiple sources. See links to the References table.

Standards with similar compositions

The following information is taken from ASM AlloyFinder 3 - see link to References table for further information.

AFNOR 30NCD2 (France)
DIN 30NiCrMo2-2 (Germany)
DIN WNr 1.6545 (Germany)
UNI 7356(74) 30NiCrMo2KB (Italy)
DGN B-203 8630 (Mexico)
DGN B-297 8630 (Mexico)
NMX-B-300(91) 8630 (Mexico)
UNE F.129 (Spain)
AMS 6280 (USA)
AMS 6281 (USA)
AMS 6530 (USA)
AMS 6535 (USA)
AMS 6550 (USA)
AMS 7496 (USA)
ASTM A29/A29M(93) 8630 (USA)
ASTM A322(96) 8630 (USA)
ASTM A331(95) 8630 (USA)
ASTM A513(97a) 8630 (USA)
ASTM A519(96) 8630 (USA)
ASTM A752(93) 8630 (USA)
ASTM A829/A829M(95) 8630 (USA)
DoD-F-24669/1(86) 8630 (USA)
MIL-S-16974E(86) 8630 (USA)
MIL-S-18728D(83) 8630 (USA)
MIL-S-46059 G86300 (USA)
MIL-S-6050A(94) 8630 (USA)
SAE 770(84) 8630 (USA)
SAE J404(94) 8630 (USA)
AISI 8630 (USA)
COPANT 334 8630 (Venezuela)
COPANT 514 8630 (Venezuela)

Links

[ProcessUniverse](#)

[Producers](#)

[Reference](#)

[Shape](#)

General properties

Designation

AISI 4340

UNS number

G43400

Density

7.8e3 - 7.9e3 kg/m³

Price

* 5.77 - 6.34 NOK/kg

Tradenames

A-1270, AFORA (Aceros Afora S.A.) (SPAIN); A-1272, AFORA (Aceros Afora S.A.) (SPAIN);

Composition overview

Composition (summary)

Fe/.38-.43C/.7-.9Cr/1.65-2Ni/.6-.8Mn/.15-.35Si/.2-.3Mo/<.035P/<.04S

Base

Fe (Iron)

Composition detail

Element	Min	Max	Unit
C (carbon)	0.38	0.43	%
Cr (chromium)	0.7	0.9	%
Fe (iron)	95.1	96.3	%
Mn (manganese)	0.6	0.8	%
Mo (molybdenum)	0.2	0.3	%
Ni (nickel)	1.65	2	%
P (phosphorus)	0	0.035	%
S (sulfur)	0	0.04	%
Si (silicon)	0.15	0.35	%

Bio-data

RoHS (EU) compliant grades? 

Toxicity rating

Non-toxic

Mechanical properties

Young's modulus	205	213	GPa
Flexural modulus	* 205	213	GPa
Shear modulus	79	83	GPa
Bulk modulus	158	174	GPa
Poisson's ratio	0.285	0.295	
Shape factor	29		
Yield strength (elastic limit)	770	950	MPa
Tensile strength	1.15e3	1.41e3	MPa
Compressive strength	770	950	MPa
Flexural strength (modulus of rupture)	770	950	MPa
Elongation	9	15	% strain
Hardness - Vickers	325	405	HV
Fatigue strength at 10 ⁷ cycles	* 472	545	MPa
Fatigue strength model (stress range)	* 304	424	MPa
<small>Parameters: Stress Ratio = 0, Number of Cycles = 1e7</small>			
Fracture toughness	* 57	96	MPa.m ^{0.5}
Mechanical loss coefficient (tan delta)	* 3.6e-4	4.5e-4	



Thermal properties

Melting point	1.43e3	1.51e3	°C
Maximum service temperature	* 613	653	°C
Minimum service temperature	* -63	-33	°C
Thermal conductivity	* 35	50	W/m.°C
Specific heat capacity	* 440	520	J/kg.°C
Thermal expansion coefficient	11.5	13	µstrain/°C
Latent heat of fusion	* 265	280	kJ/kg

Processing properties

Carbon equivalency 0.415 - 0.565

Electrical properties

Electrical resistivity * 18 - 27 μohm.cm

Optical properties

Transparency Opaque

Durability: flammability

Flammability Non-flammable

Durability: fluids and sunlight

Water (fresh) Acceptable
 Water (salt) Limited use
 Weak acids Limited use
 Strong acids Unacceptable
 Weak alkalis Acceptable
 Strong alkalis Limited use
 Organic solvents Excellent
 UV radiation (sunlight) Excellent
 Oxidation at 500C Acceptable

Geo-economic data for principal component

Principal component Iron
 Typical exploited ore grade 45.1 - 49.9 %
 Minimum economic ore grade 25 - 70 %
 Abundance in Earth's crust 3.9e4 - 4.31e4 ppm
 Abundance in seawater 2.38e-4 - 2.63e-4 ppm
 Annual world production 1.14e9 - 1.26e9 tonne/yr
 Reserves 7.51e10 - 8.3e10 tonne

Main mining areas

China, Brazil, Australia, India, Russia.

Primary material production: energy, CO2 and water

Embodied energy, primary production 32 - 38 MJ/kg
 CO2 footprint, primary production 2.01 - 2.22 kg/kg
 NOx creation * 12.6 - 13.9 g/kg
 SOx creation * 21.5 - 23.8 g/kg
 Water usage 36.9 - 111 l/kg

Eco-indicators for principal component

Eco-indicator 95 110 millipoints/kg
 Eco-indicator 99 198 millipoints/kg

Material processing: energy

Casting energy * 4.06 - 4.48 MJ/kg
 Forging, rolling energy * 3.59 - 3.97 MJ/kg
 Metal powder forming energy * 37.8 - 41.7 MJ/kg
 Vaporization energy * 25.1 - 27.7 MJ/kg
 Conventional machining energy (per unit wt removed) * 7.38 - 8.16 MJ/kg
 Non-conventional machining energy (per unit wt removed) * 47 - 52 MJ/kg

Material processing: CO2 footprint

Casting CO2 * 0.244 - 0.269 kg/kg
 Forging, rolling CO2 * 0.287 - 0.318 kg/kg
 Metal powder forming CO2

	* 3.02	- 3.34	kg/kg
Vaporization CO2	* 2.01	- 2.22	kg/kg
Conventional machining CO2 (per unit wt removed)	* 0.59	- 0.653	kg/kg
Non-conventional machining CO2 (per unit wt removed)	* 3.76	- 4.16	kg/kg

Material recycling: energy, CO2 and recycle fraction

Recycle	✓		
Embodied energy, recycling	* 9.28	- 10.3	MJ/kg
CO2 footprint, recycling	* 0.562	- 0.621	kg/kg
Recycle fraction in current supply	39.9	- 44	%
Downcycle	✓		
Combust for energy recovery	✗		
Landfill	✓		
Biodegrade	✗		
A renewable resource?	✗		

Possible substitutes for principal component

Iron is the least expensive and most widely used metal. In most applications, iron and steel compete either with less expensive nonmetallic materials or with more expensive materials having a property advantage. Iron and steel compete with lighter materials, such as aluminum and plastics, in the motor vehicle industry; aluminum, concrete, and wood in construction; and aluminum, glass, paper, and plastics in containers.

Notes

Typical uses

High tensile applications; General engineering parts; Through-hardened gears; Connecting rods and bolts; Gun barrels;

Other notes

A very popular, versatile steel. It can be heat-treated to produce a wide range of tensile strengths in moderate sections.

Reference sources

Data compiled from multiple sources. See links to the References table.

Standards with similar compositions

The following information is taken from ASM AlloyFinder 3 - see link to References table for further information.

IAS IRAM 4340 (Argentina)
 EN 10083/1(91)A1(96) 1.6582 (Belgium)
 EN 10083/1(91)A1(96) 1.7037 (Belgium)
 EN 10083/1(91)A1(96) 34CrNiMo6 (Belgium)
 EN 10083/1(91)A1(96) 34CrS4 (Belgium)
 BDS 6354 40ChN2M (Bulgaria)
 BDS 6354(74) 35Ch2N2M (Bulgaria)
 GB 3077(88) 40CrNiMoA (China)
 GB 8162(87) 40CrNiMoA (China)
 GB/T 3078(94) 40CrNiMoA (China)
 GB/T 3079(93) 40CrNiMoA (China)
 CSN 416341 16341 (Czech Republic)
 AFNOR NFA35551(75) 35NCD6 (France)
 DIN 40NiCrMo6 (Germany)
 DIN 40NiCrMo8-4 (Germany)
 DIN WNr 1.6562 (Germany)
 DIN WNr 1.6565 (Germany)
 MSZ 61(85) NCMo5 (Hungary)
 IS 1570 40Ni2Cr1Mo28 (India)
 IS 1570 40NiCr1Mo15 (India)
 UNI 5332(64) 40NiCrMo7 (Italy)
 UNI 6926(71) 40NiCrMo7 (Italy)
 UNI 7356(74) 40NiCrMo7KB (Italy)
 UNI 7845(78) 40NiCrMo7 (Italy)
 UNI 7874(79) 40NiCrMo7 (Italy)
 JIS G4103(79) SNCM439 (Japan)
 JIS G4103(79) SNCM8 (Japan)
 JIS G4108(94) SNB24-1 (Japan)
 JIS G4108(94) SNB24-2 (Japan)
 JIS G4108(94) SNB24-3 (Japan)
 JIS G4108(94) SNB24-4 (Japan)
 JIS G4108(94) SNB24-5 (Japan)
 DGN B-203 4340 (Mexico)
 DGN B-297 4340 (Mexico)
 NMX-B-300(91) 4340 (Mexico)
 AS 1444(96) 4340 (NSW Australia)
 PNH84030/04 36HNMA (Poland)
 PNH84030/04 40HNMA (Poland)
 GOST 4543 40Ch2N2MA (Russian Federation)
 GOST 4543(61) 38ChNWA (Russian Federation)
 GOST 4543(71) 36Ch2N2MFA (Russian Federation)
 GOST 4543(71) 38Ch2N2MA (Russian Federation)
 GOST 4543(71) 40Ch2N2MA (Russian Federation)
 UNE 36012(75) 35NiCrMo4 (Spain)
 UNE 36012(75) 40NiCrMo4 (Spain)
 UNE 36012(75) 40NiCrMo7 (Spain)
 UNE 36012(75) F.1272 (Spain)
 ISO 683-8 4 (Switzerland)
 ISO 683-8 4A (Switzerland)
 ISO 683-8 4b (Switzerland)
 ISO R683-8 4A (Switzerland)
 ISO R683-8 4b (Switzerland)
 BS 4670 818M40 (United Kingdom)
 BS 970/3(91) 817M40 (United Kingdom)
 AMS 6359 (USA)
 AMS 6409 (USA)
 AMS 6414 (USA)
 AMS 6415 (USA)
 AMS 6454 (USA)
 ASTM A29/A29M(93) 4340 (USA)
 ASTM A322(96) 4340 (USA)
 ASTM A331(95) 4340 (USA)
 ASTM A372 Type VII (USA)
 ASTM A506(93) 4340 (USA)
 ASTM A519(96) 4340 (USA)
 ASTM A646(95) Grade 7 (USA)
 ASTM A752(93) 4340 (USA)
 ASTM A829/A829M(95) 4340 (USA)
 DoD-F-24669/1(86) 4340 (USA)

warranty is given for the accuracy of this data. Values marked * are estimates.

Links

ProcessUniverse

Producers

Reference

Shape

General properties

Designation

MMC: CermeTi-20TiC(p)

Density	* 4.52e3	-	4.58e3	kg/m ³
Price	* 613	-	858	NOK/kg

Composition overview

Composition (summary)

Ti-6Al-4V/20%TiC(p)

Base Ti (Titanium)

Composition detail

Al (aluminum)	5	%
Ti (titanium)	72	%
TiC (titanium carbide)	20	%
Titanium carbide (particulate)	20	%
V (vanadium)	3.2	%

Bio-data

RoHS (EU) compliant grades? 

Toxicity rating Non-toxic

Mechanical properties

Young's modulus	139	-	158	GPa
Flexural modulus	* 139	-	158	GPa
Shear modulus	* 52.1	-	59.3	GPa
Bulk modulus	* 140	-	160	GPa
Poisson's ratio	* 0.33	-	0.35	
Shape factor	14			
Yield strength (elastic limit)	943	-	1.04e3	MPa
Tensile strength	959	-	1.05e3	MPa
Compressive strength	* 950	-	1.04e3	MPa
Flexural strength (modulus of rupture)	* 959	-	1.04e3	MPa
Elongation	0.3	-	0.31	% strain
Hardness - Vickers	* 240	-	270	HV
Fatigue strength at 10 ⁷ cycles	* 336	-	364	MPa
Fatigue strength model (stress range)	* 239	-	280	MPa
<u>Parameters:</u> Stress Ratio = 0, Number of Cycles = 1e7				
Fracture toughness	18.4	-	28	MPa.m ^{0.5}
Mechanical loss coefficient (tan delta)	* 8e-4	-	0.002	



Thermal properties

Melting point	1.63e3	-	1.66e3	°C
Maximum service temperature	380	-	430	°C
Minimum service temperature	-273			°C
Thermal conductivity	* 5.5	-	6	W/m.°C
Specific heat capacity	* 584	-	591	J/kg.°C
Thermal expansion coefficient	* 7.72	-	8.36	µstrain/°C
Latent heat of fusion	290	-	295	kJ/kg

Electrical properties

Electrical resistivity	* 178	-	191	µohm.cm
------------------------	-------	---	-----	---------

Optical properties

Transparency Opaque

Durability: flammability

Flammability Non-flammable

Durability: fluids and sunlight

Water (fresh)	Excellent
Water (salt)	Excellent
Weak acids	Excellent
Strong acids	Acceptable
Weak alkalis	Excellent
Strong alkalis	Acceptable
Organic solvents	Excellent
UV radiation (sunlight)	Excellent
Oxidation at 500C	Excellent

Geo-economic data for principal component

Principal component	Titanium		
Typical exploited ore grade	15.2	-	16.8 %
Minimum economic ore grade	2	-	30 %
Abundance in Earth's crust	5.32e3	-	5.88e3 ppm
Abundance in seawater	4.56	-	5.04 ppm
Annual world production	1.16e5	-	1.28e5 tonne/yr
Reserves	4.94e7	-	5.46e7 tonne

Primary material production: energy, CO2 and water

Embodied energy, primary production	* 1.4e3	-	1.55e3 MJ/kg
CO2 footprint, primary production	* 105	-	116 kg/kg
NOx creation	* 420	-	464 g/kg
SOx creation	* 840	-	928 g/kg

Material processing: energy

Casting energy	* 5.05	-	5.58 MJ/kg
Metal powder forming energy	* 47	-	52.1 MJ/kg
Vaporization energy	* 30.9	-	34.2 MJ/kg
Non-conventional machining energy (per unit wt removed)	* 57.9	-	64 MJ/kg
Advanced composite molding energy	* 10	-	22 MJ/kg

Material processing: CO2 footprint

Casting CO2	* 0.303	-	0.335 kg/kg
Metal powder forming CO2	* 3.76	-	4.17 kg/kg
Vaporization CO2	* 2.47	-	2.74 kg/kg
Non-conventional machining CO2 (per unit wt removed)	* 4.63	-	5.12 kg/kg
Advanced composite molding CO2	* 1.5	-	1.65 kg/kg

Material recycling: energy, CO2 and recycle fraction

Recycle	✓		
Embodied energy, recycling	* 350	-	387 MJ/kg
CO2 footprint, recycling	* 2.62	-	2.9 kg/kg
Recycle fraction in current supply	21.8	-	24.1 %
Downcycle	✓		
Combust for energy recovery	✗		
Landfill	✓		
Biodegrade	✗		
A renewable resource?	✗		

Possible substitutes for principal component

There are few substitutes for titanium in aircraft and space use without some sacrifice of performance. For industrial uses, high-nickel steel, zirconium, and, to a limited extent, the superalloy metals may be substituted. In certain applications, ground calcium carbonate, precipitated calcium carbonate, kaolin, and talc compete with titanium dioxide as a white pigment.

Notes

Typical uses

Aerospace: domed rocket cases, missile fins, aircraft engine components

Reference sources

Data compiled from multiple sources. See links to the References table.

Links

ProcessUniverse

Producers

Reference

Shape

Appendix E

SL design standard; ISO 13628-7:2005

Reproduction of the standard is not allowed.

ISO 13628-7:2005(E)

Please look up section 6.7.1 "*Safety joint or weak link*", page 119.

Appendix F

1. Maximum Bending Loads on Riser System for Connected Mode Operation
2. Schematic Representation of Riser System for Kristin Workover Riser
3. Riser Joint Interface Drawing

Table 4.6.2-3 Maximum Bending Loads on Riser System for Connected Mode Operations (kNm) 100% of Riser Tension from Ruckers with 25 Te (+/-23Te) Overpull at EDP Connector All Pressure Conditions							
Location	Node	Operating Limit					
		Hs=7.5m (-10 degs)	Hs=6.7m (-5 degs)	Hs=5.5m (-3 degs)	Hs=5.5m (3 degs)	Hs=6.7m (5 degs)	Hs=7.5m (10 degs)
CT_SPOOL_FLG	274	0	0	0	0	0	0
FLOWHEAD_FLG	271	21	14	13	12	16	19
FLOWHEAD_ADP	270	24	16	16	14	18	21
LAND_JT	248 - 270	144	94	63	52	108	128
USURFPUP_JT	238 - 248	184	121	79	64	93	166
TJ_TOP	233 - 238	187	123	81	67	84	168
TJ_BOT	212 - 233	187	123	81	67	84	168
URISER_JT	177 - 212	72	47	29	25	34	70
ULV_ADP	176	31	18	14	17	25	40
LV_BODY	175	32	19	14	17	25	40
LLV_ADP	174	32	19	14	17	26	41
LPUP_JTS	168 - 174	19	13	14	17	16	22
MRISER_JTS	61 - 168	47	27	18	24	36	59
SAFETY_JT	61	47	27	18	24	36	59
LRISER_JTS	48 - 61	505	284	177	205	329	561
SJ_PIPE	42 - 48	587	329	205	238	378	647
SJ_T6	41	662	370	230	268	423	725
SJ_T5	32	1002	556	345	403	621	1071
SJ_T4	26	1326	732	453	531	805	1394
SJ_T3	23	1574	867	537	630	946	1639
SJ_T2	20	1708	940	581	683	1020	1769
SJ_T1	19	1748	961	595	698	1042	1808
SJ_CONN	19	1748	961	595	698	1042	1808
EDP	16	2054	1125	693	818	1212	2108
WCP Flange	12	2418	1310	796	955	1411	2470
WCP Connector	11	2507	1354	820	987	1460	2559
TREE	5	2833	1507	894	1101	1633	2889
WHD	1	3250	1693	973	1237	1849	3317

The utilisation factors have been presented for 3°, 5° and 10° vessel offset based on $F_d=0.67$, $F_d=0.8$ and $F_d=1.0$ respectively.

Schematic Representation of Riser System Configured for Wireline Intervention

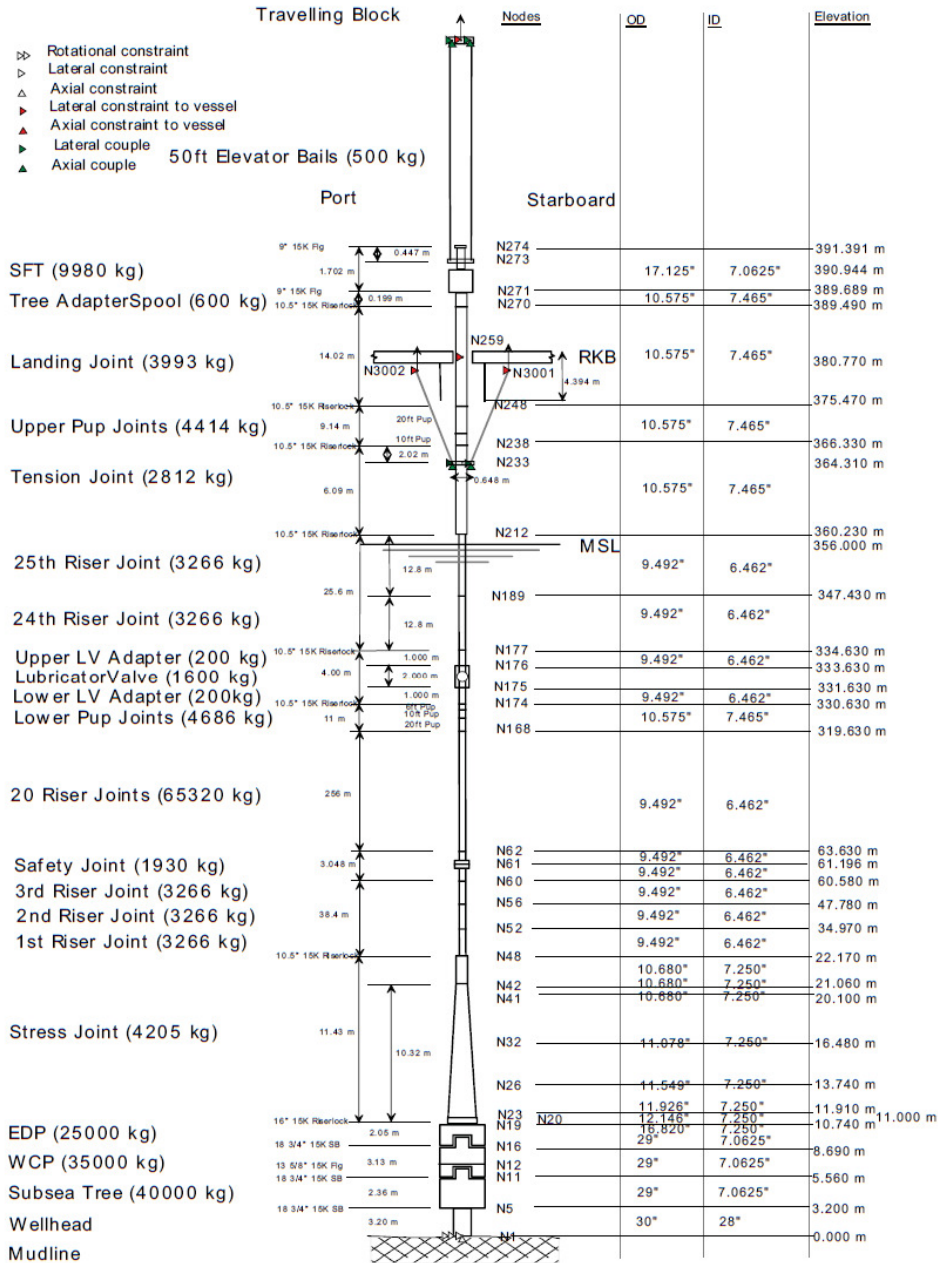
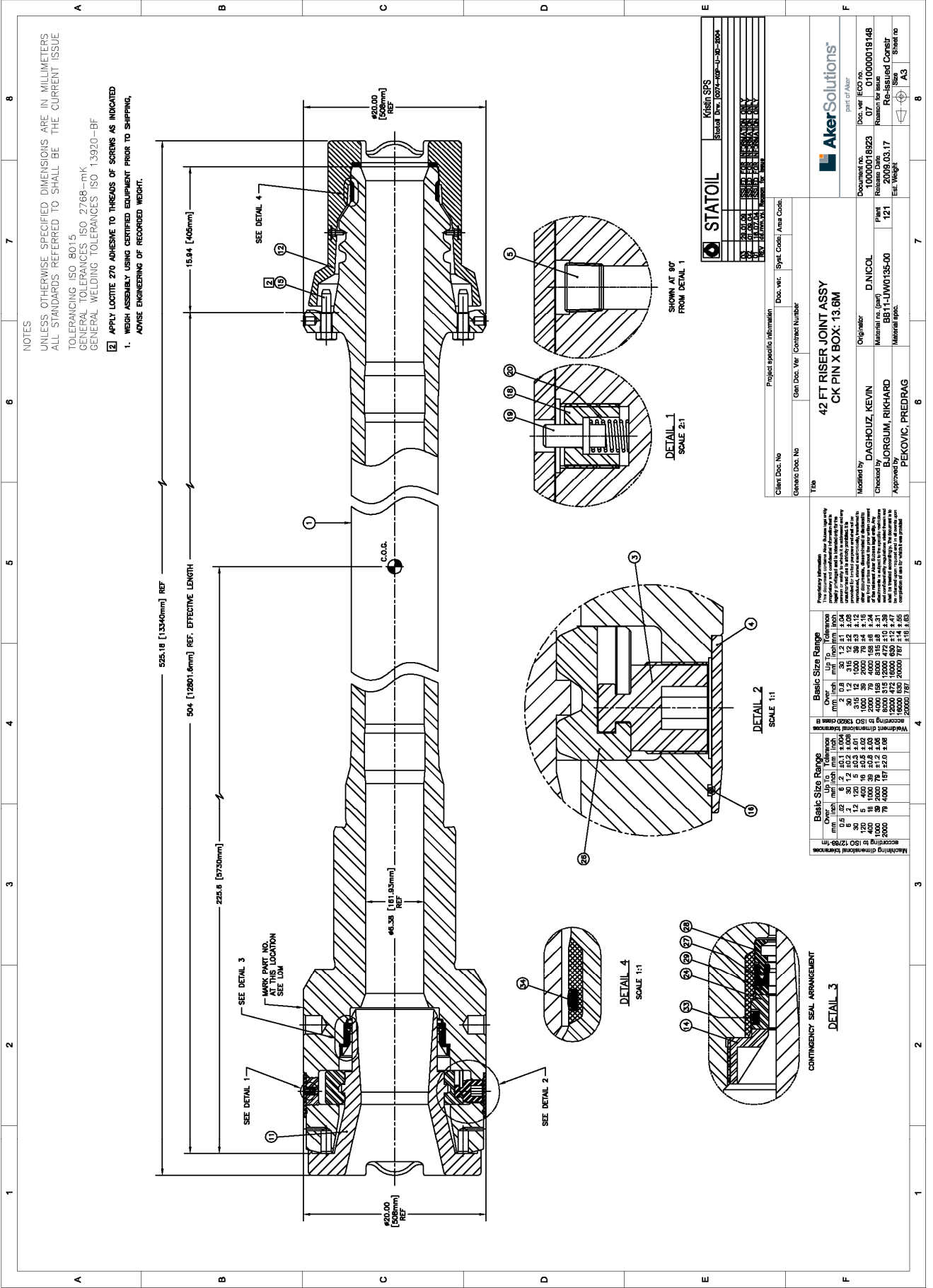


Figure 3.7.3-1



NOTES
 UNLESS OTHERWISE SPECIFIED DIMENSIONS ARE IN MILLIMETERS
 ALL STANDARDS REFERRED TO SHALL BE THE CURRENT ISSUE
 TOLERANCING ISO 8015
 GENERAL TOLERANCES ISO 2768-mK
 GENERAL WELDING TOLERANCES ISO 13920-BF
 [2] APPLY LOCTITE 270 ADHESIVE TO THREADS OF SCREWS AS INDICATED
 1. WEIGH ASSEMBLY USING CERTIFIED EQUIPMENT PRIOR TO SHIPPING,
 ADVISE ENGINEERING OF RECORDED WEIGHT.

STATOIL	
part of Akros	Kristian SPS
Doc. ref.	1000018923
Revision	07
Released Date	2009.03.17
Author	PERKOVIC, KEVIN
Checked by	BJORNUM, RIKHARD
Approved by	PERKOVIC, PREDRAG
Material spcs.	BB11-JVW01355-00
Plant	121
Material no.	D.NICOL
Original no.	07
Doc. ref.	010000019148
Re-issued Constr	
Sheet no	AS

Client Doc. No.	Gen Doc. No.	Gen Doc. Ver.	Commer Number	Doc. ver.	Spcl. Code	Area Code
<p>42 FT RISER JOINT ASSY CK PIN X BOX: 13.8M</p>						
Modified by	DAGHOUZ, KEVIN	Original no.	D.NICOL	Doc. ref.	07	010000019148
Checked by	BJORNUM, RIKHARD	Material no.	BB11-JVW01355-00	Released Date	2009.03.17	Re-issued Constr
Approved by	PERKOVIC, PREDRAG	Material spcs.		Plant	121	Sheet no

Basic Size Range		Basic Size Range		Basic Size Range	
mm	inch	mm	inch	mm	inch
1000	39.37	1000	39.37	1000	39.37
1200	47.24	1200	47.24	1200	47.24
1500	59.06	1500	59.06	1500	59.06
2000	78.74	2000	78.74	2000	78.74
2500	98.43	2500	98.43	2500	98.43
3000	118.11	3000	118.11	3000	118.11
3500	137.80	3500	137.80	3500	137.80
4000	157.48	4000	157.48	4000	157.48
4500	177.17	4500	177.17	4500	177.17
5000	196.85	5000	196.85	5000	196.85
5500	216.54	5500	216.54	5500	216.54
6000	236.22	6000	236.22	6000	236.22
6500	255.91	6500	255.91	6500	255.91
7000	275.59	7000	275.59	7000	275.59
7500	295.28	7500	295.28	7500	295.28
8000	314.96	8000	314.96	8000	314.96
8500	334.65	8500	334.65	8500	334.65
9000	354.33	9000	354.33	9000	354.33
9500	374.02	9500	374.02	9500	374.02
10000	393.70	10000	393.70	10000	393.70

Basic Size Range		Basic Size Range		Basic Size Range	
mm	inch	mm	inch	mm	inch
1000	39.37	1000	39.37	1000	39.37
1200	47.24	1200	47.24	1200	47.24
1500	59.06	1500	59.06	1500	59.06
2000	78.74	2000	78.74	2000	78.74
2500	98.43	2500	98.43	2500	98.43
3000	118.11	3000	118.11	3000	118.11
3500	137.80	3500	137.80	3500	137.80
4000	157.48	4000	157.48	4000	157.48
4500	177.17	4500	177.17	4500	177.17
5000	196.85	5000	196.85	5000	196.85
5500	216.54	5500	216.54	5500	216.54
6000	236.22	6000	236.22	6000	236.22
6500	255.91	6500	255.91	6500	255.91
7000	275.59	7000	275.59	7000	275.59
7500	295.28	7500	295.28	7500	295.28
8000	314.96	8000	314.96	8000	314.96
8500	334.65	8500	334.65	8500	334.65
9000	354.33	9000	354.33	9000	354.33
9500	374.02	9500	374.02	9500	374.02
10000	393.70	10000	393.70	10000	393.70

